A Novel Hybrid Model for Oblique Machining Induced Residual Stresses and Distortions on Thin Parts

by

Omar Fergani

A Thesis Submitted to the
Graduate School of Engineering
in Partial Fulfilment of the Requirements for
The Degree of

Master of Science
in
Mechanical Engineering

Koc University
December 2012

Koc University

Graduate School of Sciences and Engineering

This is to certify that I have examined this copy of a master's thesis by

Omar Fergani

and have found that it is complete and satisfactory in all respects,

and that any and all revisions required by the final

examining committee have been made.

Committee Members:

_____

Ismail Lazoglu, Ph. D. (Advisor)

_____

Erdem Alaca, Ph. D.

_____

Canadinc Demircan, Ph. D.

_____

Ozgur Birer, Ph. D.

_____

Kerem Pekkan, Ph. D.

Date: _____

ABSTRACT

Residual stresses are critical factors in the performance of mechanical components. Residual stress state may directly affect the fatigue life, fracture initiations, corrosion resistance and distortions of engineering parts. Although the residual stresses are very critical in mechanical engineering parts such as thin airplane and rocket parts, jet engine parts, bearings, etc., there is a lock of fast and precise model in the literature for for residual stress estimations.

Thin parts are very commonly used in Aerospace Industry. Most of the thin parts in Aerospace applications are manufactured by oblique machining processes such as milling. Due to the mechanical and thermal loading during the machining processes, the stress states of parts may change significantly.

This thesis aims to develop an enhanced solution for the very significant engineering problem of the industry. Although the problem is very practical, its solution is very challenging due to fact that it requires advanced modeling of the processes. The objective of this research is to develop a method of predicting residual stress in the milling process based on a hybrid model associating analytical and experimental approach. The model considers all possible machining parameters and the material properties are associated to the residual stress field. The newly developed model uses elasto-plastic constitutive behavior and numerical algorithm to estimate the plastic strain and residual stresses once the cutting forces were accurately calculated. Relaxation procedure is also applied upon residual stresses in order to simulate the deflection when the plate is free of forces.

Experimental machining tests are performed on Mori Seiki NMV 5000 DCG CNC Machine on Aerospace Aluminum Alloy Al7050 as well as on Steel 2842 and Titanium Alloy Ti-Al6-V4 for the model validations. X-Ray Diffraction measurements are performed for residual stresses on various machining conditions. Relationships between

micro hardness and microstructure of the parts and residual stresses are also investigated in details. 3D thin part deformations are also simulated and validated with the 3D CMM measurements.

ÖZET

Artık gerilmelerın, talaşlı imalatla üretilmiş parçaların üretim performanslarında önemli bir rolü vardır. Yorulma ömrü, korozyon dayanımı ve distorsiyon, artık gerilmelerden etkilenen parça özellikleridir. Yani, artık gerilme dağılımı imal edilmiş herhangi bir parçanın genel kalitesiyle doğrudan ilişkilidir. Uzun yıllar boyunca, araştırmacılar artık gerilmeleri matematiksel, ampirik veya sonlu elemenlarla modelleme yoluyla ya da deneysel olarak incelemişlerdir. Her ne kadar bu konu üzerinde çok sayıda kayda değer araştırma yapılmışsa da, artık gerilmeleri önceden tahmin etme yöntemlerini geliştirmek adına yapılabilecek daha birçok çalışma vardır. Bu araştırmanın amacı, frezeleme işlemi esnasında artık gerilmeleri önceden tahmin edecek, analitik ve deneysel yaklaşımları birleştiren hibrit bir modeli baz alan bir metot geliştirmektir.

Çalışma, frezeleme artık gerilmelerinin oluşum sürecinin deneysel olarak anlaşılmasına odaklanacaktır. Kesme parametreleri ve malzeme özelliklerinin artık gerilme alanı ile ilişkili olduğu bir model oluşturulması konusunda bugüne kadar birtakım çalışmalar yürütülmüştür. Artık gerilme oluşumu nedeniyle meydana gelen malzeme özelliklerindeki değişimler incelenmiş ve mikroyapı ve artık gerilme arasında bir korelasyon oluşturulmaya çalışılmıştır. Artık gerilmeler sebebiyle oluşan distorsiyonlar modellenmiş ve basit bir geometri için doğrulanmıştır. Bu konuda ileride yapılabilecek çalışmalar ve geliştime olanakları sunulmuştur.

ACKNOWLEDGEMENTS

I would like to thank my advisor Dr. Ismail Lazoglu for guiding and supporting me in this research. His enthusiasm about the manufacturing technologies made this work productive.

I would like to thank the jury members Dr. Erdem Alaca, Dr. Demircan Canadinc, Dr. Kerem Pekkan, Dr. Ozgur Birer for accepting to be present in my thesis defence and for the reviewing of the thesis. I am thankful to Dr. Erdem Alaca for sharing his knowledge and to Dr. Demircan Canadinc without whom the microstructure discussion part wouldn't be possible.

The experimental part of this research would not be possible without the collaboration with ENSAM ParisTech. I would like to express my gratitude for Dr. El Mansori, Deputy General Director of ENSAM ParisTech and Dr. Ali Mkaddem for welcoming me in at ENSAM and for supporting me financially.

I would like to thank Dr. Sebastien Jegou from the Mecasurf laboratory at ENSAM Aix en Provence, with whom I worked many hours on the X-ray diffraction measurements.

I would like to express my respect for my colleagues at the Manufacturing and Automation Research Centre (MARC), with whom I had good memories; thanks to Ugur, Erdem, Suat and Ali for the help during my stay here. Thank you Muzzafer Buttun for the technical support.

Last but not the least; I would like to express my gratitude my mother, father, sister and brother. Without their support and encouragement I wouldn't be the person I am today.

TABLE OF CONTENTS

List of Tables

List of Figures

Nomenclature

Table of Contents

Chapter 1: Introduction **15**

Chapter 2: Literature Review **21**

2.1 Overview 21

2.2 Residual stress modeling 22

2.3 Experimental studies 25

2.4 Thin part deflection 26

Chapter 3: Residual stress modeling and deflection 30

3.1 Introduction 30

3.2 The hybrid aspect of the model 31

3.2.1Equivalent & Hydrostatique stress on the surface 33

3.2.2Pressure distribution design 36

3.2.3Microstructure consideration 39

3.3 Analytical model for residual stress 41

3.3.1Elastic Plastic model 41

3.3.2Analytical solution 45

3.3.3Relaxation procedure 50

3.4 Deflection model 51

Chapter 4: Experimental methodology and results 55

4.1 Introduction 55

4.2 Material characterization 60

4.3 Residual stress measurements 64

4.3.1X-ray diffraction method 64

4.3.2Experimental results 67

4.3.2.1Residual stress in Steel 2842 72

4.3.2.2Residual stress in Al7050 74

4.4 Hardness investigation 77

4.4.1Vickers test 77

4.4.2Hardness depth profile for Steel 2842 80

4.5 Deflection validation 82

4.5.1Experimental setup 82

4.5.2Metrology validation 83

Chapter 5: Results and discussions 88

5.1 Introduction 88

5.2 Part deflection 88

5.3 Residual stress 95

5.4 Hardness and residual stress 106

5.5 Milling and SPD similarities 108

Conclusion **112**

Bibliography **115**

Vita **121**

LISTE OF TABLES

Table 1: Composition of Steel 2842 62
Table 2: TiAl6V4 concentration results 62
Table 3: TiV6 concentration results 63
Table 4: Al 7050 concentration results 63
Table 5: Cutting conditions 70
Table 6: Hardness measures 81
Table 7: Cutting parameters for residual stress 96

LISTE OF FIGURES

Figure 1: Oblique cutting configuration 16
Figure 2: Milling operation 17
Figure 3: The mechanics of cutting in the milling tool [49] 18
Figure 4: Distortion of a part due to residual stresses [Safran] 20
Figure 5: Tool path in the milling process 32
Figure 6: Uncut chip thickness 33
Figure 7: Investigated points and forces 34
Figure 8: Equivalent and Hydrostatique stresses per location of the cutter 35
Figure 9: (a) Oblique cutting (b) Ballend mill pressure generation (c) Endmill pressure generation 38
Figure 10: Residual stress investigation methodology 40
Figure 11: Return mapping algorithm for Drucker-Prager 42
Figure 12: Yielding surface Drucker-Prager criteria[Wikipedia] 44
Figure 13: Parallelepiped inclusion 49
Figure 14: Half-space model 51
Figure 15: Effect of a force on the whole body [38] 55
Figure 16: EDX (Energy Dispersive X-ray) 61
Figure 17: Normal and shear stress tensors 64
Figure 18: The diffraction principle of X-ray 65
Figure 19: 2Ω setup for residual stress investigation 67
Figure 20: D500 Siemens x-ray machine 67
Figure 21: Electro-polisher 68
Figure 22: Metrology setup to measure the depth 69
Figure 23: x-ray during measurement 69
Figure 24: Five axis CNC machine MORI SEIKI 70
Figure 25: SEM picture of a worn tool 71
Figure 26: SEM picture of a fresh tool 72

Figure 27: Residual stress σ_{xx} in steel 2842 73
Figure 28: Residual stress σ_{yy} in steel 74
Figure 29: Residual stress σ_{xx} in Aluminum for fresh and warn tool in Aw1 and Af1 75
Figure 30: Residual stress σ_{yy} in Aluminum for fresh and warn tool in Aw1 and Af1 76
Figure 31: Residual stress σ_{xx} in Aluminum for fresh and warn tool in Aw2 and Af2 76
Figure 32: Residual stress σ_{yy} in Aluminium for fresh and warn tool in Aw2 and Af2 77
Figure 33: Vicker test details 78
Figure 34: Tested part in the resin 79
Figure 35: Polishing of the surface 79
Figure 36: Hardness machine Leyca 80
Figure 37: Hardness before and after milling 81
Figure 38: Experimental setup for machining 82
Figure 39: Distorted part 83
Figure 40: Distortion acquisition process 85
Figure 41: CMM machine 86
Figure 42: Technique used 86
Figure 43: Path definition on Catia v4 87
Figure 44: Matlab surface generation from the recorded data 87
Figure 45: Experimental distortion of Al7050 part (Depth of cut of 2mm, Spindle speed of 8000 rpm, feed per tooth 0.2 mm/rev) 90
Figure 46: The CMM profile of the deflected Al7050 part (Depth of cut of 2mm, Spindle speed of 8000 rpm, feed per tooth 0.2 mm/rev) 91
Figure 47: CMM profile side view (Depth of cut of 2mm, Spindle speed of 8000 rpm, feed per tooth 0.2 mm/rev) 91
Figure 48: Simulated deflection 92
Figure 49: Micro milling experimental setup 93
Figure 50: Tool used 94
Figure 51: Micro deflection (20x5 mm) 94
Figure 52: White light interferometer obtained result 95
Figure 53: Experimental residual stresses in the x direction of Steel 2842 for (S01, S02, S03) 97
Figure 54: Simulated residual stress in x direction for the case S01, Steel 2842 97
Figure 55: Simulated residual stress in x direction for the case S02, Steel 2842 98
Figure 56: Simulated residual stress in x direction for the case S03, Steel 2842 98
Figure 57: Experimental residual stresses in the y direction of Steel 2842 99
Figure 58: Simulated residual stresses in the y direction for the case S01 of Steel 2842.. 100
Figure 59: Simulated residual stresses in the y direction for the case S02 of Steel 2842.. 100
Figure 60: Simulated residual stresses in the y direction for the case S03 of Steel 2842.. 101

Figure 61: Experimental residual stress for Al7050 (Feed 0.075, Spindle speed of 8000 rpm, depth of cut 1mm), x direction 102
Figure 62: Experimental residual stress for Al7050 (Feed 0.075, Spindle speed of 8000 rpm, depth of cut 1mm), y direction 103
Figure 63: Simulated residual stress for Al7050 (Feed 0.075mm/rev, Spindle speed of 8000 rpm, depth of cut 1mm) 103
Figure 64: Experimental residual stress for Al7050 (Feed 0.2 mm/rev, Spindle speed of 8000 rpm, depth of cut 1mm), x direction 104
Figure 65: Experimental residual stress for Al7050 (Feed 0.2 mm/rev, Spindle speed of 8000 rpm, depth of cut 1mm), y direction 105
Figure 66: Simulated residual stress for Al7050 (Feed 0.2 mm/rev, Spindle speed of 8000 rpm, depth of cut 1mm) 105
Figure 67: Harness before and after milling on Steel 2842 107
Figure 68: Hardness vs. residual stress 108
Figure 69: Chip formation process [45] 110
Figure 70: The change of the grain size during the machining [45] 111

NOMENCLATURE

d	axial depth of cut
σ	Stress field
μ	Lame coefficient
ν	Poisson's coefficient
θ	geometrical constant
λ	Lame coefficient
ε^*	Relaxed strain – Eigenstrain
ε^p	Plastic strain
ε^e	Elastic strain
ε^{th}	Thermal strain
$\Delta\sigma$	Residual stress
E	Young Modulus
u_{ij}	Displacement field
Ω	Integration domain, Eshelby's inclusion domain
F_a	Axial force
F_r	Radial force
P_a	Axial pressure
P_r	Radial pressure
a	Half contact length
(x,y,z)	Coordinates parameters
G_{ij}	Green function

Chapter 1

INTRODUCTION

Residual stress is one of the major parameters in the study of surface quality and reliability of any mechanical part. The understanding of residual stress distribution is a major challenge the manufacturing industry is dealing with. The residual stresses are in fact directly affecting the crack propagation on the surface, the resistance to fatigue and the part distortion. One may define residual stresses as locked-in stresses without application of any exterior forces. This is the most basic definition that may be found in the literature. Residual stresses can be caused by thermal or mechanical effects. The plastic deformation generates a permanent displacement of the crystal structure, and the thermally induced residual stress is the consequence of change in the volume of the material. During the cutting of metals, both of these effects are produced. The plastic deformation is due to the chip formation and the contact between the tool and the part. The friction and the plastic deformation produce thermal residual stress. Therefore, modeling the residual stress distribution is very challenging both mathematically and technically. Many researchers have focused on that topic [5, 6, 7], most of them has been studying residual stress in orthogonal cutting due to the simplicity of the physical modeling in that case. Other types

of manufacturing processes, such as milling and turning have also been studied. Most of the work done is based on empirical fitting and statistical estimations [33, 34]. Models based on FEM have been used since the emergence of strong computing capabilities [11, 12, 13]. FEM methods have been able to produce sufficiently informative results in predicting residual stress due to cutting. However, the FEM models have made little effort to clarify the mechanisms which give rise to the machining induced residual stresses. Additionally, FEM still requires significant computational power, and can be time prohibitive. Changes in the cutting conditions require re-computing of the model. Because of this, use of FEM as a means of production guidance has been restricted.

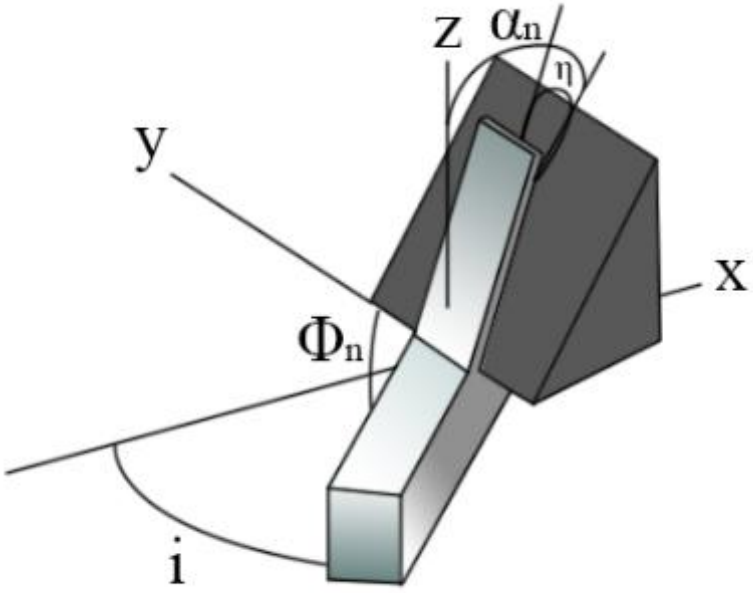

Figure 1: Oblique cutting configuration

The target of this research is to build the basis for the modeling of residual stress in the milling using analytical techniques. In fact, the complex kinematics of the milling

operation obliged us to use experimental calibration results to construct a pressure distribution equivalent to the one applied by the tool on the workpiece. Figure 2 shows the contact area during the slot milling. The oblique aspect of the milling operation makes the modeling more complex. Figure 1 shows the principle of the oblique cutting mechanism that defines the bases of the milling. Altintaş [36] in his book established the basics of the modeling of forces in milling. The model equations were derived from the mechanics of oblique cutting defined by the schemas of figure.3.

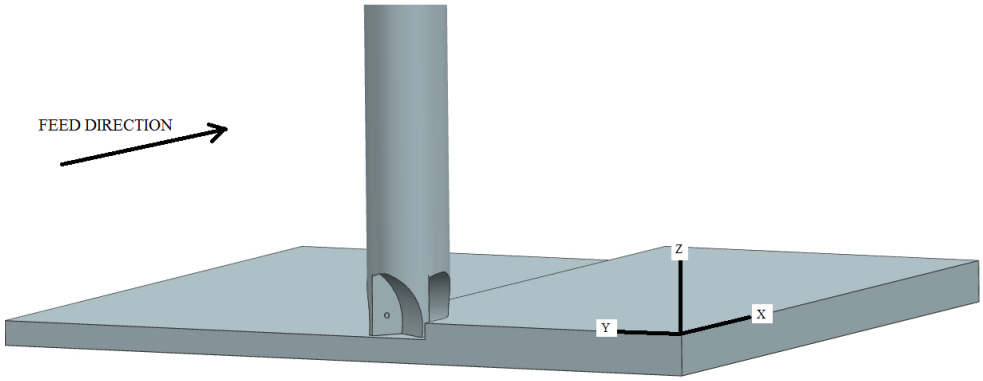

Figure 2: Milling operation

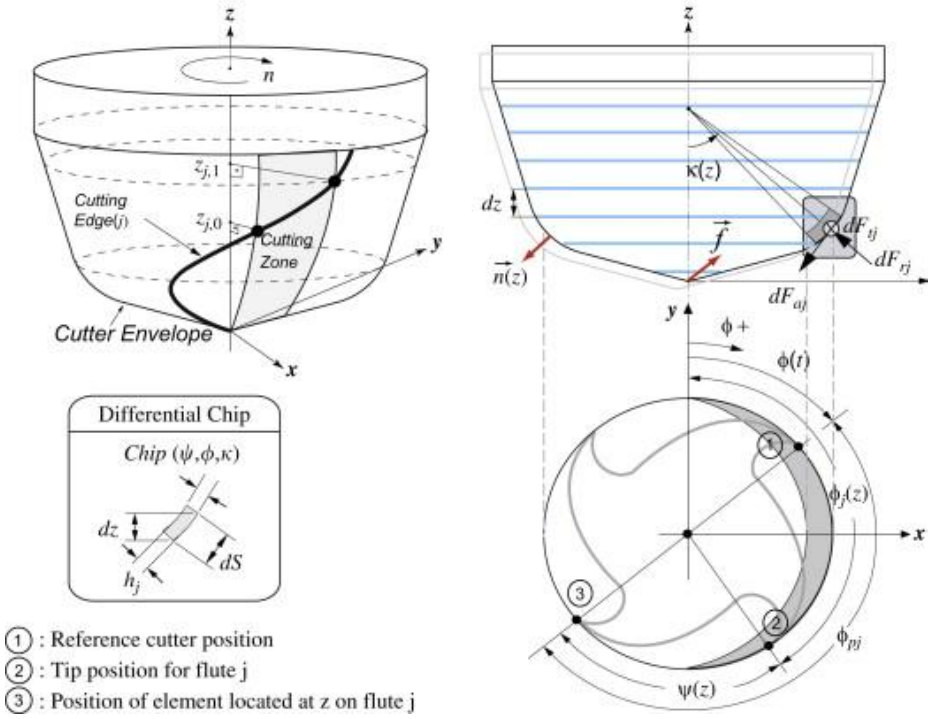

Figure 3: The mechanics of cutting in the milling tool [49]

The pressure applied by the tool to the part is then estimated using a Hetzian contact solution. Hertz [35] was the first to propose an analytical form for the most used pressure distribution. Hertzian contact stress refers to the localized stresses that develop as two curved surfaces come in contact and deform slightly under the imposed loads. This amount of deformation is dependent on the modulus of elasticity of the material in contact. The analytical code is estimating the plastic strain based on an elastic-plastic constitutive algorithm. In this work, since the thermal effect is not studied, the use of the common Johnson-Cook [50] model was avoided. A Drucker-Prager [51] elastic-plastic model was implemented. Once the plastic strain is known, the relaxation procedure is applied to come out with the residual stress. In this analytical work the distortion which is one of the main effects of the residual stress is investigated. An analytical model to calculate the surface

displacement is introduced and adapted for the residual stress case. Only simple geometries such as a point, line or plane can be taken into account. This is due to the analytical aspect of the proposed solution.

Experiments were necessary to validate the simulation results. Experiments are designed for validating and investigating different aspects of the residual stresses. During the experimental work, residual stresses are investigated using x-ray diffraction technique. In this work, the relationship between the residual stress distribution and the microstructure changes in the surface was investigated. The similarities concerning the microstructure changes with processes such as SPD (Severe Plastic Deformation) are established. The hardness of the Steel part was investigated before and after the manufacturing. A relation between hardness and residual stress is established based on the experimental outputs. On the other hand, the macro effects of residual stress in a manufactured part are studied. The distortion is usually taking place for a large thin part as shown in the figure bellow. In this study, the deflection of a milled thin Aluminium part is investigated theoretically and experimentally, figure.4. The geometrical error in the final part is explored using CMM (coordinate measuring machine). The materials used for the experiments are mostly from aerospace and automotive industry such as Al7050, Steel 2842, and TiAl6V4.

Figure 4: Distortion of a part due to residual stresses [Safran]

The thesis presents the output of this research in the following order: In chapter 1, a literature review on the residual stress and its effects is presented. The deflection of a part under stress constraints is also reviewed. Chapter 2 concentrates on the analytical modeling of the residual stress generated by milling based on a hybrid model associating simulation and experimental calibration will be presented. A quick review of the kinematics of oblique machining is made. The distortion model is derived and simulated. Chapter 3 presents the full experimental setup for both residual stress and distortion validation. The theoretical and practical side of the uses of x-ray machine and hardness is detailed. Experimental results are all summarized in this chapter. In Chapter 4, the results of simulations and experiments are compared and discussed.

In the conclusion, the outputs of this research are summarized. Future research opportunities are presented.

Chapter 2

LITERATURE REVIEW

2.1 Overview

Residual stress induced by metal cutting processes has been studied intensely for the last sixty years. Many researchers have been investigating the distribution and the modeling of residual stress using different techniques. In this review, part 2.2 will be reviewing the progression of the modeling of residual stress using different methods. Analytical modeling will be presented and compared to the finite element modeling. The finite element uses evolution and benefit will be seen. New methods of modeling of residual stress will be exposed, such as the hybrid modeling where analytical and experimental background is implemented in a finite element code to simulate the distribution of residual stresses. In each part the advantages and inconvenient are going to be presented and analyzed. In section 2.3, the experimental studies on the residual stress are presented. The evolution from destructive methods to non destructives method is seen. Special importance is going to be given to the x-ray diffraction method for the residual stress determination and the evolution of the sensitivity of the results. Final section 2.5, will review the literature about

the distortion and deflection of part due to residual stress. After the review, a summary of new potential path on the future of the research in the residual stress will be presented.

2.2 Residual Stress Models

Many researchers since 1920 started to model the physics of the metal cutting operation [1], [2]. Their analytical modeling founded the basis of the residual stress modeling. Cutting parameters and material properties have been the main focus of researchers in the residual stress modeling. In fact, relating the residual stress analytical models proposed by Chiu [3] and Love [4] and the cutting parameters was the priority to optimize the machining process. Recently, many researchers are focusing on the uses of analytical solution to model residual stress. Lazoglu [5] used a couple mechanical and thermal modeling of the cutting process to model the residual stress in the orthogonal cutting operation. Most of the works done analytically are based on the elasto-plastic contact framework that Johnson has proposed [6]. Jacobus [7] presented also one of the most accurate analytical models. The research utilized an incremental plasticity model, similar to that used by Merwin and Johnson [8]. Rather than assume a stress field in the workpiece, the model assumed a form for the deformation of the material beneath the tool. Residual stress was modelled in a coordinate frame with respect to the tool. The deformation parameters were treated as a function of the edge radius and the depth of cut. The parameters were calibrated from experimental tests and an optimization procedure. The work also provided a rationale for the effect of thermal loads and mechanical loads on the residual stress generated in machining. Mittal and Liu continued modelled the residual stress in hard turning [9].The model suppose that the residual stress profiles fit a polynomial profile that was a function of depth into the workpiece. The coefficients of the

polynomial were individual functions of the machining parameters. Therefore, the determination of a large number of coefficients was a complicated part. Additionally, it did not provide any physical understanding into the residual stress formation. El-Axir [10] and Sridhar [11] modelled residual stress in hard turning of new material such as Titanium. They investigated the influence of tool parameter on the residual stress.

In contrast to the analytical modeling that was the first to be introduced, FEM was used due to the progress in the computing technology. Commercial packages offer interesting and flexible simulation conditions. Okushima and Kakino [12] were one of the first to apply analysis to residual stress prediction for the machining process. The effect of the tool edge and the thermal effect of temperature distribution produced in metal cutting were modelled. The modeling results were compared with experimental data measured by x-ray diffraction. Residual stresses were measured in the cutting direction and across the cutting direction. The conclusion of their work was that the mild cutting parameters were necessary to minimize the residual stress distribution. Lin [13] used a finite element method to determine the strain field in the workpiece. Using the strain field, the concept of particle flow was employed to determine the stress history of the strain history of the material. In this paper, the authors used the residual stress modeling method introduced by Merwin and Johnson. Lin incorporated the thermal and the mechanical load in his model. In another related work, Lin used the same modeling methodology to study the residual stress, but this time the tool wear was taken into account.

Shih [14] developed a plane-strain finite element simulation of orthogonal metal cutting. The research incorporated detailed material modeling including effects of elasticity, viscoplasticity, temperature, large strain, and high strain-rate. Experiments have been made to validate the model. The comparison between experimental and simulation results show

very good agreement. However, the paper does not explain the mechanics of the generation of residual stress during the machining.

Hua [15, 16] used DEFORM 2D, which is a Lagrangian implicit code to simulate orthogonal cutting of AISI 52100. The work focused on analyzing the effect of feed rate, workpiece hardness, and cutting edge on the subsurface residual stress formation in hard turning. The results were compared with experimental data and showed reasonable agreement between model predictions and experimental data. K.c.Ec [17] presented another finite element model based on a thermal elastic viscoplastic of the material. He used remeshing technique to increase the accuracy of the simulation results. Z.T.Tang [18] investigated the tool flank wear of the residual stress distribution for aluminium alloy. He presented an integral work about the modeling and the validation of the model experimentally. He used an explicit FEM code on abaqus.

After the utilization of FEM and analytical method, some researchers are proposing hybrid model [19], where the simulation is made using half FEM while the load historic is introduced from experimental and analytic simulations. This model shows a very high accuracy and gave the possibility to visualize the 3D field of residual stress in the orthogonal cutting. However, this method is time consuming and can be used only in research application due to its complexity.

The introduction of FEM in the domain of residual has enhanced the research and the quality of modeling. However, FEM rarely explain the physical phenomenon behind residual stress. Further, the uses of FEM have high computing cost which makes it industrial uses hard. FEM can be time prohibitive. Changes in the cutting conditions require re-computing the model. Because of this, use of FEM as a means of for production guidance has been restricted. In the other hand, analytical solutions were the first to be used for simulating residual stress. They give good results and the simulation time is very small

comparing to FEM. More and more researchers are working on increasing the accuracy and implementing them in the industry. However, they still suffer from a big dependency on the experimental calibrations and the number of hypothesis. The analytical models cover various aspects of sources of residual stress and mechanisms that affect the profiles. However, a thorough model for predicting residual stress with consideration of the oblique cutting is still unavailable.

2.3 Experimental studies

The previous section focused on the review of existing model to predict residual stresses in the machining field. Experimental investigation of residual stress is definitely the best way to understand the distribution and the effect of the cutting process. However, it is obvious that it's hard to be implemented for many reasons. The most obvious one is the cost of the solution; huge investments have to done on the machines and human resources. Further, technical problem can immerge depending on the size of the part and the portability of the residual stress process. Many companies are offering new mobile X-ray diffraction solution, however all these complexities make the dependency on the simulation very high.

Henriksen [20] was the pioneer on the machining induced residual stress. He investigated the residual stresses in the low carbon steel in orthogonal cutting. He was the first to attribute the majority of the remaining stress to the mechanical loading. After, a vague of researcher tried to understand the effect of cutting parameters on the residual stress. Most of works have been done in the orthogonal cutting. Sadat [21] investigated the effect of feed rate, cutting speed and depth of cut on residual stress distribution on turning process. He used deflection etching to measure the residual stress profiles. A direct relation between the increase of depth of cut and the increases of absolute residual stress value was

established. In another work Sadat [22] did the same experiment but this time on Inconel 718. The conclusion of his work shows that the depth of the residual stress picks increases with the increase of cutting speed. Liu and Barash [23] have demonstrated a unique relationship between four process parameters and residual stresses. The variables included the length of the shear plane, tool flank wear, shape of the cutting edge, and the depth of cut. The shape of the cutting edge determined the residual stress pattern near the machined surface. Additionally, the research found that tool flank wear increased cutting temperature. They also found that smaller depths of cut did not necessarily produce low subsurface stresses. They concluded that a lower degree of constraint in the deformation process produces a lower level of residual stress. Xie and Bayoumi [24] also investigated the effect of tool wear on residual stress in machining. They found similar results and concluded that tool wear impacted residual stress. The experimental work has produced very important knowledge about the residual stress in the machining. Mechanical loading for example is more responsible for generating compressive stress. However thermal loading is more likely to generate tensile stress.

2.4 Thin part deflection

The distortion of a part can occur during the manufacturing process or while the tool is removed. The deformations occurring during the machining have taken the interest of many researchers [25], [26]. Most of this research is about thin wall deformation. The purpose was to propose corrective actions on the cutting parameters to avoid or minimize the distortion. The geometrical errors due to residual stresses relaxation still remain under-addressed; a recent review however, noticed it importance on the surface integrity field [27]. Despite open literature has reported the role of the phenomenon on altering the quality of finished parts, only a small number of models were developed in this topic [28].

Different types of models have been proposed and used to simulate workpiece deformations in the machining field. Finite element analysis is the most wide used; the advantage of this technique is its ability to simulate complexes geometries and processes [29]. However, many problems have been reported concerning long computational time. Further, the number of assumptions made during the modeling of the cheap removal process makes the results less accurate. Analytical models can be used to predict such phenomenon [30], [31]. Its main advantage is the short computing time and the large optimization opportunities and industrial application offered. Love [32] has demonstrated an analytical model to predict residual deformations due to an elasto-pastic contact. In his work, he was the first to link the stress to the distortion. These precedent works all proved the important of prediction residual stress in the understanding of large part distortions. In another field, [33] used an analytical model to predict the photo induced deformation. However, no analytical model predicting the post machining distortion of a thin part due to the milling residual stresses was reported in the literature.

Empirical and analytical model can be improved to investigate the effect of the cutting parameters. Most of the research has been conducted using FEM, the large computing time is restricting more and more the uses of it. Many of the models are based on an orthogonal approach and limited to orthogonal conditions. Extending the modeling capabilities to more complex operations such as milling and turning will enhance the value of analytical residual stress modeling. Also, concerning the experimental investigation, methods such as x-ray and hole drilling are the most used. Rather than the process difficulty. The results are not usually accurate. Modern techniques such as ultrasound investigation should be studied. Other aspect such as the effect of the cutting fluid on the residual stress generation can be important to understand. The relation between the residual stress and the microstructure is also very important; in fact linking the residual stress to the

microstructure is a big challenge. The effect of the wear on the residual stress is critical; a deeper investigation has to be done for a better understanding of the wear effect on the surface quality.

This study tries to fill the gap in the research about residual stress in the milling operation. Various topics going from the tool wear to the microstructure passing by residual stresses are studies. Deflection and distortion due to the residual stress are to be investigated. The theory is validated using different material under x-ray diffraction measurements. Therefore this thesis will be divided into the following elements:

- Modeling
    - Design of pressure distribution
    - Elasto-Plastic model
    - Residual stresses modeling
    - Distortion prediction

- Experimental validation
    - Residual stress validation
        - Steel
        - Aluminium
    - Distortion validation
        - Aluminium
    - Hardness profile

- Results and discussions
    - Residual stress
    - Deflection

- Hardness and residual stress
- SPD similarities

Chapter 3

Residual Stress and Deflection Modelling

3.1 Introduction

This chapter will focus on the modeling of residual stress for the milling. Only mechanical loading is taken into account. Therefore, all the thermal aspects of the problem are neglected here. In contrast with orthogonal cutting where the mechanistic approach is clear, the oblique cutting makes the understanding and the modeling of many parameters more complex. Therefore, during the entire modeling approach, the aspect of oblique cutting is investigated. After modeling and predicting cuttings forces, the contact surface between the tool and the workpiece is investigated either experimentally of theoretically as it has been done in [5, 35]. In fact, during the modeling, the applied pressure by the tool on the part is estimated based on a Hertzian type of distribution. This pressure generates a plastic deformation. In this study, a plastic model is incorporated to the analytical solution. The Drucker-Prager model is used and more details about its implementation are offered. Finally, using the pioneer work [37,38,39,40], the distribution of residual stresses is derived for a specific geometry. The present work is inspired by a previous one which was done for

a cubic form. Details about the residual stress process is given and the physics behind is explained. The last modeling part focuses on the deflection prediction. Complex mathematical equations are solved. Green's function is used to determine the effect of a force on all the points of the geometry [39]. The advantages of the model and its limitations are exposed. Finally, an outline about the simulation is proposed, many aspects of the computational work and some basic comparisons with other modeling method is presented.

3.2 The hybrid aspect of the model

This work presents for the first time a methodology to predict residual stress in the milling operation. Most of the previous work has studied the residual stress generated by the orthogonal cutting operation [5]. The simplicity and the geometrical approximations of the orthogonal cutting process made the modeling and the understanding of residual stress easier. During the milling process, the complexity increases and the understanding of the mechanics become complicated [36]. All the existing tentative for milling and other manufacturing process were made on FEM or using experimental fitting [17, 22].More recently [52] proposed a semi analytical approach to model residual stress in milling, Altough all the effects were considered the simulation results were not satisfying for the surface residual stress. In fact, many parameters contribute to this increase of complexity:

- Tool geometry becomes very critical. In fact, during the milling operation the affected zone is large and different contact areas exist depending on the number of teeth. (Figure.6)
- The tool path is important. In fact, the residual stress distribution is not uniform and changes following the location inside the path of the tool. (Figure.5)

- The applied load is changing during the milling process. The unloaded chip variation following Martelotti [41] curve defines the variation of the cutting force and therefore the variation of the pressure distribution.

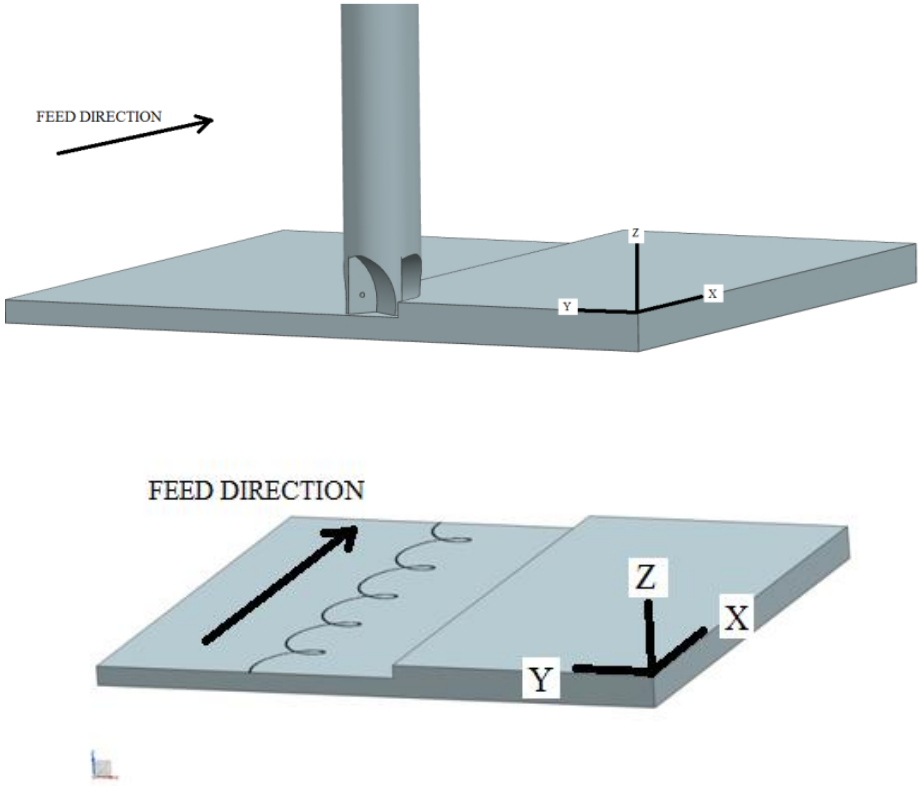

Figure 5: Tool path in the milling process

In this chapter, the basic of understanding the residual stress profile in a milled part is investigated. A global understanding of the relation between the cutters positions presented in Figure. 5 and the hydrostatique and equivalent stresses distribution on the surface are proposed in figure 8. A better understanding of the relation between the macro parameters of milling (forces) and the equivalent stress distribution is established. The second approach will concern the development of a relation between the micro residual

stress (Residual stress in a single grain) and the macro residual stress (Total residual stress in the part). This comes through the study of the material used in the experiment. The relation between micro and macro residual stress will help us to identify the error factor during the estimation. Finally, a better modeling method will be introduced for future work.

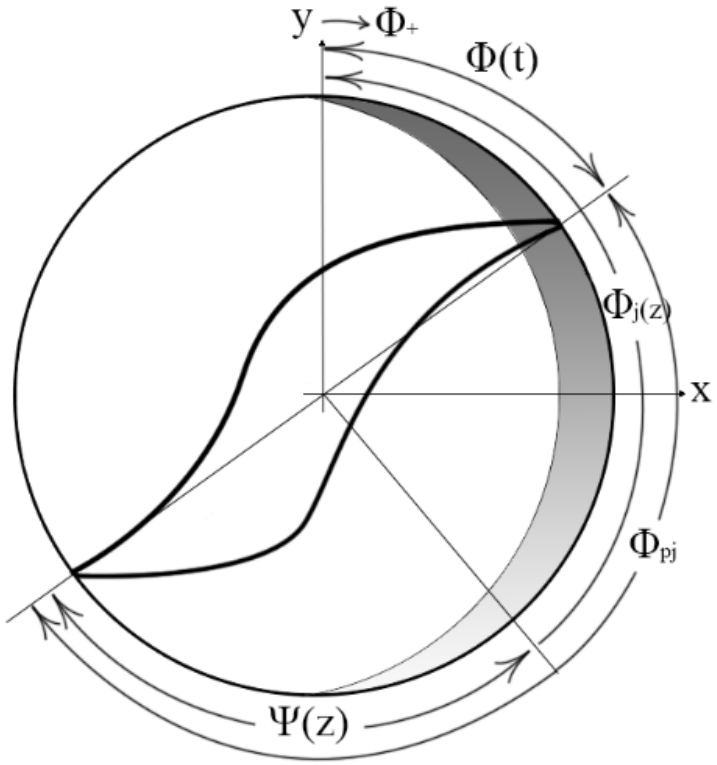

Figure 6: Uncut chip thickness

3.2.1 Equivalent and hydrostatique stress on the surface

During the cutting operation, the endmill teeth shear the material. Shear intensity and removal volume change considering the location of the cutter. In this case, a kinematic study of the milling tool during the shearing operation is necessary. A global relation between the location of the cutter, the forces variations and the equivalent stress remaining

on the part is established. These relations offer us the opportunity to better understand the relation between the cutting mechanics and the residual stress on the part surface. The outputs of this study were used directly in the enhancement of the simulation results by taking realistic input data.

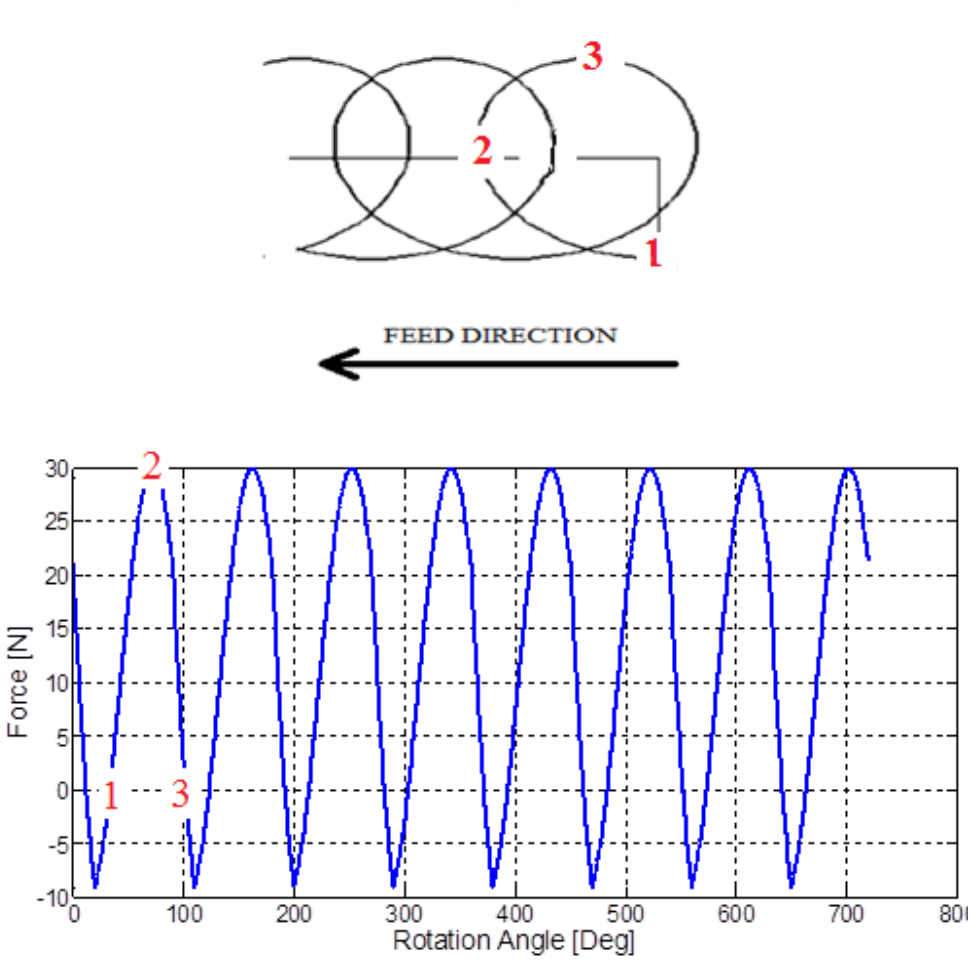

Figure 7: Investigated points and forces

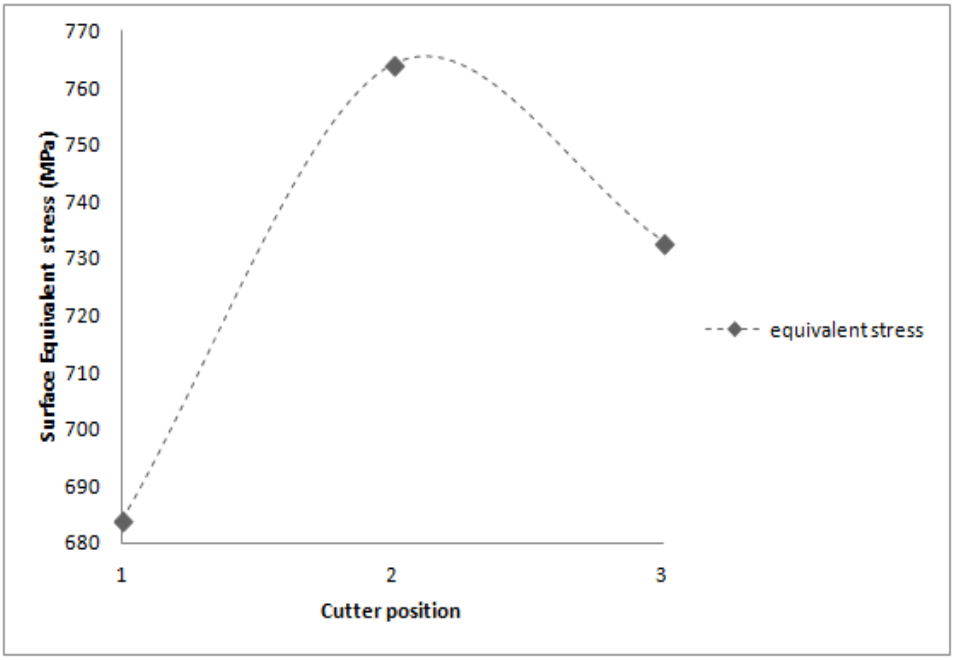

(a)

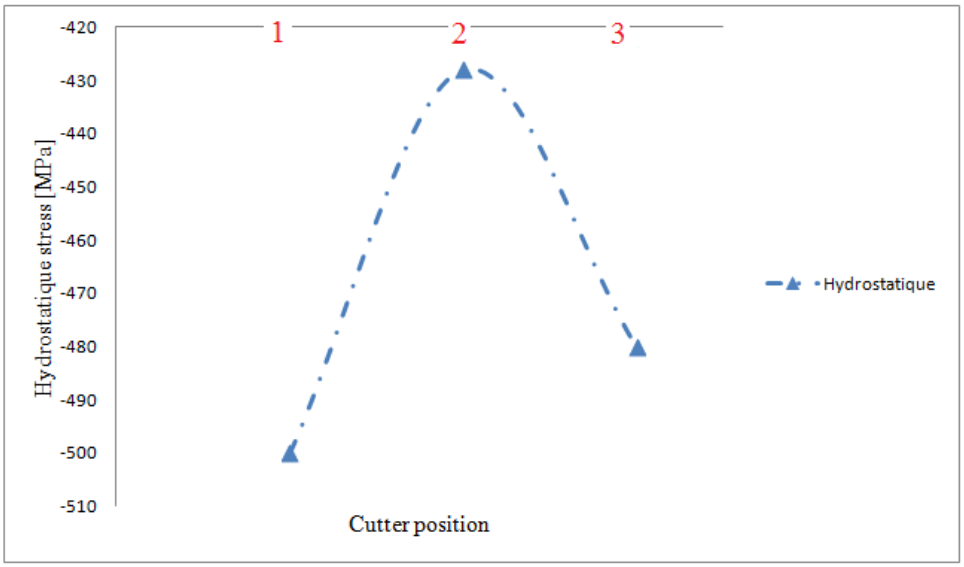

(a)

Figure 8: (a) Equivalent and (b) Hydrostatique stresses per location of the cutter

During the milling operation, the cutting process can be divided into three main critical areas. The shearing operation starts at point **1**, when the tool just engaged the workpiece. The sheared volume just has initiated and the maximum value is not yet reached. The force diagram of the milling operation is also correlating with this fact. Point **2** represents the maximum sheared volume, which is corresponding to the maximum needed force. Also, this is generating the maximum equivalent stress on the surface. Point **3** represents the exit point. This correlation between the cutter position, forces and surface equivalent stress remind us of Martelotti's [41] work on the uncut cheap thickness as shown via figures 7-8.

The impact on the surface is shown through the equivalent surface stress. Figures are correlating and they show that the kinematics, the kinetics and the residual stress distribution on the surface are correlating in a very evident way.

3.2.2 Pressure distribution design

Although analytical modeling gives deeper knowledge about the phenomenon involved in the physical modeling, it is based on different approximations and hypotheses. The mechanical loading applied by the tool on the workpiece surface is one of them. The best approach is the uses of a Hertzian pressure profile to model it. The procedure is fully predictive and it takes as input the maximum cutting forces during the milling operation. The force prediction model proposed by Altintas [36] is used here.

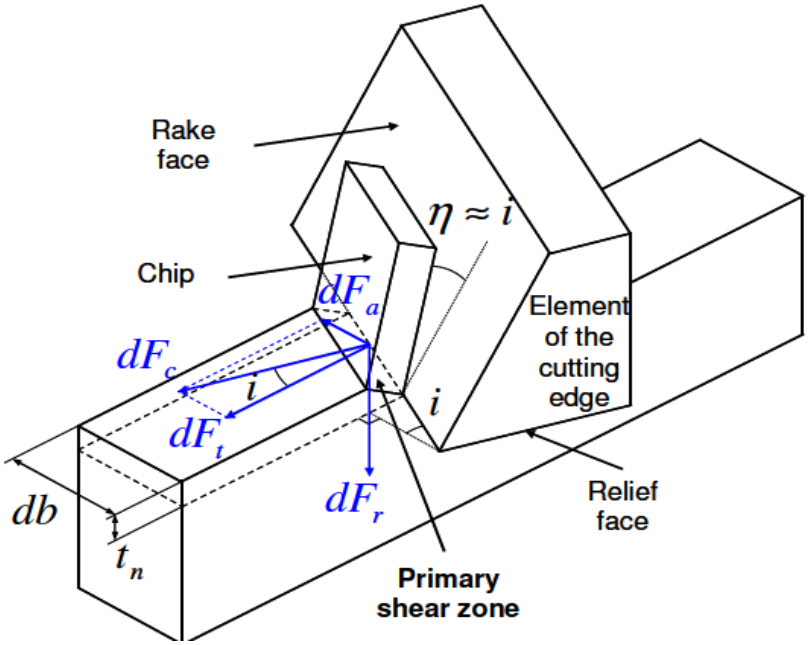
Rake face
Chip
$\eta \approx i$
dF_a
dF_c
i
dF_t
dF_r
i
Element of the cutting edge
Relief face
db
t_n
Primary shear zone

(a)

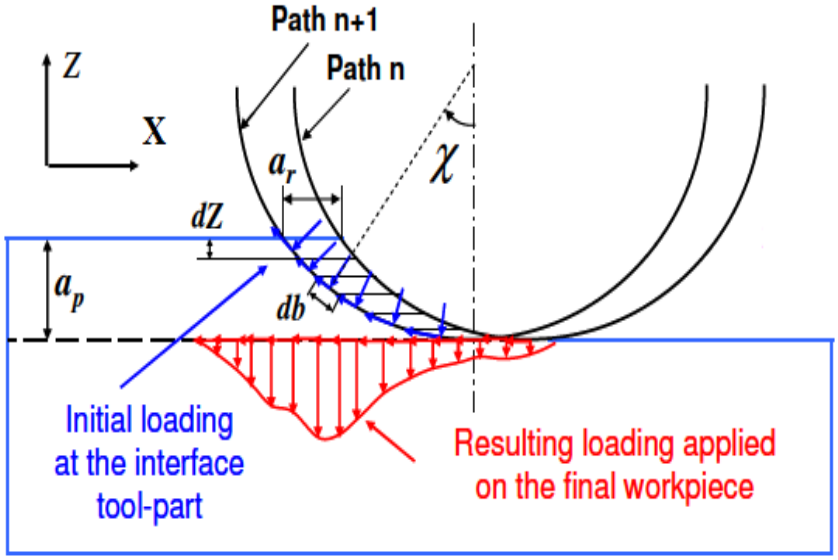
Path n+1
Path n
Z
X
a_r
χ
dZ
a_p
db
Initial loading at the interface tool-part
Resulting loading applied on the final workpiece

(b)

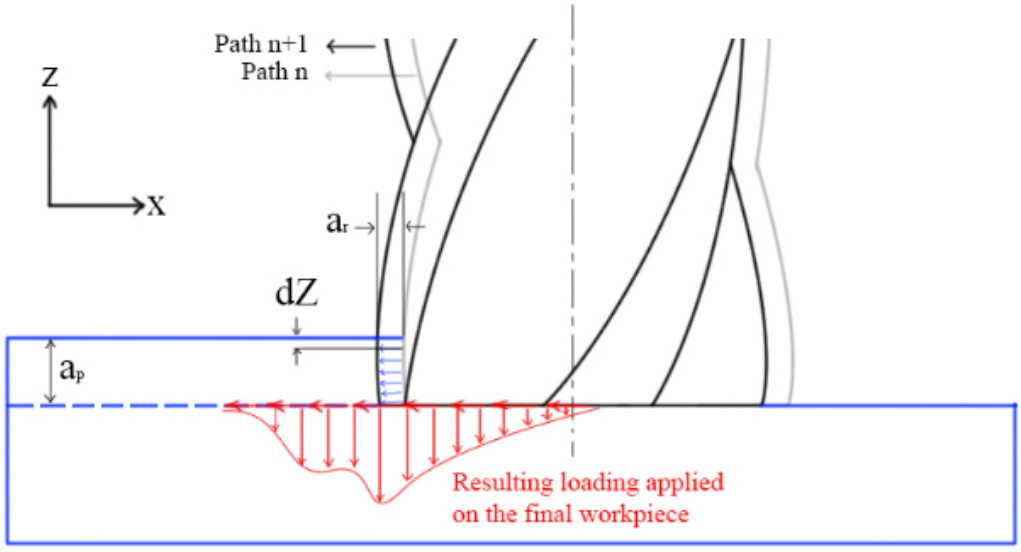

(c)

Figure 9: (a) Oblique cutting (b) Ballend mill pressure generation (c) Endmill pressure generation

Using the solution given by Hertz [35], the axial and radial pressure applied by the tool is designed. Figure and equation (3.2.2.1) explain the principle.

$$dP_r = \frac{2dF_r}{\pi a.db} \qquad (3.2.2.1)$$

$$dP_a = \frac{2dF_a}{\pi a.db}$$

Where $F_r\ and\ F_r$ are respectively the radial and the axial forces applied by the tool on the workpiece as shown in figure 9. Also, a, db are the half contact length and the width of the cut.

For the residual stress implementation, the stress generated by the pressure distribution is needed. Johnson [48] proposed an analytical solution for the components

$$\sigma_{xx}^{mechanical} = -\frac{2z}{\pi}\int_{-a}^{a}\left(\frac{p(s)(x-s)^2 + q(s)(x-s)^3}{((x-s)^2+z^2)^2}\right)ds$$

$$\sigma_{zz}^{mechanical} = -\frac{2z^3}{\pi}\int_{-a}^{a}\left(\frac{p(s) + q(s)(x-s)}{((x-s)^2+z^2)^2}\right)ds$$

$$\sigma_{xz}^{mechanical} = -\frac{2z^2}{\pi}\int_{-a}^{a}\left(\frac{p(s)(x-s) + q(s)(x-s)^2}{((x-s)^2+z^2)^2}\right)ds$$

$Where\ p$ is the normal force distribution, and q the tangential force distribution calculated from equation (3.2.2.1) x, z are the distances from the contact point a half contact length and s the integration variable. This procedure is necessary to implement the stress generated by the tool. Experimental measure on the tool is necessary. SEM (Scanning electron microscope) was used in the research to estimate the half contact length.

3.2.3 Microstructure consideration

The nature of the simulated material is very critical in the accuracy of the residual stress prediction. Materials are composed of grains. Every grain has different elastic-plastic behaviour due to the different chemical constitution of the material and the crystal orientation. The size of each grain is changing depending on the processing history of the material. In this model, a hypothesis is made about the nature of the material. In the modeling and simulation work, materials are considered isotropic. However during the validation part, all the experiments have been done on orthotropic materials. Therefore, every grain develops a different residual stress accumulation. However, it is proved that the residual stress is directly connected to the microstructure of a material.

A new approach based on experimental analysis allows us to determine the error coefficient between the macro residual stress and the residual stress of each grain. The experimental work is based on material characterization, X-ray diffraction measurement and calibration. The understanding of the range difference of the produced residual stress between all the grains is important to determine the error factor. This will help a lot when comparing results with simulations. The proposed process is described in figure.10 below.

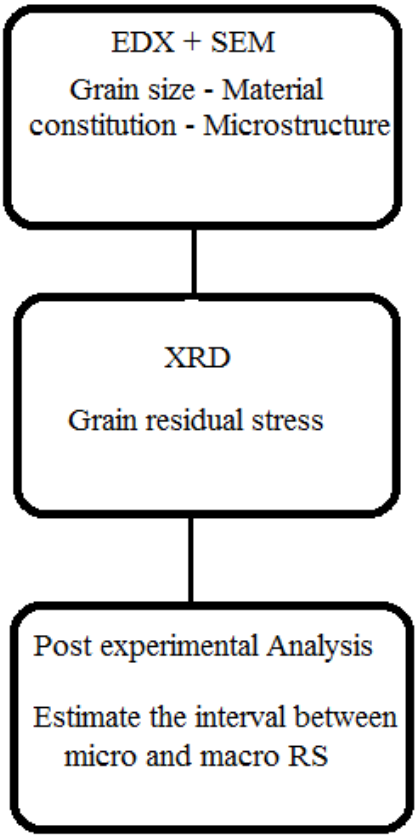

Figure 10: Residual stress investigation methodology

The second aspect of the methodology is connected to the simulation part. As described above the residual stress generated depends on the cutter location, therefore, the final residual stress distribution will be related directly to the kinematics of the milling process. In this work only three point of the cutting procedure as described in figure 7-8. The simulation is going to be done for three different forces intensities and therefore pressure distributions.

3.3 Analytical model for residual stress

In this part of the thesis the theoretical approach to build the analytical model for the prediction of residual stress is presented. The steps will be explained going from the force prediction model to the residual stress prediction.

3.3. 1 Elastic-Plastic model

The constitutive material behaviour is a critical part of this work. In fact metal cutting operation generates elastic-plastic behaviour of the material. Literature offers a large spectrum of existing models to simulate the material deformation during the cutting parameters. In this work, a comparative study has been made to chose the most appropriate model to simulate the residual stress in the near surface of a machined part. For this many parameters have to be compared.

During the milling operation, the material removal process generates very intense plastic deformation and large strains and strain–rates. Further, the literature noticed that residual stresses are mainly located in the near surface. Therefore, the first 50 μm are to be

investigated. During all this work, the thermal effect on residual stress is neglected. Only mechanical loading is investigated, thus, there is no need for a thermo-elastic-plastic model. The use of Johnson Cook [50] model was excluded. After the benchmark, the use of Drucker-Prager model was decided. It is the closest model to the requirements the model. The Drucker-Prager material model is non-linear. Therefore, it is integrated with an iterative numerical scheme. In this thesis a simple Newton-Raphson scheme is used in the material subroutine. Return mapping algorithm used for the numerical resolution of the non-linear equations of the model. Details are presented bellow.

1. Compute $\boldsymbol{\sigma}^{\mathrm{tr}}$ and $\varepsilon^{\mathrm{e\ tr}}$.
2. Spectrally decompose $\boldsymbol{\sigma}^{\mathrm{tr}}$ and $\varepsilon^{\mathrm{e\ tr}}$
3. Check if $F \leq 0$
   (a) If yes, the material is still in the elastic region. Set the following variables, then exit the loop.
   $\boldsymbol{\sigma} = \boldsymbol{\sigma}^{\mathrm{tr}}$, $\boldsymbol{\kappa}_{n+1} = \boldsymbol{\kappa}_n$, $\lambda_{n+1} = \lambda_n$
   (b) If no, the material is in yielding. Continue to the next step.
4. Newton-Raphson iterations on to converge on a solution of $\boldsymbol{x}$.
5. Set $\lambda_{n+1} = \lambda_n + \Delta\lambda$
6. Calculate the consistent tangent operator for the global iteration loop.
7. Compute the final stresses in original coordinate system where the values σ_A^{tr} are the values of $\boldsymbol{\sigma}$ from $\boldsymbol{x}$, and the directions m_A^{tr} are the same spectral directions found in Step 2.

Figure 11: Return mapping algorithm for Drucker-Prager

Where σ^{tr} and ε^{etr} are the spectral stress and strain,

Pressure-dependent materials require advanced material models to predict yielding. A commonly used yield criterion is the two-invariant Mohr-Coulomb model presented bellow, where the σ_i's correspond to principal stresses, c is the cohesion, and φ is the friction angle. On the π-plane, the Mohr-Coulomb yield surface is similar to a distorted Tresca yield surface with lower tensile strengths and higher compressive strengths.

$$F(\sigma_1, \sigma_2, \sigma_3, K) = |\sigma_A - \sigma_B| - K \leq 0 \tag{3.3.1}$$

$$K = 2c\cos\varphi - (\sigma_A + \sigma_B)\sin\varphi \tag{3.3.2}$$

This work will derive the Drucker-Prager smoothed approximation to the Mohr-Coulomb plasticity model, including a detailed account of the integration algorithm and numerical implementation. The Drucker-Prager yield surface and plastic potential are defined by

$$\begin{aligned} F &= q + \alpha p \\ G &= q + \beta p \end{aligned} \tag{3.3.3}$$

The hardening laws are given by

$$\begin{cases} \hat{\alpha}(\lambda) = \alpha_0 + \frac{2\alpha\sqrt{k\lambda}}{k+\lambda} \\ \hat{\beta}(\lambda) = \hat{\alpha}(\lambda) - \beta_0 \end{cases} \tag{3.3.4}$$

All the necessary derivatives for the integration procedure described in the algorithm are included here. Material constants are α, k, α_0, β_0. Additionally, K is the bulk modulus, v is the Poisson's ratio, E is the Young's modulus, and μ is one of the Lame constants. λ in the cumulative plastic multiplier.

$$F = q + \alpha p = \sqrt{\frac{3}{2}}\|\sigma - p\delta\| + \alpha p \tag{3.3.5}$$

Derivation for all the necessary functions are presented:

$$\frac{\partial F}{\partial \sigma} = \frac{\alpha}{3} + \frac{1}{2\sqrt{\sigma_1^2 + \sigma_2^2 - \sigma_2\sigma_3 + \sigma_3^2 - \sigma_1(\sigma_2 + \sigma_3)}} \begin{bmatrix} 2\sigma_1 - \sigma_2 - \sigma_3 \\ -\sigma_1 + 2\sigma_3 - \sigma_3 \\ -\sigma_1 - \sigma_2 + 2\sigma_3 \end{bmatrix}$$

$$\frac{\partial F}{\partial K} = \begin{bmatrix} \frac{\partial F}{\partial \alpha} \\ \frac{\partial F}{\partial \beta} \end{bmatrix} = \begin{bmatrix} \frac{1}{3}(\sigma_1 + \sigma_2 + \sigma_3) \\ 0 \end{bmatrix}$$

$$G = q + \beta p = \sqrt{\frac{3}{2}} \|\sigma - p\delta\| + \beta p$$

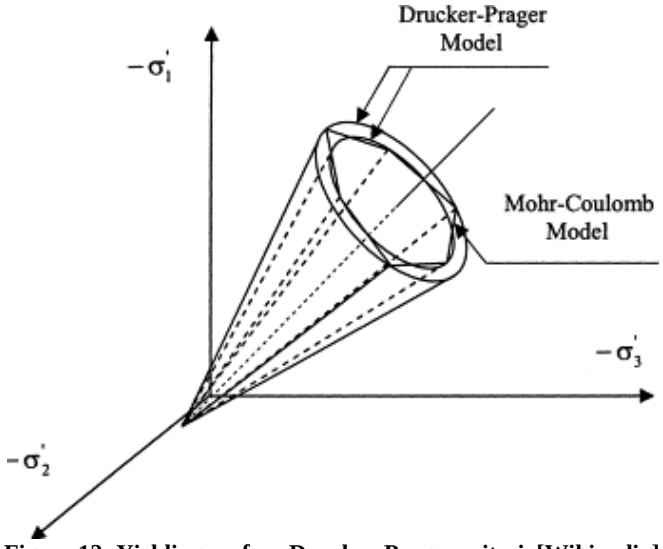

Figure 12: Yielding surface Drucker-Prager criteria[Wikipedia]

More details about the implementation of the model are given bellow.

$$g = \frac{\partial G}{\partial \sigma} = \frac{\beta}{3} + \frac{1}{2\sqrt{\sigma_1^2 + \sigma_2^2 - \sigma_2\sigma_3 + \sigma_3^2 - \sigma_1(\sigma_2 + \sigma_3)}} \begin{bmatrix} 2\sigma_1 - \sigma_2 - \sigma_3 \\ -\sigma_1 + 2\sigma_3 - \sigma_3 \\ -\sigma_1 - \sigma_2 + 2\sigma_3 \end{bmatrix}$$

$$\frac{\partial G}{\partial \sigma} = A \begin{bmatrix} (\sigma_2 - \sigma_3)^2 & (\sigma_1 - \sigma_3)(\sigma_3 - \sigma_2) & (\sigma_1 - \sigma_2)(\sigma_2 - \sigma_3) \\ (\sigma_1 - \sigma_3)(\sigma_3 - \sigma_2) & (\sigma_1 - \sigma_3)^2 & (\sigma_1 - \sigma_2)(\sigma_3 - \sigma_1) \\ (\sigma_1 - \sigma_2)(\sigma_2 - \sigma_3) & (\sigma_1 - \sigma_2)(\sigma_3 - \sigma_1) & (\sigma_1 - \sigma_2)^2 \end{bmatrix}$$

$$A = \frac{3}{4(\sigma_1 + \sigma_2 - \sigma_2\sigma_3 + \sigma_3^2 - \sigma_1(\sigma_2 + \sigma_3))^{3/2}}$$

$$\frac{\partial g}{\partial K} = \frac{1}{3}\begin{bmatrix} 0 & 1 \\ 0 & 1 \\ 0 & 1 \end{bmatrix}$$

$$K(\lambda) = \begin{bmatrix} \alpha(\lambda) \\ \beta(\lambda) \end{bmatrix} = \begin{bmatrix} \alpha_0 + \dfrac{2\alpha\sqrt{k\lambda}}{k+\lambda} \\ \alpha - \beta_0 \end{bmatrix}$$

$$h = \frac{\partial K}{\partial \lambda} = \frac{\alpha k(k-\lambda)}{\sqrt{k\lambda}(k+\lambda)^2}\begin{bmatrix} 1 \\ 1 \end{bmatrix}$$

$$\frac{\partial h}{\partial \sigma} = \begin{bmatrix} 0 & 0 & 0 \\ 0 & 0 & 0 \end{bmatrix}$$

$$\frac{\partial h}{\partial \lambda} = -\frac{\alpha k^2(k^2 + 6k\lambda - 3\lambda^2)}{2(k\lambda)^{3/2}(k+\lambda)^3}\begin{bmatrix} 1 \\ 1 \end{bmatrix}$$

3.3.2 Analytical solution

On the contrary to the orthogonal cutting where the kinematics is defined and simple, the modeling of residual stresses in the oblique cutting is a difficult task. Milling differs from orthogonal cutting in several key areas. In milling, the relative orientation between the cutter tip and the newly generated surface varies during the cut. An additional result of the cutter rotation is the uncut chip thickness during chip formation. Furthermore, depending on the geometry of the milling cutter, the surface being generated can be attributed to different parts of the cutter. These factors can affect the residual stresses generated from milling.

The second difficulty faced during the modeling is the geometrical aspect of the concerned workpiece. In fact, one may think that residual stresses are depending only on the machining force distribution and material properties. However, a geometrical aspect of the part is very critical. This geometrical aspect can be compared to a boundary conditions effect on the FEM simulations. Chiu [43] was the first to derive the equation of the residual stresses in a cubic inclusion. The utilisation of the Eshelby [47] inclusion was necessary for a more accurate modeling. During all the modeling the hypothesis of semi-infinite body is used. The adaptation of the inclusion theory made by Eshelby [47] is therefore necessary. In the following, equations of residual stress are presented and they were inspired by the previous work of Chiu [43].

The last important problem of the modeling is the material aspect. Most of the used materials in the industry are not isotropic. Many grains are existing and make the residual stress change from a grain to another. During the simulation work the material properties introduced are based on the hypothesis of an isotropic material. Therefore, a difference between the experimental results and the simulation is predicable. In fact, there are two solutions for this problem; the first one is to find experimentally a correcting factor between the X-rays diffraction results and the simulations. This is the solution that is mainly used in the industry. The second approach is to make many simulations using different materials properties corresponding to each grain and superpose them. This technique gives accurate results, however the computing time is lonrger and it is technically not applicable.

Near to the surface, a rectangular inclusion is supposed. The plastic field P_f is defined as:

$$P_f = \begin{pmatrix} \frac{-\varepsilon^p}{2} & 0 & 0 \\ 0 & \frac{-\varepsilon^p}{2} & 0 \\ 0 & 0 & \varepsilon^p \end{pmatrix} \tag{3.4.1}$$

$$\varepsilon^p \; is \; the \; plastic \; strain$$

The case of a cubic inclusion containing a plastic deformation has been studied by Lin [37]. Here we are interested about the residual stress field in parallelepiped inclusion. Therefore, the problem can be formulated mathematically as:

$$div\ \sigma = 0$$

$$\sigma = L{:}\,(\varepsilon - \varepsilon^p) \tag{3.4.2}$$

$$\sigma.\vec{n} = 0$$

With: ε defining the zero displacement fields at the infinite. Let's consider that

$$\sigma = -2\mu\varepsilon^p + \Delta\sigma$$
$$div\ \Delta\sigma = 2\mu\ div\ \varepsilon^p \tag{3.4.3}$$

Then the problem becomes determining the stress profile induced by the volume force on the volume Ω

$$2\mu\ div\ \varepsilon^p$$

And on the surface (3.4.4)

$$2\mu\varepsilon^p.\vec{n}$$

However, since ε^p is constant on the volume Ω only surface forces are needed. This problem can be easily solved since the calculus of the stress profile generated by a point located force somewhere in a semi-infinite body is known. This problem was introduced and solved by Mandlin [38]. This problem is adapted for the case of forces generated by milling operations.

Suppose that the tool is generating a force $\vec{F}$ (Fx, Fy, Fz) on the part. The force is considered here as point applied force. It is applied at the point (0, 0, d). Here d is the depth of cut. It is demonstrated in [37] that the stress field can be written as:

$$\sigma_{xx} = \frac{\mu}{2(1-\nu)}\left\{2(1-\nu)\frac{\partial B_x}{\partial x} - \frac{\partial^2 B_x}{\partial x^2} + 2\nu\frac{\partial B_y}{\partial y} - y\frac{\partial^2 B_y}{\partial x^2} + 2\nu\frac{\partial B_z}{\partial z} - z\frac{\partial^2 B_z}{\partial x^2} - \frac{\partial^2 \beta}{\partial x^2}\right\}$$

$$\sigma_{yy} = \frac{\mu}{2(1-\nu)}\left\{2(1-\nu)\frac{\partial B_y}{\partial y} - \frac{\partial^2 B_y}{\partial y^2} + 2\nu\frac{\partial B_x}{\partial x} - x\frac{\partial^2 B_x}{\partial y^2} + 2\nu\frac{\partial B_z}{\partial z} - z\frac{\partial^2 B_z}{\partial y^2} - \frac{\partial^2 \beta}{\partial y^2}\right\}$$

$$\sigma_{zz} = \frac{\mu}{2(1-\nu)}\left\{2(1-\nu)\frac{\partial B_z}{\partial z} - z\frac{\partial^2 B_z}{\partial z^2} + 2\nu\frac{\partial B_x}{\partial x} - x\frac{\partial^2 B_x}{\partial z^2} + 2\nu\frac{\partial B_y}{\partial y} - y\frac{\partial^2 B_y}{\partial z^2} - \frac{\partial^2 \beta}{\partial z^2}\right\} \quad (3.4.5)$$

$$\sigma_{xy} = \frac{\mu}{2(1-\nu)}\left\{(1-2\nu)\left(\frac{\partial B_x}{\partial y} + \frac{\partial B_y}{\partial x}\right) - x\frac{\partial^2 B_x}{\partial x \partial y} - y\frac{\partial^2 B_y}{\partial x \partial y} - z\frac{\partial^2 B_z}{\partial x \partial y} - \frac{\partial^2 \beta}{\partial x \partial y}\right\}$$

$$\sigma_{xz} = \frac{\mu}{2(1-\nu)}\left\{(1-2\nu)\left(\frac{\partial B_x}{\partial z} + \frac{\partial B_z}{\partial x}\right) - x\frac{\partial^2 B_x}{\partial x \partial z} - y\frac{\partial^2 B_y}{\partial x \partial z} - z\frac{\partial^2 B_z}{\partial y \partial z} - \frac{\partial^2 \beta}{\partial x \partial z}\right\}$$

$$\sigma_{yz} = \frac{\mu}{2(1-\nu)}\left\{(1-2\nu)\left(\frac{\partial B_y}{\partial z} + \frac{\partial B_z}{\partial y}\right) - x\frac{\partial^2 B_x}{\partial y \partial z} - y\frac{\partial^2 B_y}{\partial y \partial z} - z\frac{\partial^2 B_z}{\partial y \partial z} - \frac{\partial^2 \beta}{\partial y \partial z}\right\}$$

where $\overrightarrow{B}$ and β are Papkovish functions given as:

$$B_x = \frac{F_x}{4\pi\mu}\left(\frac{1}{R_1} - \frac{1}{R_2}\right)$$

$$B_y = \frac{F_y}{4\pi\mu}\left(\frac{1}{R_1} + \frac{1}{R_2}\right)$$

$$B_z = \frac{(xF_x + yF_y)}{2\pi\mu}\left[\frac{(1-2\nu)}{R_2(R_2+z+d)} - \frac{D}{R_2^3}\right] + \frac{F_z}{4\pi\mu}\left[\frac{1}{R_1} + \frac{3-4\nu}{R_2} + \frac{2d(z+d)}{R_2^3}\right]$$

$$\beta = \frac{(xF_x + yF_y)}{2\pi\mu}\left[\frac{\nu(1-2\nu)}{R_2} - \frac{(1-2\nu)z}{R_2(R_2+z+d)} - (1-\nu)(1-2\nu)\frac{(R_2+z+d)}{R_2(R_2+z+d)}\right] + \frac{F_z}{4\pi\mu}\left[4(1-\nu)(1-2\nu)\log(R_2+z+d) - \frac{d}{R_1} - \frac{(3-4\nu)d}{R_2}\right] \quad (3.4.6)$$

with

$$R_1 = \sqrt{x^2 + y^2 + (z-d)^2}$$

$$R_2 = \sqrt{x^2 + y^2 + (z+d)^2}$$

From these equations, it is easy to derive the stress tensor$\Delta\sigma$. As an example, the way to find $\Delta\sigma_{xx}$ is shown, the other stresses can be found following the same technique. In fact $\Delta\sigma_{xx}$ is the sum of six terms, each of term is the results of derivation on each face of the rectangular volume. Therefore $\Delta\sigma_{xx}$ can be written:

$$\Delta\sigma_{xx} = C_{x=-\frac{a}{2}} + C_{x=\frac{a}{2}} + C_{y=-\frac{b}{2}} + C_{y=\frac{b}{2}} + C_{z=0} + C_{z=d} \quad (3.4.7)$$

$C_{f(x,y,z)=0}$ is the integration on the surface of the rectangular volume included in the surface with the equation $f(x,y,z)=0$. After doing the calculus on a formal mathematical solver. the following analytical solution is found:

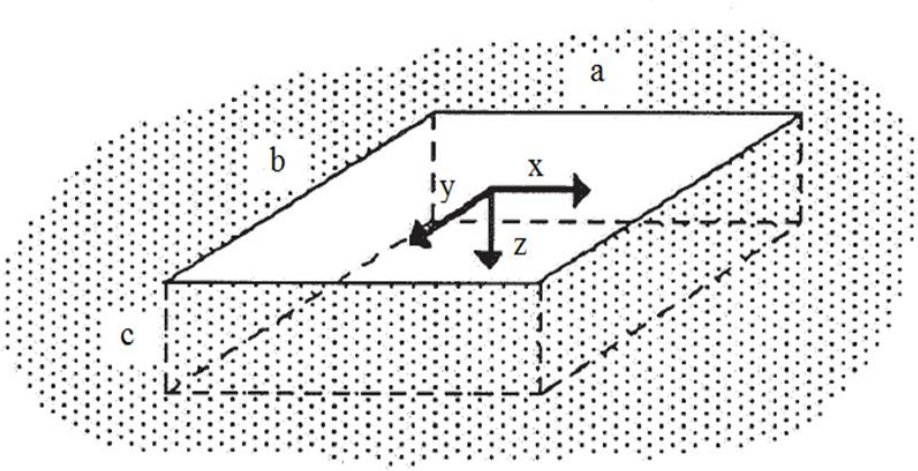

Figure 13: Parallelepiped inclusion

Geometrical parameters are defined as follows; figure 13 shows the physical model

$x_1 = x - \frac{a}{2}$, $x_2 = x + \frac{a}{2}$, $y_1 = y - \frac{b}{2}$, $y_2 = y + \frac{b}{2}$, $z_1 = z - d$, $z_2 = z + d$,

$$r_{ijk} = \sqrt{x_i^2 + y_j^2 + z_k^2} \quad i,j,k = 1 \; or \; 2$$

$$r_{ij0} = \sqrt{x_i^2 + y_j^2 + z_0^2} \quad i,j = 1 \; or \; 2$$

3.3.3 Relaxation procedure

When the unloading is complete, i.e. mechanical and thermal loading no longer exists (cutting forces are too far away and the temperature of the point of interest has decreased to ambient temperature), a certain distribution of stresses and strains is obtained. This distribution, however, does not correspond to the actual residual stress and strain distribution σ_{ij}^r and ε_{ij}^r respectively, due to the stress invariant assumption [42]. It is expected that:

(1) $\epsilon_{xx}^r = 0$ (to ensure planarity of the surface after deformation), and

(2) $\sigma_{zz}^r = \sigma_{xz}^r = 0$ (to retain equilibrium and a traction-free surface). Therefore, the following stress and strain increments are enforced:

$$\begin{aligned} d\epsilon_{xx} &= -\frac{\epsilon_{xx}}{M} \\ d\sigma_{zz} &= -\frac{\sigma_{zz}}{M} \\ d\sigma_{xz} &= -\frac{\sigma_{xz}}{M} \end{aligned} \qquad (3.6.1)$$

After M steps, ϵ_{xx} , σ_{zz} and σ_{xz} are reduced to zero. In this work, the relaxation is supposed to be elastic. ϵ_{xx} , σ_{zz} and σ_{xz} are token as output from the elastic plastic model

after the yielding occurs. This method was used in [5] and shows very reliable results. The same procedure is used in FEM simulation of residual stress; however the computing time takes very large time comparing to the analytical solution. At the end of the relaxation procedure, the resulting σ_{xx} and σ_{yy} are set equal to the corresponding residual stress $\sigma_{xx}^{r}\ and\ \sigma_{yy}^{r}$ components and respectively.

3.4 Deflection modeling

The aim of this work is to link the residual stress accumulated by a workpiece and the possible deflection of the part. Rather than residual distribution, the deflection or geometrical accuracy of a part is important. No analytical model was reported in the literature. Many industries are using FEM with long computational time to generate the geometrical error. In this part, a prediction model of the deflection in the case of the milling of a very thin part is proposed. The machined part should have a very basic geometry. In fact, due to the analytical nature of the model, introducing complex geometries is mathematically a very difficult task. Therefore, here the part is a semi infinite body, elastic plastic and with a sharp geometry. A rectangular volume is studied here.

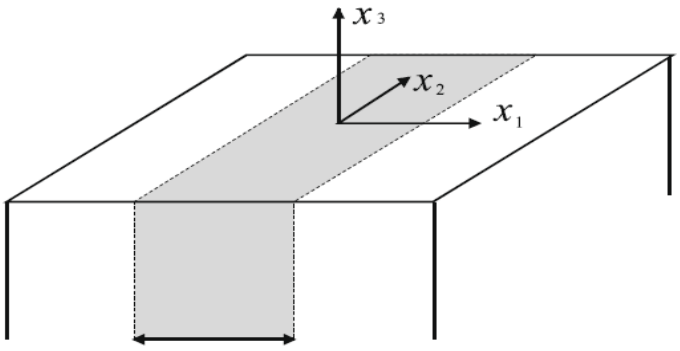

Figure 14: Half-space model

Denote the total displacement in a half-place by u_i. Consequently, total strain is

$$\varepsilon_{ij} = \frac{1}{2}.\left(\frac{\partial u_i}{\partial x_j} + \frac{\partial u_j}{\partial x_i}\right) \tag{3.7.1}$$

$$\varepsilon_{ij} - \varepsilon_{ij}{}^{*}: elastic\ strain$$

For the analytical model, the equations are solved within a half-space. $\varepsilon_{ij}{}^{*}$: is the relaxed plastic strain, and ε_{ij} is the total strain called eigenstrain. Therefore, the constitutive law is written as:

$$\sigma_{ij} = \frac{\mathrm{E}}{1+\nu}.\left((\varepsilon_{ij} - \varepsilon_{ij}{}^{*}) + \frac{\nu}{1+2\nu}(\varepsilon_{kk} - \varepsilon_{kk}{}^{*})\delta_{ij}\right) \tag{3.7.2}$$

E and ν are Young modulus and Poisson's coefficient respectively. The stresses satisfy the equilibrium equation

$$\frac{\partial \sigma_{ij}}{\partial x_j} = 0 \tag{3.7.3}$$

The following boundary conditions can be introduced to represent the free surface:

$$x_3 = 0\ and\ \sigma_{i3} = 0 \tag{3.7.4}$$

The symmetry of the residual stress implies:

$$u_i = u_i(x_1, x_3) \tag{3.7.5}$$

Therefore, the strain matrices M_e can be written

$$M_e = \begin{pmatrix} \frac{\partial u_1}{\partial x_1} & \frac{1}{2}.\left(\frac{\partial u_2}{\partial x_1}\right) & \frac{1}{2}.\left(\frac{\partial u_1}{\partial x_3}+\frac{\partial u_3}{\partial x_1}\right) \\ \frac{1}{2}.\left(\frac{\partial u_2}{\partial x_1}\right) & 0 & \frac{1}{2}.\left(\frac{\partial u_2}{\partial x_3}\right) \\ \frac{1}{2}.\left(\frac{\partial u_1}{\partial x_3}+\frac{\partial u_3}{\partial x_1}\right) & \frac{1}{2}.\left(\frac{\partial u_2}{\partial x_3}\right) & \frac{\partial u_3}{\partial x_3} \end{pmatrix} \quad (3.7.6)$$

Therefore the stresses on the surface can be estimated using the generalized Hook law as

$$\begin{aligned}
\sigma_{11} &= \frac{E}{(1+\nu).(1-2\nu)}\left[(1-\nu).\frac{\partial u_1}{\partial x_1}+\nu.\frac{\partial u_3}{\partial x_3}-(1-\nu).{\varepsilon_{11}}^* \right. \\
&\qquad \left. -\nu({\varepsilon_{11}}^*+{\varepsilon_{33}}^*)\right] \\
\sigma_{22} &= \frac{E}{(1+\nu).(1-2\nu)}\left[(\nu).\frac{\partial u_1}{\partial x_1}+\nu.\frac{\partial u_3}{\partial x_3}-(1-\nu).{\varepsilon_{22}}^*-\nu({\varepsilon_{11}}^* \right. \\
&\qquad \left. +{\varepsilon_{33}}^*)\right] \\
\sigma_{33} &= \frac{E}{(1+\nu).(1-\nu)}\left[(\nu).\frac{\partial u_1}{\partial x_1}+(1-\nu).\frac{\partial u_3}{\partial x_3}-(1-\nu).{\varepsilon_{22}}^* \right. \\
&\qquad \left. -\nu({\varepsilon_{11}}^*+{\varepsilon_{33}}^*)\right] \\
\sigma_{12} &= \frac{E}{2.(1+\nu)}\left[\frac{\partial u_2}{\partial x_1}-\ 2.{\varepsilon_{12}}^*\right] \\
\sigma_{13} &= \frac{E}{2.(1-\nu)}\left[\frac{\partial u_3}{\partial x_1}+\frac{\partial u_1}{\partial x_3}-\ 2.{\varepsilon_{13}}^*\right] \\
\sigma_{23} &= \frac{E}{2.(1+\nu)}\left[\frac{\partial u_2}{\partial x_3}-\ 2.{\varepsilon_{23}}^*\right]
\end{aligned} \quad (3.7.7)$$

The substitution of these equations into the equilibrium equations (1.3) gives:

$$
\begin{aligned}
&2.(1-\nu).\frac{\partial^2 u_1}{\partial {x_1}^2}+(1-2.\nu).\frac{\partial^2 u_1}{\partial {x_3}^2}+\frac{\partial^2 u_3}{\partial x_1.\partial x_3}\\
&\qquad=2.(1-\nu).\left(\frac{\partial {\varepsilon_{11}}^*}{\partial x_1}+\frac{\partial {\varepsilon_{13}}^*}{\partial x_3}\right)+2.\nu(\frac{\partial {\varepsilon_{22}}^*}{\partial x_1}+\frac{\partial {\varepsilon_{33}}^*}{\partial x_3}\\
&\qquad-\frac{\partial {\varepsilon_{13}}^*}{\partial x_3})\\
&2.(1-\nu).\frac{\partial^2 u_3}{\partial {x_1}^2}+(1-2.\nu).\frac{\partial^2 u_3}{\partial {x_3}^2}+\frac{\partial^2 u_1}{\partial x_1.\partial x_3}\\
&\qquad=2.(1-\nu).\left(\frac{\partial {\varepsilon_{13}}^*}{\partial x_1}+\frac{\partial {\varepsilon_{33}}^*}{\partial x_3}\right)+2.\nu(\frac{\partial {\varepsilon_{11}}^*}{\partial x_3}+\frac{\partial {\varepsilon_{22}}^*}{\partial x_3}\\
&\qquad-\frac{\partial {\varepsilon_{13}}^*}{\partial x_1})\\
&\frac{\partial^2 u_2}{\partial {x_1}^2}+\frac{\partial^2 u_2}{\partial {x_3}^2}=2.\left(\frac{\partial {\varepsilon_{12}}^*}{\partial x_1}+\frac{\partial {\varepsilon_{23}}^*}{\partial x_3}\right)
\end{aligned}
\tag{3.7.8}
$$

By applying the boundary condition $x_3 = 0$, equation (3.7.8) becomes

$$
\begin{aligned}
&\frac{\partial u_1}{\partial x_3}+\frac{\partial u_3}{\partial x_1}=2.{\varepsilon_{13}}^*\\
&\frac{\partial u_2}{\partial x_3}+\frac{\partial u_3}{\partial x_2}=2.{\varepsilon_{23}}^*\\
&\nu.\frac{\partial u_1}{\partial x_1}+(1-\nu)\frac{\partial u_3}{\partial x_1}=\nu.{\varepsilon_{11}}^*+\nu.{\varepsilon_{22}}^*+(1-\nu).{\varepsilon_{33}}^*
\end{aligned}
\tag{3.7.9}
$$

During the milling operation, the tool is moving following a cutting direction, therefore, the plastic deformation in each point is affecting the entire surface. For this, the displacement of each point of the workpiece surface is the result of the accumulation of the force action on a point A and the effect of this force on another point C on the same surface of the workpiece as introduced by [38] and illustrated by Figure.15.

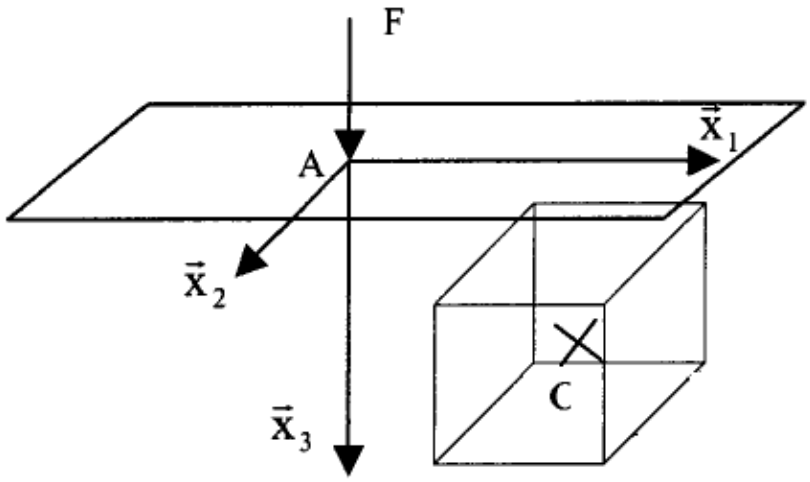

Figure 15: Effect of a force on the whole body [38]

For this, the Green's function is taken into account for this event, and we consider an elastic body in an equilibrium state with two forces acting on it, the traction over the surface area and the body forces act on a point unit volume, therefore

$$C_{ijkl}.u_{kl} + b_j = 0, \tag{3.7.10}$$

As explained before, the workpiece is considered as an infinite homogenous body. The Green's function will help to contract the equation for the displacement field in response to virtual forces applied inside the body that represent the residual stress. The residual stress is the stress supported by the body in a fixed reference configuration in absence of external forces. Thus the residual stress T satisfies the equilibrium equation

$$\nabla.T = 0$$

$$T = T^T$$

In the boundary of the body ∂B with outward unit normal n, the zero traction condition apply (3.7.11)

$$T.n = 0$$

For the set of virtual forces F_j induced by the residual stress, the gradient of the generated displacement can be defined as

$$u_{i,m} = G_{ij,m}(x - x')F_j \tag{3.7.12}$$

Therefore,

$$C_{kpim}G_{ijmp}(x - x') + \delta_{jk}\delta(x - x') = 0, \tag{3.7.13}$$

Equation (3.7.14) is equivalent to (3.7.10) when the body force is a delta function:

$$b_k = \delta_{jk}\delta(x - x') \tag{3.7.14}$$

The equation (3.7.14) can be solved using Fourier transformation. The elastic Green's function $g_{km}(k)$ is related to the Green's function as

$$g_{ij}(k) = \int_{-\infty}^{\infty} e^{ikx} G_{ij}\,(x)\,dx$$

$$G_{ij}(x) = \frac{1}{(2\pi)^3} \int_{-\infty}^{\infty} e^{-ikx} g_{ij}\,(k)\,dk \tag{3.7.15}$$

These governing equations for the surface displacement can be written in a discrete way similar to what Chui [43, 44] proposed. The volume where the eigenstrain is not equal to zero Ω is divided into N elements. The displacement generated by those N elements can be written

$$u(A) = 2.\mu \sum_{n=1}^{N} \int_{\Omega} \varepsilon_{ij,n}{}^{p}(M) \,.\, \varepsilon_{ij,n}{}^{p}(A)\,d\Omega \tag{3.7.16}$$

$$u(A) = 2.\mu \sum_{n=1}^{N} \int_{\Omega} \varepsilon_{ij,n}{}^{p}(M) \,.\, \varepsilon_{ij,n}{}^{p}(A)\, d\Omega = \sum_{n=1}^{N} \varepsilon_{ij,n}{}^{p}(M) \,.\, D_{ij}$$

$$with \tag{3.7.17}$$

$$K_{ij} = \mu. \iiint \left(u_{ij}{}^{*} + u_{ji}{}^{*}\right) dx_1\, dx_2 dx_3$$

where A is the current point and M the integration point. This formula is calculating the strain at M generated by a unit normal load applied at A.

$$\begin{aligned} K_{ij} = {} & D_{ij}(a_1 + \Delta x_1, a_2 + \Delta x_2, a_3 + \Delta x_3) - D_{ij}(a_1 + \Delta x_1, a_2 + \\ & \Delta x_2, a_3 - \Delta x_3) - D_{ij}(a_1 + \Delta x_1, a_2 - \Delta x_2, a_3 + \Delta x_3) + \\ & D_{ij}(a_1 + \Delta x_1, a_2 - \Delta x_2, a_3 - \Delta x_3) - D_{ij}(a_1 - \Delta x_1, a_2 + \Delta x_2, a_3 + \\ & \Delta x_3) + D_{ij}(a_1 - \Delta x_1, a_2 + \Delta x_2, a_3 - \Delta x_3) + D_{ij}(a_1 - \Delta x_1, a_2 - \\ & \Delta x_2, a_3 + \Delta x_3) - D_{ij}(a_1 - \Delta x_1, a_2 - \Delta x_2, a_3 - \Delta x_3) \end{aligned} \tag{3.7.18}$$

The functions D can be integrated the following way:

$$\begin{aligned} D_{11}(x,y,z) &= \frac{1}{\pi}\left[-\nu \,\mathrm{x} \ln\,(y+R) - (1-2\nu)\mathrm{z}\tan^{-1}\,\left(\frac{y+z+R}{x}\right)\right] \\ D_{22}(x,y,z) &= \frac{1}{\pi}\left[-\nu \,\mathrm{y} \ln(x+R) - (1-2\nu)\mathrm{z}\tan^{-1}\,\left(\frac{y+z+R}{y}\right)\right] \\ D_{12}(x,y,z) &= \frac{1}{\pi}[-2\nu\,\mathrm{R} - (1-2\nu)\mathrm{z}\ln(\mathrm{z}+\mathrm{R})] \\ D_{13}(x,y,z) &= \frac{1}{\pi}\left[2\,\mathrm{x}\tan^{-1}\,\left(\frac{y+z+R}{x}\right) + \mathrm{y}\ln(z+R)\right] \\ D_{23}(x,y,z) &= \frac{1}{\pi}\left[2\,\mathrm{y}\tan^{-1}\,\left(\frac{y+z+R}{y}\right) + \mathrm{x}\ln(z+R)\right] \\ D_{33}(x,y,z) &= \frac{1}{\pi}\Big[2(1 \\ &\quad - \nu)\,(2\mathrm{z}\tan^{-1}\,\left(\frac{y+z+R}{z}\right) + xln(y+R) \\ &\quad + yln(x+R) - \frac{z}{2}\theta\Big] \end{aligned} \tag{3.7.19}$$

With

$$\theta = -2\ \tan^{-1}(\frac{xy}{zR})$$
$$R = \sqrt{(x^2 + y^2 + z^2)}$$

In this chapter, the governing equations used to model the generated deflection due to residual stresses were presented. An analytical solution to the part deflection has been introduced. Only simple geometries can be solved due to the analytical aspect. In the next chapter, the experimental work is going to be presented to validate the outputs of this chapter.

Chapter 4

EXPERIMENTAL METHODOLOGY & RESULTS

4.1 Introduction

Research around the residual stress induced by any process is very challenging. Different investigation techniques exist. There are two main categories for measuring the residual stress, destructive and non-destructive methods. Hole drilling technique was the most used in the past. The development of new products and process helped the emergence of new technologies such as x-ray, which give us the possibility to explore better the distribution of the residual stress in the near surface and the surface. However, it is very demanding concerning the knowledge and the information about the material. Different materials were used in the validation of this work. Other very new techniques have started being used in situ, such as ultrasound measurement. For more accurate modeling, the characterization of the materials used was necessary. EDX (Energy Dispersive X-ray) technology offers us an easy and fast way to analyze the material and to explore their behaviour before any testing or modeling. In this chapter, the experimental procedure and some theory behind the residual stress and material characterization is presented. The micro hardness test is also developed here for Steel. Details about the metrological process used to estimate the

deflection of the thin plate is explained. CMM (Coordinate Measures Machine) dispositive to explore the deformation of the thin plate is contained in this part. All the conclusions and comparative studies are presented in the next chapter.

4.2 Material characterization

This investigation work can be located is between two fields: material science and manufacturing technologies. Technically speaking, the fields are quite different however, they are extremely complementary. To understand better the work done in this thesis, knowledge on the material chemical composition and atomic structure is important. A characterization work has been done for all the used materials. In this part, the maximum details about Steel 2842, Al7050 and Titanium alloy are presented using an EDS.

Energy-dispersive x-ray spectroscopy (EDS or EDX) is an analytical technique used for the elemental analysis or chemical characterization of a sample. It relies on the investigation of an interaction of some source of x-ray excitation and a sample. Its characterization capabilities are due in large part to the fundamental principle that each element has a unique atomic structure allowing unique set of peaks on its x-ray spectrum. To stimulate the emission of characteristic x-rays from a specimen, a high-energy beam of charged particles such as electrons or protons, or a beam of x-rays, is focused into the sample being studied. At rest, an atom within the sample contains ground state (or unexcited) electrons in discrete energy levels or electron shells bound to the nucleus. The incident beam may excite an electron in an inner shell, ejecting it from the shell while creating an electron hole where the electron was. An electron from an outer, higher-energy shell then fills the hole, and the difference in energy between the higher-energy shell and the lower energy shell may be released in the form of an x-ray. The number and energy of the x-ray emitted from a specimen can be measured by an energy-dispersive spectrometer. As the energy of the x-

ray is characteristic of the difference in energy between the two shells, and of the atomic structure of the element from which they were emitted, this allows the elemental composition of the specimen to be measured.

An EDX (Energy dispersive X-ray) machine was used to quantify the amount of each chemical agent in the material. Machine is presented in the figure bellow. The results of the experiments are presented in Tab.1-4.

Figure 16: EDX (Energy Dispersive X-ray)

Steel 2842		
Formula	Z	Mass Concentration%
Fe	26	86,85
Cr	24	10,21
Mn	25	1,393
S	16	0,337
Ni	28	0,284
Si	14	0,248
Na	11	0,24
Mo	42	0,174
Cu	29	0,111
V	23	0,102
Cl	17	0,034
K	19	0,015

Table 1: Composition of Steel 2842

TiAl6v4		
Formula	Z	Mass Concentration%
Ti	22	85,06
Al	13	6,56
Fe	26	4,25
V	23	3,5
P	15	0,134
Si	14	0,11
Ca	20	0,106
Cu	29	0,101
Zn	30	0,086
Cl	17	0,046
S	16	0,028
K	19	0,016

Table 2: TiAl6V4 concentration results

Ti 4V		
Formula	Z	Mass Concentration%
Ti	22	87,4
Al	13	6,87
V	23	3,69
Fe	26	1,47
P	15	0,136
Ca	20	0,0876
Zn	30	0,0871
Mg	12	0,086
Cu	29	0,083
Si	14	0,034
Cl	17	0,024
Ni	28	0,018
S	16	0,017

Table 3: TiV6 concentration results

Al7050		
Formula	Z	Mass Concentration%
Al	13	88,29
Zn	30	5,025
Mg	12	2,14
Cu	29	1,959
Ti	22	1,62
P	15	0,474
Ca	20	0,182
Fe	26	0,122
Si	14	0,092
Zr	40	0,0376
S	16	0,034
Cr	24	0,012
Ag	47	0,011
Ni	28	0,005

Table 4: Al 7050 concentration results

4.3 Residual stress measurement

4.3.1 X-ray method

In measuring residual stress using x-ray diffraction (XRD), the strain in the crystal lattice is measured and the associated residual stress is determined from the elastic constants assuming a linear elastic distortion of the appropriate crystal lattice plane. Since x-rays impinge over an area on the sample, many grains and crystals will contribute to the measurement. The exact number is dependent on the grain size and beam geometry. Although the measurement is considered to be near surface, x-ray does penetrate some distance into the material: the penetration depth is dependent on the anode, material and angle of incidence. Hence the measured strain is essentially the average over a few microns depth under the surface of the specimen.

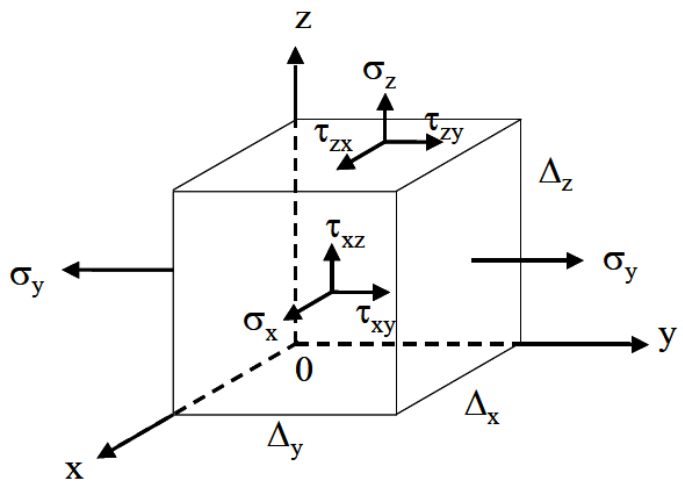

Figure 17: Normal and shear stress tensors

Consider a crystalline material made up of many crystals, where a crystal can be defined as a solid composed of atoms arranged in a pattern periodic in three dimensions. These

periodic planes of atoms can cause constructive and/or destructive interference patterns by diffraction. The nature of the interference depends on the inter-planar spacing d, and the wavelength of the incident radiation λ.

In 1912 W. L. Bragg (1890-1971) analyzed some results from experiments conducted by the German physicist von Laue (1879-1960), in which a crystal of copper sulphate was placed in the path of an X-ray beam. A photographic plate was arranged to record the presence of any diffracted beams and a pattern of spots was formed on the photographic plate. Bragg deduced an expression for the conditions necessary for diffraction to occur in such a constructive manner.

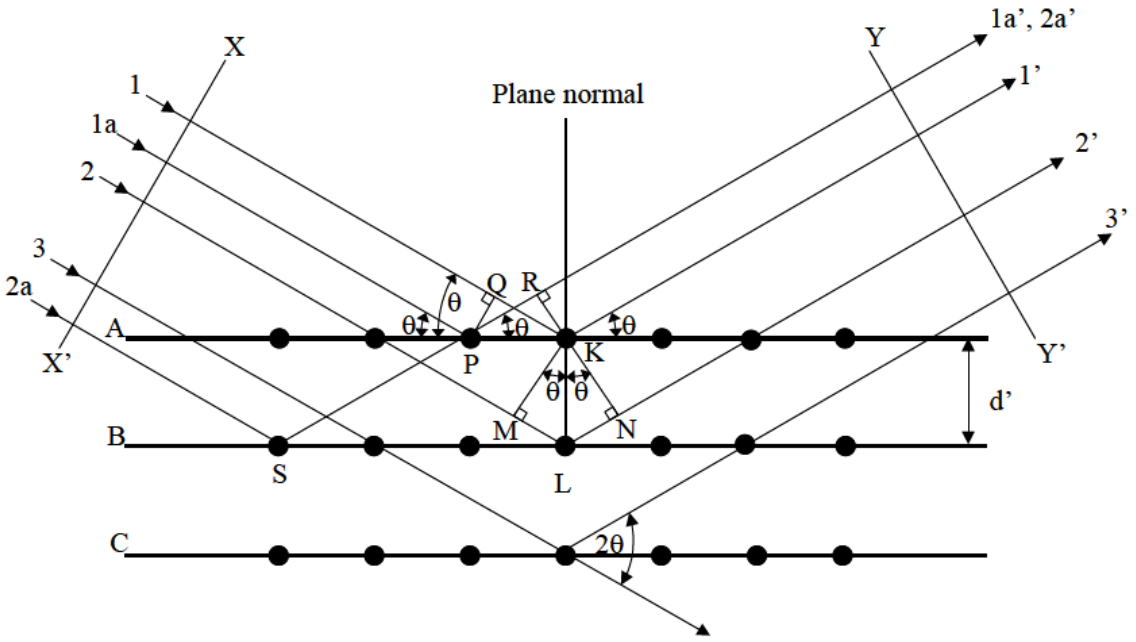

Figure 18: The diffraction principle of X-ray

Whilst it is very useful to know the strains within the material, it is more useful to know the engineering stresses that are linked to these strains. From Hooke's law we know that:

$$\sigma = E\varepsilon$$

It is also well known that a tensile force producing strain in the X-direction will produce not only a linear strain in that direction but also strains in the transverse directions. Assuming a state of plane stress exists, i.e. $\sigma_z = 0$, and that the stresses are biaxial, then the ratio of the transverse to longitudinal strains is Poisson's ratio, ν;

$$\varepsilon_x = \varepsilon_y = \varepsilon_z = -\nu\varepsilon_z = \frac{\nu\sigma_y}{E}$$

If we assume that at the surface of the material, where the X-ray measurement can be considered to have been made $\sigma_z = 0$ then:

$$\varepsilon_z = -\nu(\varepsilon_x + \varepsilon_y) = \frac{-\nu}{E}(\sigma_x + \sigma_y)$$

Thus:

$$\frac{d_n - d_0}{d_0} = \frac{-\nu}{E} + (\sigma_x + \sigma_y)$$

We wish to measure the single stress acting in some direction in the surface σ_φ. Elasticity theory for an isotropic solid shows that the strain along an inclined line

$$\varepsilon_{\phi\psi} = \frac{1+\nu}{E}\left(\sigma_1 \cos^2\phi + \sigma_2 \sin^2\phi\right)\sin^2\psi - \frac{\nu}{E}\left(\sigma_1 + \sigma_2\right)$$

If we consider the strains in terms of inter-planar spacing, and use the strains to evaluate the stresses, then it can be shown that:

$$\sigma_\phi = \frac{E}{(1+\nu)\sin^2\psi}\left(\frac{d_\psi - d_n}{d_n}\right)$$

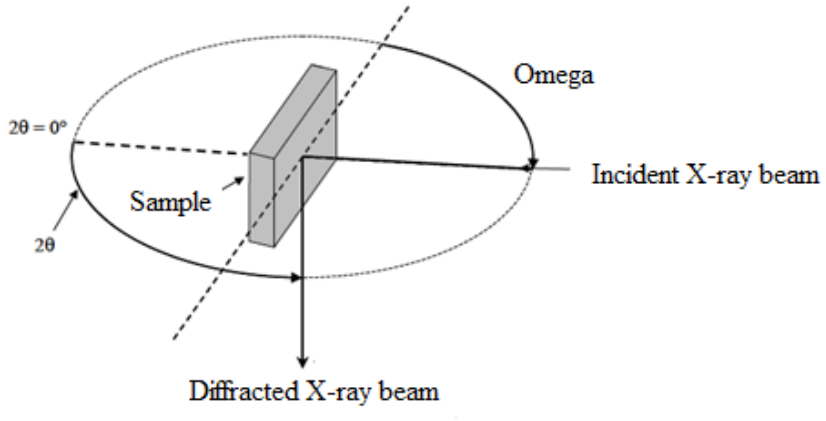

Figure 19: 2Ω setup for residual stress investigation

4.3.2 Experimental results

For the residual stress investigation, an x-ray D500 Siemens machine was used. Special precaution had to be made during the uses of an x-ray machine. The experimentation responsible was equipped by a dosimeter to estimate the quantity of radiation for security purposes.

Figure 20: D500 Siemens x-ray machine

To investigate the depth profile of residual stress, an electro polisher was used to eliminate layer by layer. Here also a specific setup has to be made to estimate the thickness eliminated by every electro polishing as shown in the following pictures.

The electro-polisher uses an intensity of 1.2 A to eliminate a layer of 10 μm. A special liquid is prepared for the operation. The average time is 40 s per layer.

Figure 21: Electro-polisher

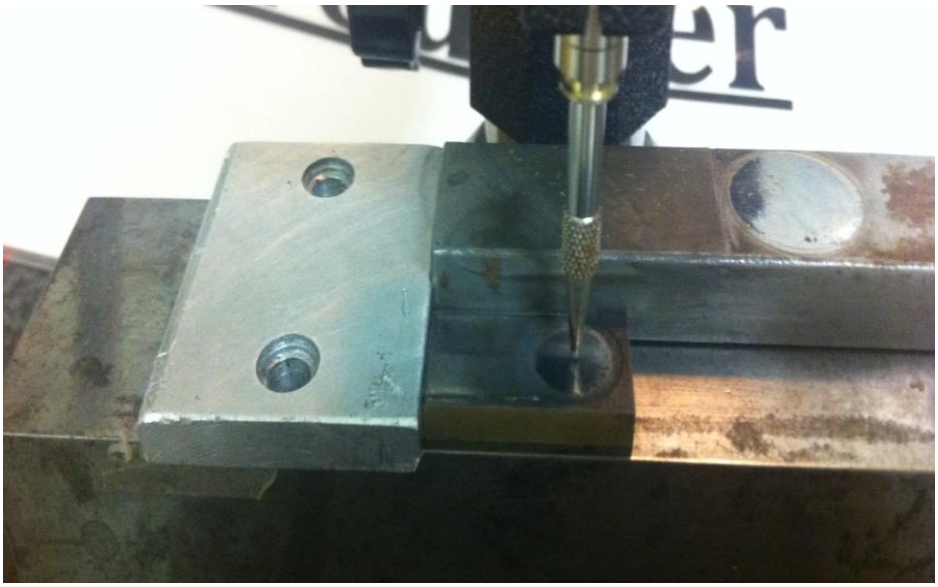

Figure 22: Metrology setup to measure the depth

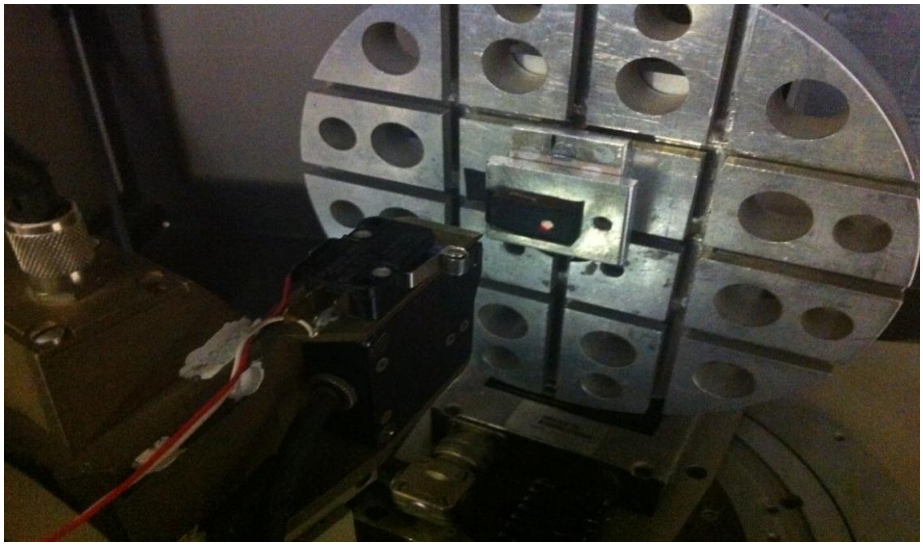

Figure 23: x-ray during measurement

During this work, not only different materials were used, but also the effect of different cutting conditions was investigated. The cutting tests were all made on a five axis machine.

Figure 24: Five axis CNC machine MORI SEIKI

The cutting parameters used for the steel 2842 and Al7050 are summarized in the following table.

	S01	**S02**	**S03**	**Af1**	**Af2**	**Aw1**	**Aw2**
Material	Steel2842	Steel2842	Steel2842	Al7050	Al7050	Al7050	Al7050
Feed Rate(mm/rev)	0.075	0.10	0.2	0.075	0.2	0.075	0.2
Spindle Speed(rpm)	4000	4000	4000	8000	8000	8000	8000
Axial Depth of Cut(mm)	2	2	2	1	1	1	1
Number of cutters	2	2	2	2	2	2	2
Wear	fresh	fresh	fresh	fresh	fresh	worn	worn

Table 5: Cutting conditions

During this research and especially for the cutting of the aluminium, not only the cutting parameters were tested but also the wear of the tool. Here we used two different tools, one fresh and one worn. The effect of the wear of the tool on the residual stress was investigated.

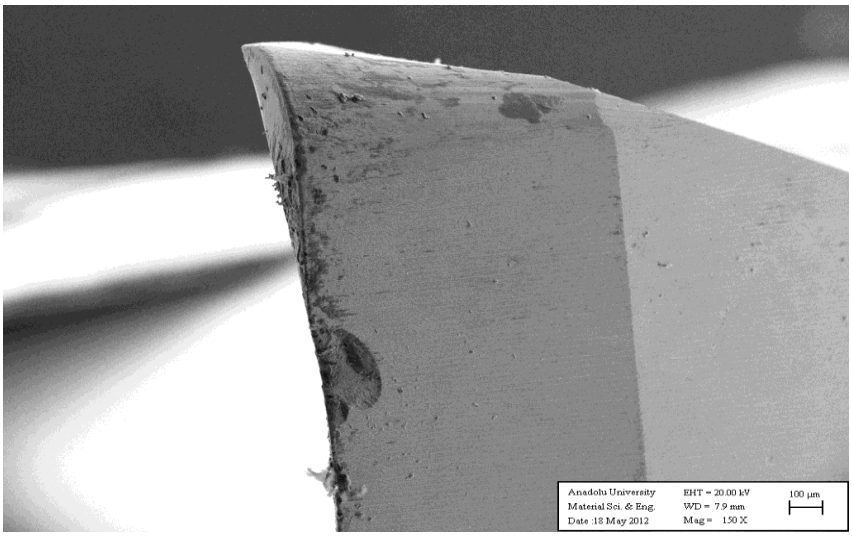

Figure 25: SEM picture of a worn tool

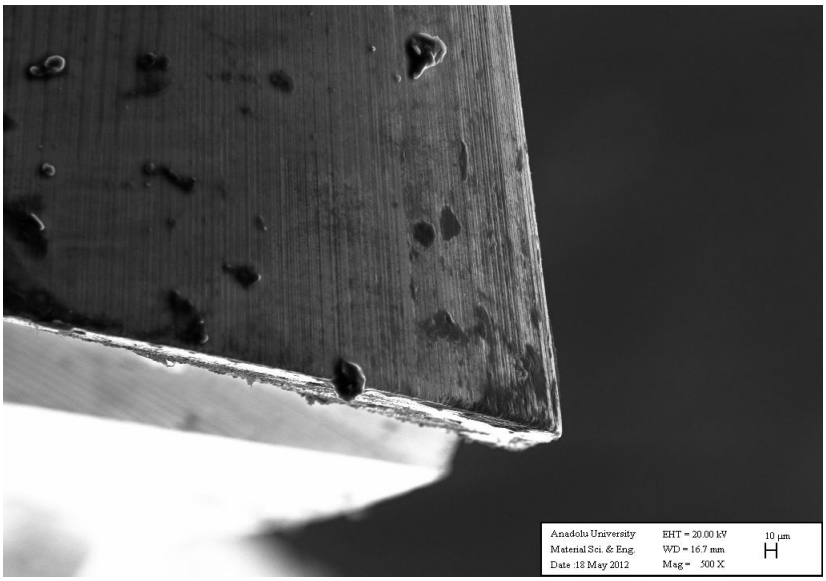

Figure 26: SEM picture of a fresh tool

To understand the effect of fresh and warn tool on forces. Force measurements were made for the same cutting parameters and the same depth of cut. The wear has a direct effect on the amount of force and therefore the amplitude and the type of residual stress on the part. During the experimental work (HT-D16R05L100) is used. It is an uncoated carbide end mill with two flutes. It is of 16mm in diameter, 100 mm in length, 0.5 mm in corner radius and 15° in Helix angle.

4.3.2.1 Residual stresses in Steel 2842

As summarized in Table 5. Residual stresses were investigated experimentally in the Steel 2842 using three different cutting conditions. The experimental residual stress was investigated following direction x and y as shown in Figure 5.

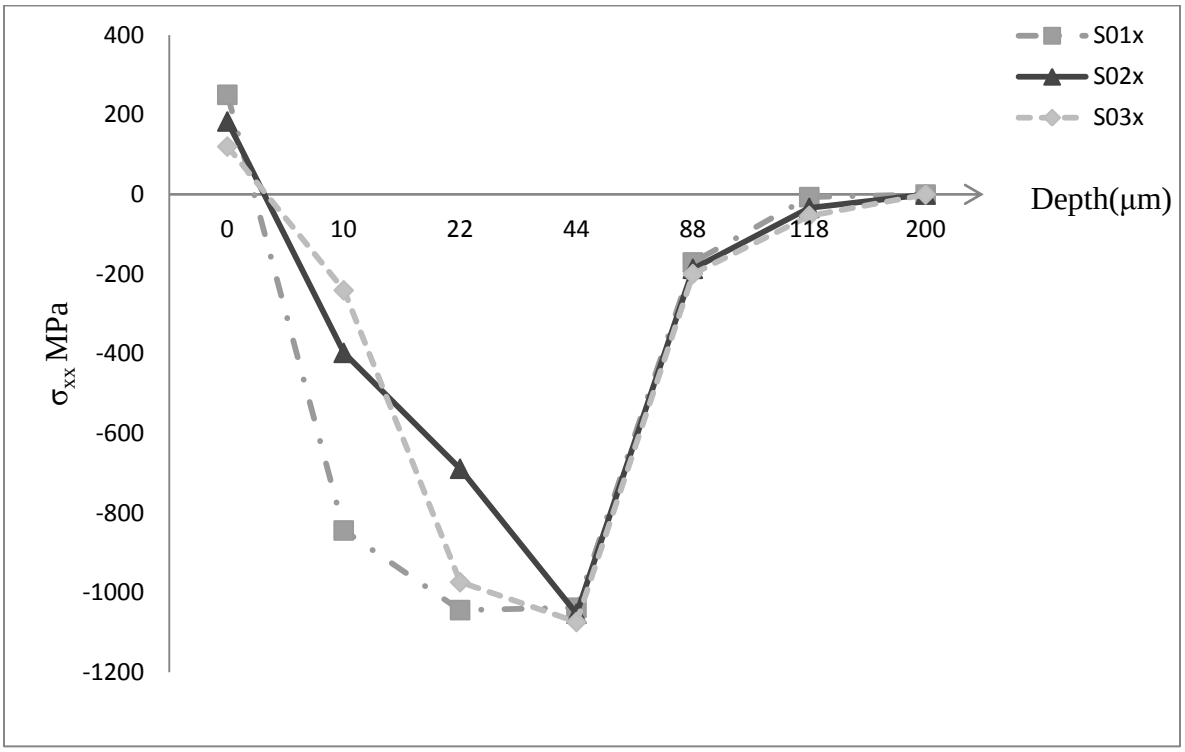

Figure 27: Residual stress σ_{xx} in Steel 2842

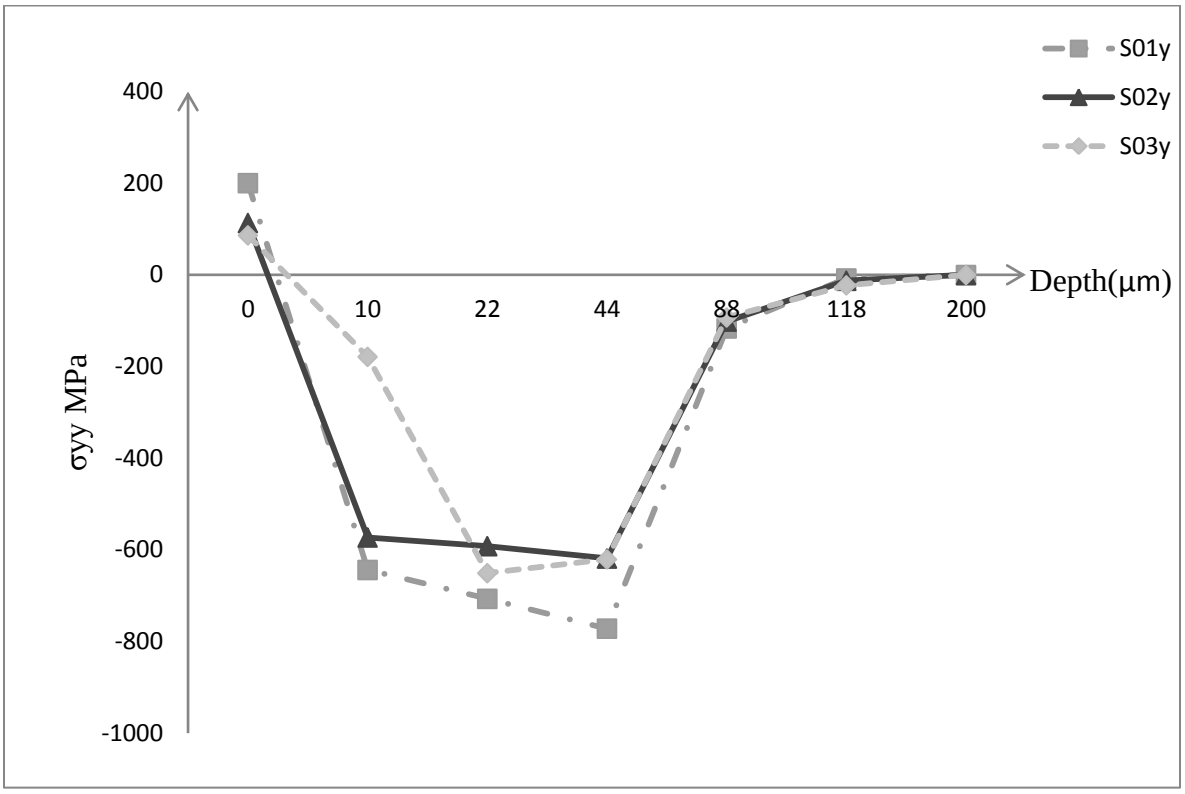

Figure 28: Residual stress σ_{yy} in Steel 2842

4.3.2.2 Residual stresses in Al 7050 part

The same experimental work has been conducted for Al 7050. For the Aluminium the effect of fresh and worn tool was investigated. Cutting conditions used are summarized in Table 5.

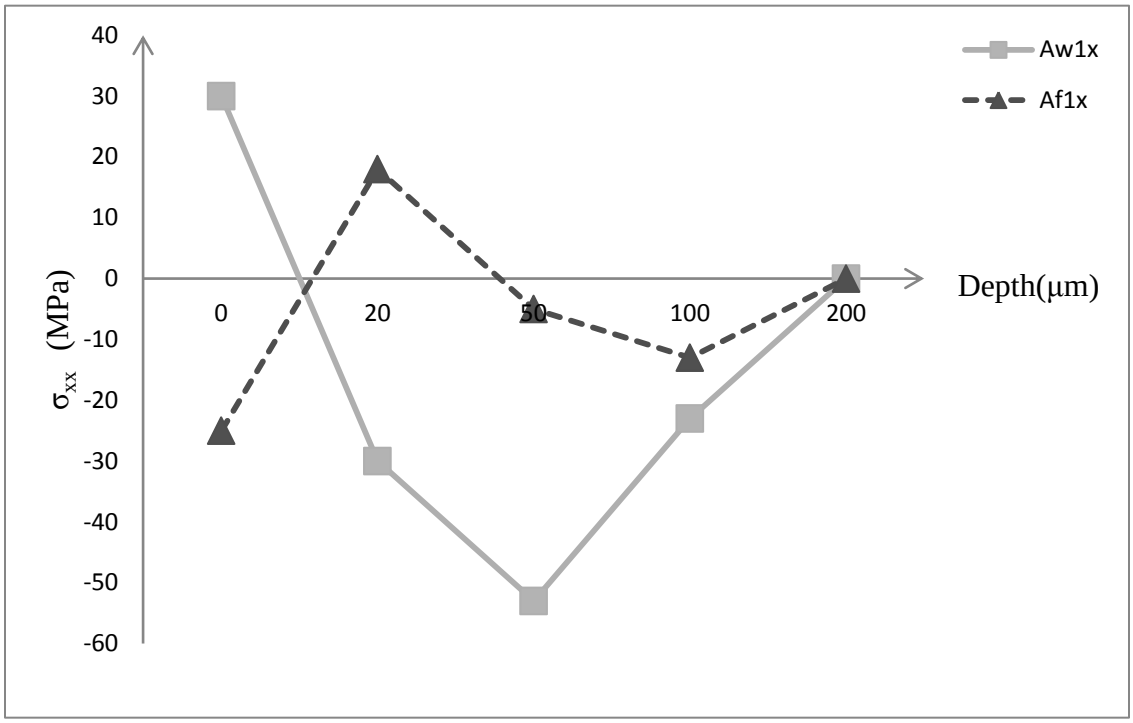

Figure 29: Residual stress σ_{xx} in Aluminium for fresh and warn tool in Aw1 and Af1

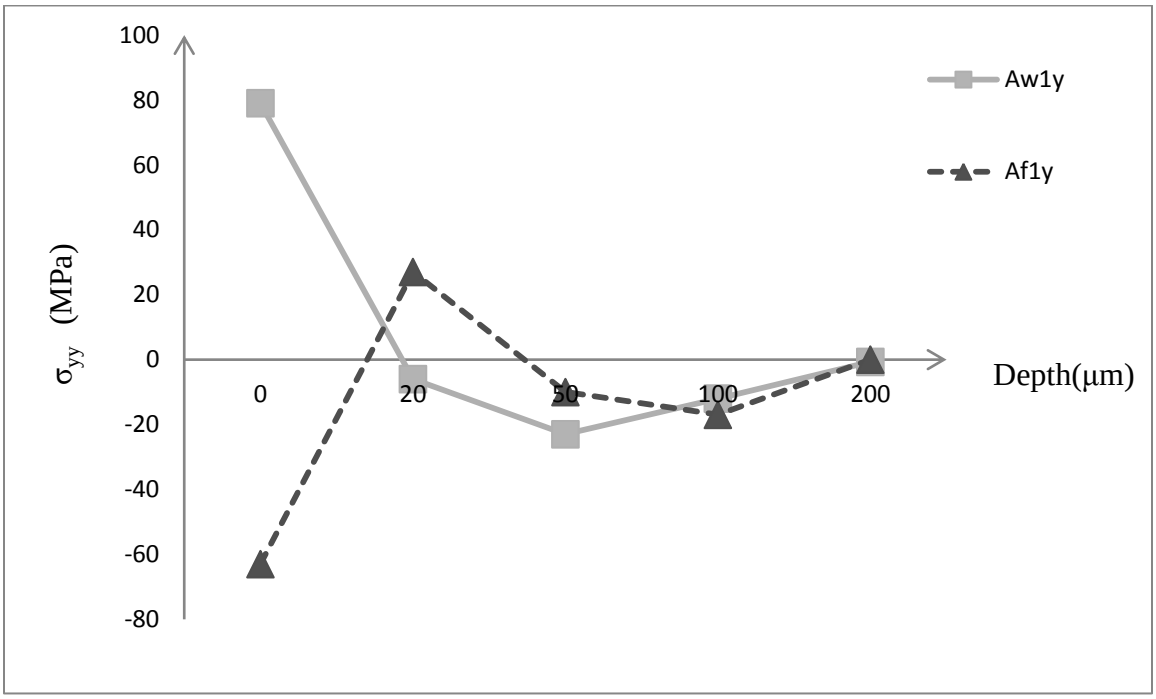

Figure 30: Residual stress σ_{yy} in Aluminium for fresh and warn tool in Aw1 and Af1

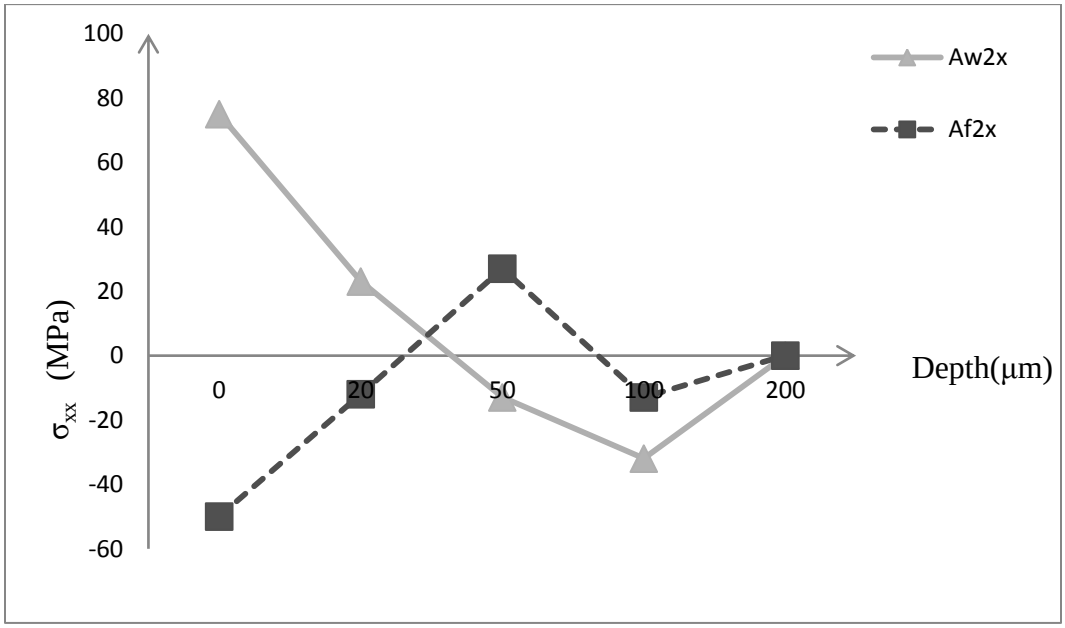

Figure 31: Residual stress σ_{xx} in Aluminium for fresh and warn tool in Aw2 and Af2

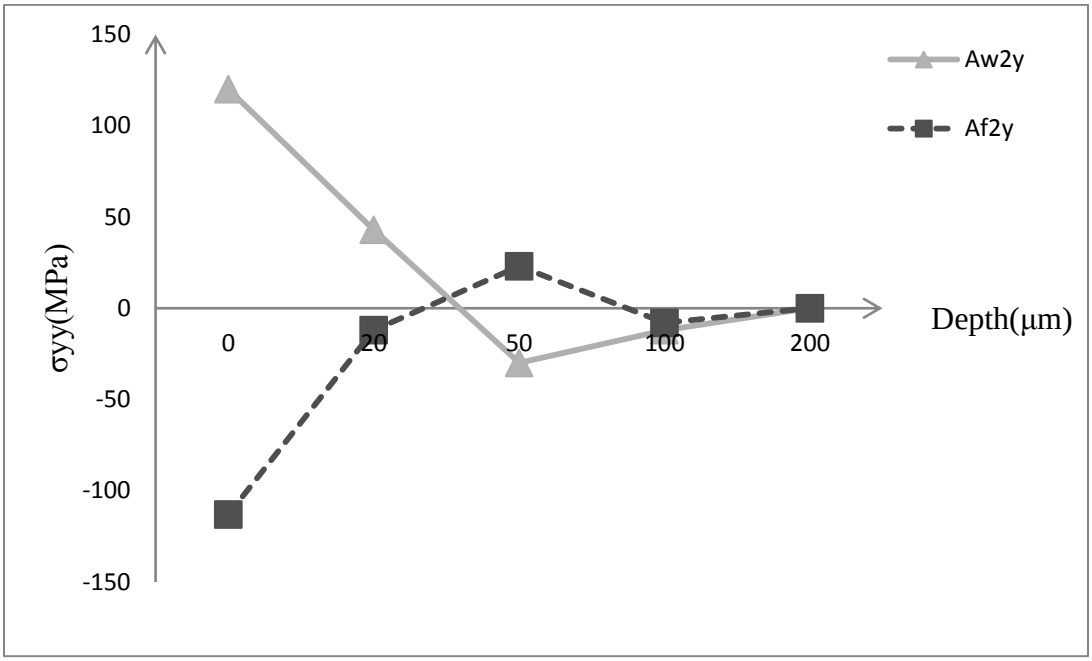

Figure 32: Residual stress σ_{yy} in Aluminium for fresh and warn tool in Aw2 and Af2

4.4 Hardness Investigation

4.4.1 Vickers test

The Vickers hardness test method consists of indenting the test material with a diamond indenter, in the form of a right pyramid with a square base and an angle of 136 degrees between opposite faces subjected to a load of 1 to 100 kgf. The full load is normally applied for 10 to 15 seconds. The two diagonals of the indentation left in the surface of the material after removal of the load are measured using a microscope and their average calculated. The area of the sloping surface of the indentation is calculated. The Vickers

hardness is the quotient obtained by dividing the kgf load by the square mm area of indentation.

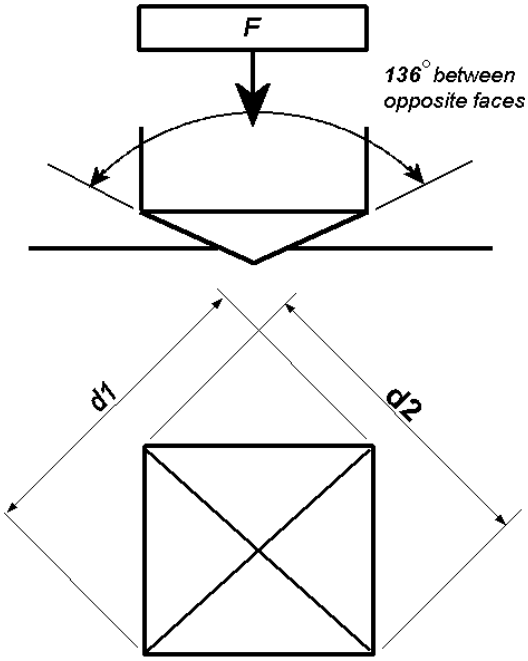

Figure 33: Vicker test details

F= Load in kgf
d = Arithmetic mean of the two diagonals, d1 and d2 in mm
HV = Vickers hardness

$$HV = \frac{2\,F \sin\frac{136°}{2}}{d^2}$$

$$HV = 1.854\,\frac{F}{d^2}$$

When the mean diagonal of the indentation has been determined the Vickers hardness may be calculated from the formula, but it is more convenient to use conversion tables. The

advantages of the Vickers hardness test are that extremely accurate readings can be taken, and just one type of indenter is used for all types of metals and surface treatments.

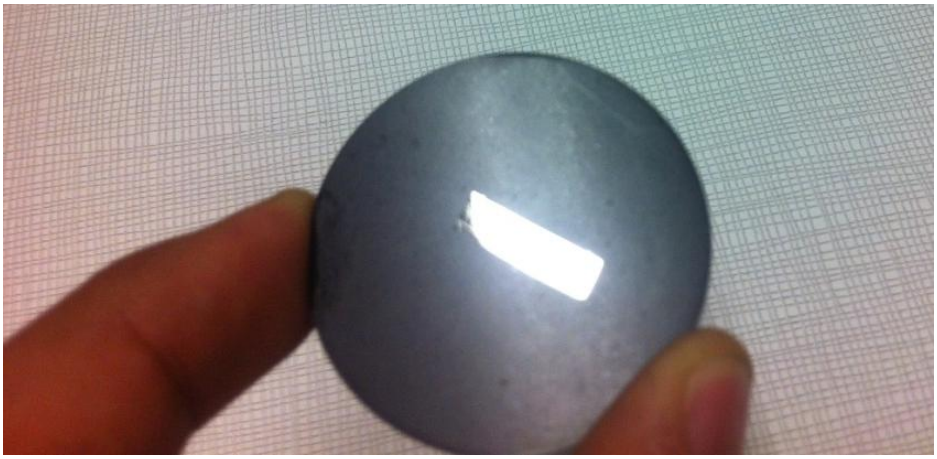

Figure 34: Tested part in the resin

Figure 35: Polishing of the surface

Figure 36: Hardness machine Leyca

4.4.2 Hardness depth profile for Steel 2842

The behaviour of steel during the machining operation has always interested researchers. First, it is very important to understand the steel reaction to mechanical and thermal load due to the intense uses in all industries. Second there is the fact that steel is metallurgically very complex. In this work, the investigation of the steel response to milling operation in terms of hardness is studied. In fact, some papers in the literature tried to link the surface roughness to the white layer thickness and the hardness. Here, the surface hardness profile was investigated using the previously presented method. The results are presented in Table.6 and Figure.

Depth (μm)	HV1	HV2	HV3	Average HV
0	649.7	649.8	651.2	649.84
30	662,90	639,90	585,50	629,43
50	552,40	607,02	577,10	578,84
100	618,30	500,00	581,00	566,43
2000	567,70	602,80	595,30	588,60
2500	595,00	570,00	590,00	585,00

Table 6: Hardness measures on milled Steel 2842

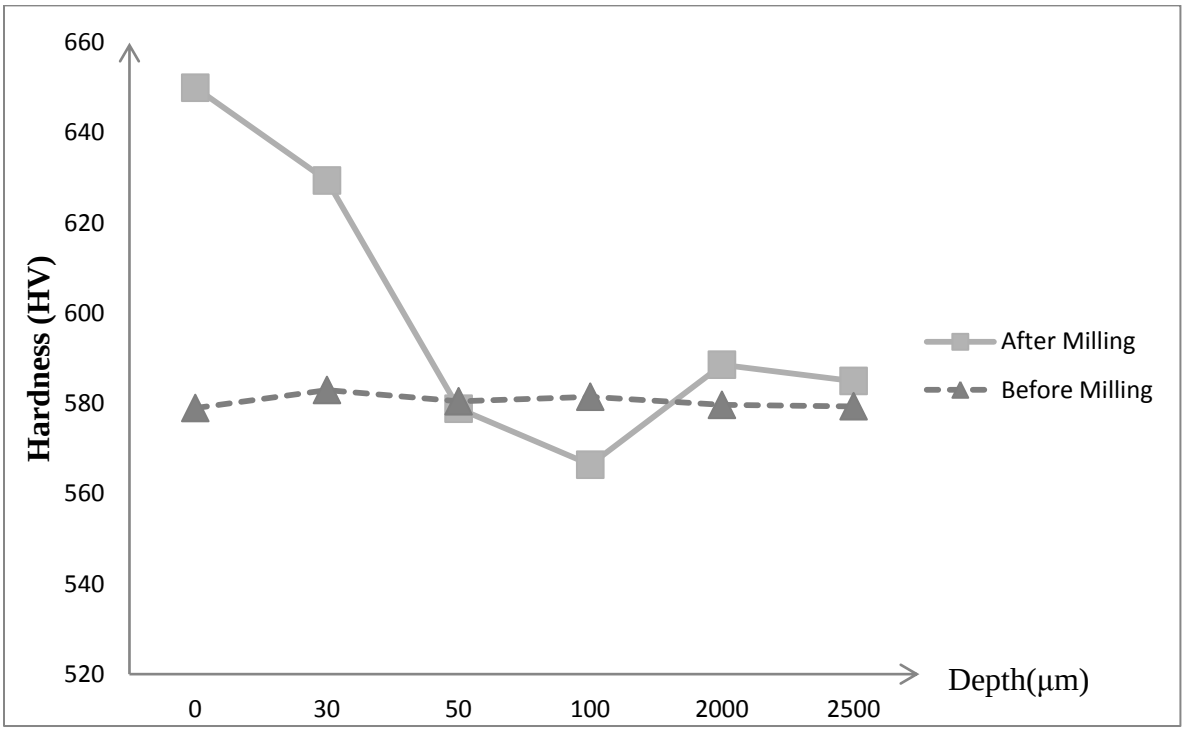

Figure 37: Hardness before and after milling

4.5 Deflection validation

4.5.1 Experimental setup

Deflection of the thin part made of Al 7050 was modelled mathematically and simulated. Validation of the simulation results is necessary. Using different materials and different cutting conditions the slot milling of a rectangular part was experienced. Forces during the cutting operation were recorded to control the inputs of the simulation and to compare the similarities between experiments and simulations. Figure shows the experimental setup.

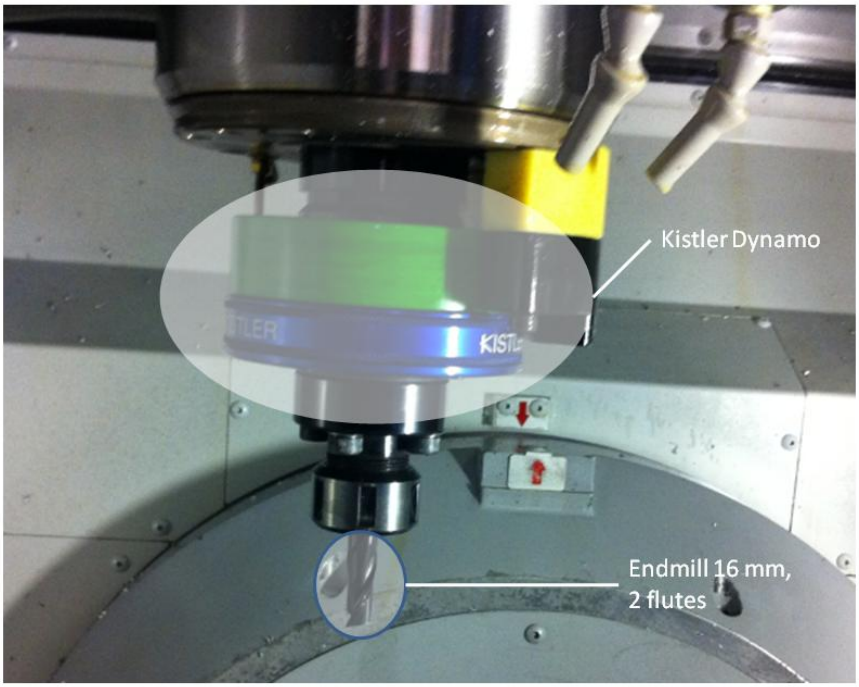

Figure 38: Experimental setup for machining

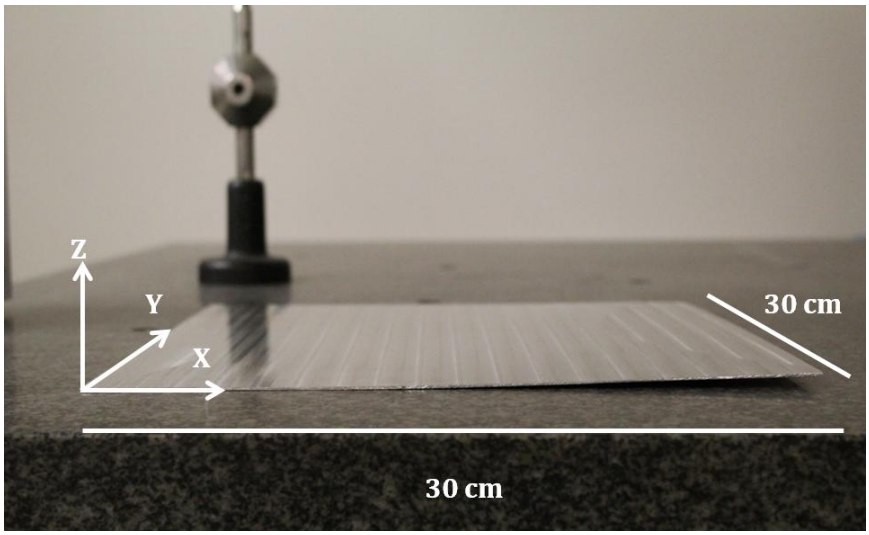

Figure 39: Distorted part

Cutting was made under cooling to decrease the effect of the thermal load since the simulation does not take thermal stress into account. The following cutting conditions were used: The tool (HT-D16R05L100) is an uncoated carbide end mill with two flutes. It is of 16mm in diameter, 100 mm in length, 0.5 mm in corner radius and 15° in Helix angle. The tests used a depth of cut of 2mm, a spindle speed of 8000 rpm and a feed/tooth of 0.2 mm rev^{-1} to obtain finished part with 2 mm in thickness

4.5.2 Metrology validation

For validation purpose, an acquisition of the real surface deflection was necessary. Metrological technologies to record the geometry error exist and are common in the manufacturing industry. CMM was used to record the surface deflection data for a better analysis work. However, this work is challenging. Since the part is a thin plate, the rigidity is very small and the CMM sensor is generating mode displacement in the part while touching the surface another deformation, which make the results non reliable.

A methodology was necessary to avoid this problem. The thin part was therefore put-on a sand bank that does not generate any deformation and protects the real form. Furthermore it is giving the necessary rigidity to the part not to be deformed during the sensing operation. Figure shows the experimental setup. The data acquisition was made on CATIA and the result matrix was saved in an IGES format. A post processing Matlab code was developed to regenerate the surface recorded by the CMM. A procedure to measure the deflection is then proposed for the future experiences. Figure.41 presents the sequence used.

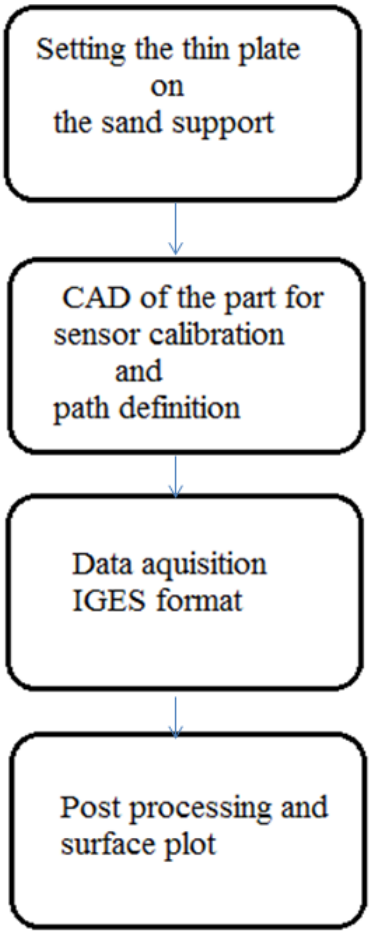

Figure 40: Distortion acquisition process

A post processing of the recorded data was made on Matlab software. Surface of the part was rebuilt and the results are presented bellow.

Figure 41: CMM machine

Figure 42-43 shows the uses of sand to fix the thin part from the external deflection that may be caused by the CMM tool.

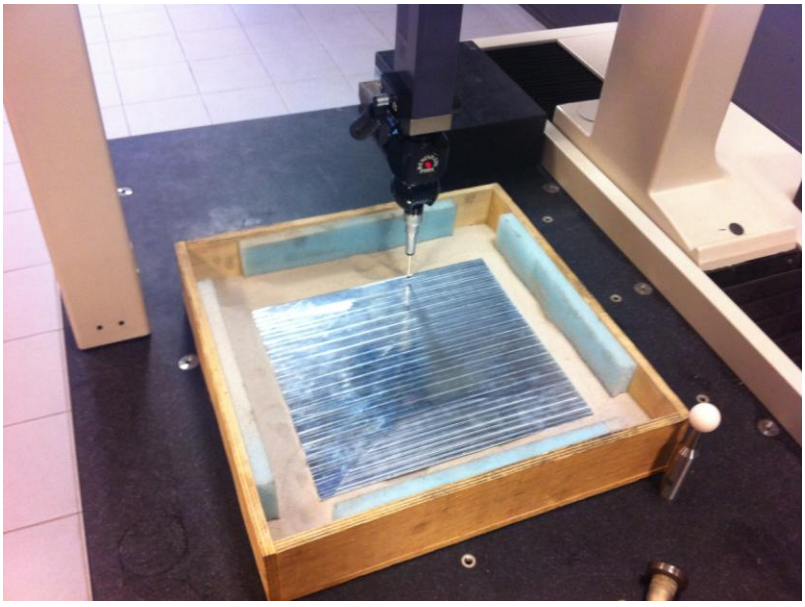

Figure 42: Technique used

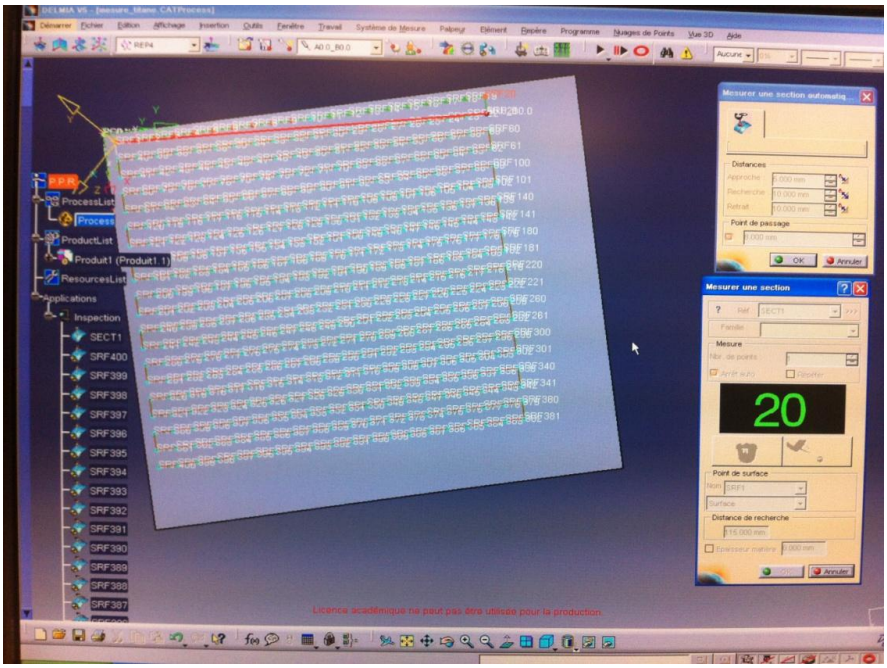

Figure 43: Path definition on Catia v4

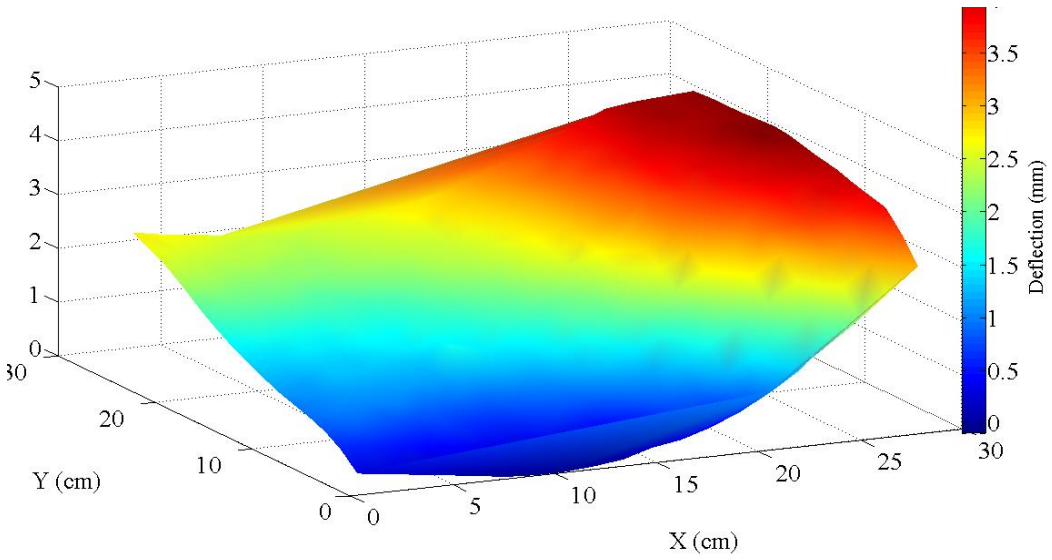

Figure 44: Matlab surface generation from the recorded data

Chapter 5

RESULTS & DISCUSSIONS

5.1 Introduction

In this chapter, the simulations and analytical results are reported and analyzed. Many physical phenomena are explained and many empirical relations are introduced. Some of the findings are not explained and hypotheses are therefore made. The first part will be about the distortion modeling. The simulation scheme and the experimental results are explained. The residual stress modeling and measurement presented the biggest challenge in this work. In fact, many new results are validated especially for the Steel 2842. Different materials are tested. New results about the hardness and its correlation with the residual stresses are also exposed. Finally, a global conclusion about the work is presented, and future possibilities are proposed.

5.2 Part deflection

Modeling of deflection of a thin part is a great challenge. While many FEM packages are able to predict it, there are many inconvenient factors such as the large

computing time (from hours to days). Analytical modeling presents a good opportunity to enhance the results for simple geometries. Analytical modeling is straightforward for simple geometries such as a line or plane. Therefore, in this study, we were limited to the study of a plane. Many aerospace parts are in the form of a plane such as some components of the wing. Established equations of the distortion of a plastically deformed and elastically relaxed part have been derived in chapter 3. A post processing was established to mesh the geometry and to calculate the deflection of each separated element of the mesh. All the calculated deflections are then associated in a defined orientation. In the simulation process, the thermal residual stress effect on the distortion is not studied. Only mechanical loading and therefore the relaxed plastic strain is taken as an input. Experiments have been made to validate the results. The output of the experiments is in concordance with the simulation. Even though the intensity in not accurately predicted, the deflection gradient is validated.

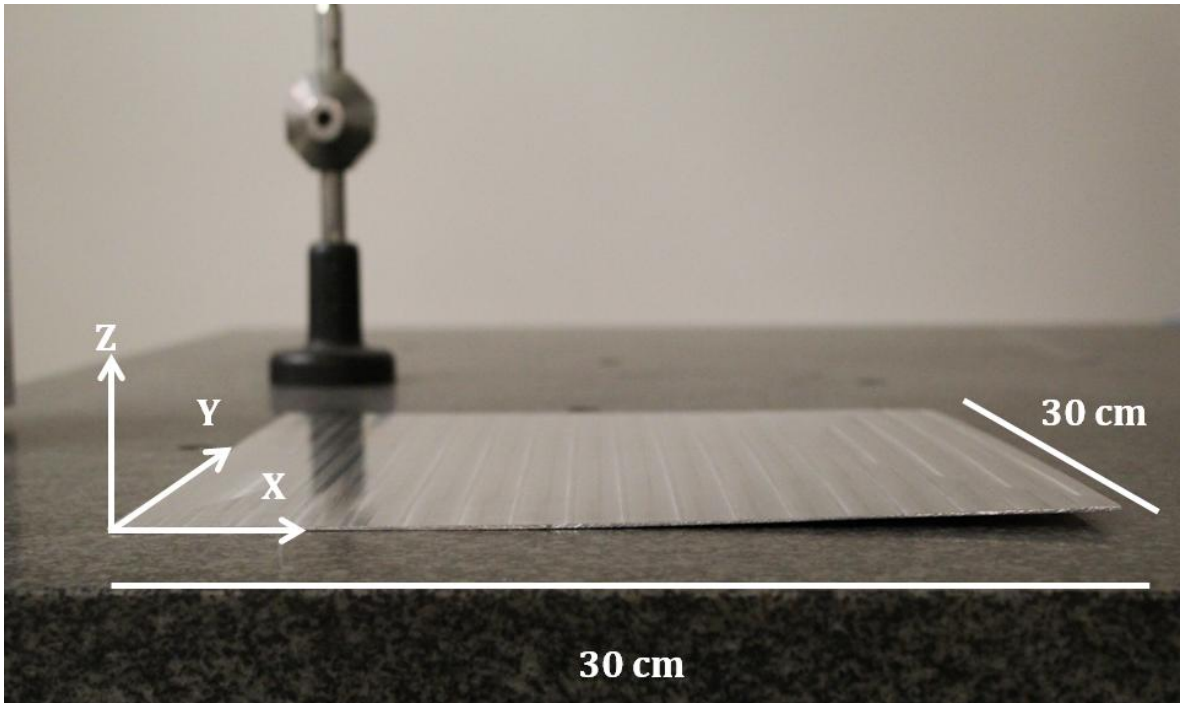

Figure 45: Experimental distortion of Al7050 part (Depth of cut of 2mm, Spindle speed of 8000 rpm, feed per tooth 0.2 mm/rev)

Figure 43 shows the obtained deflection after milling the part. Multi-pass dry milling tests have been conducted on Al7050 (Al 88.29%, Zn 5.02%, Mg 2.14%, Ti 1.62%) specimen of 50 mm in thickness, 300 mm in length and width. The material is of 2.83g/mm^3 density, 71.5×10^3 MPa Young's modulus, and 0.33 Poisson ratio. Cutting forces were measured using Kistler dynamometer. The tool (HT-D16R05L100) is an uncoated carbide end mill with two flutes. It is of 16mm in diameter, 100 mm in length, 0.5 mm in corner radius and 15° in Helix angle. The tests used a depth of cut of 2mm, a spindle speed of 8000 rpm and a feed/tooth of 0.2 mm rev^{-1} to obtain finished part with 2 mm in thickness. The deflection taking place immediately after detachment of the part from the fixations was measured using a Coordinate Measuring Machine (CMM) model Mitutoyo BHN506. Figure 44 and 45 shows the obtained profile with the measure of the deflection.

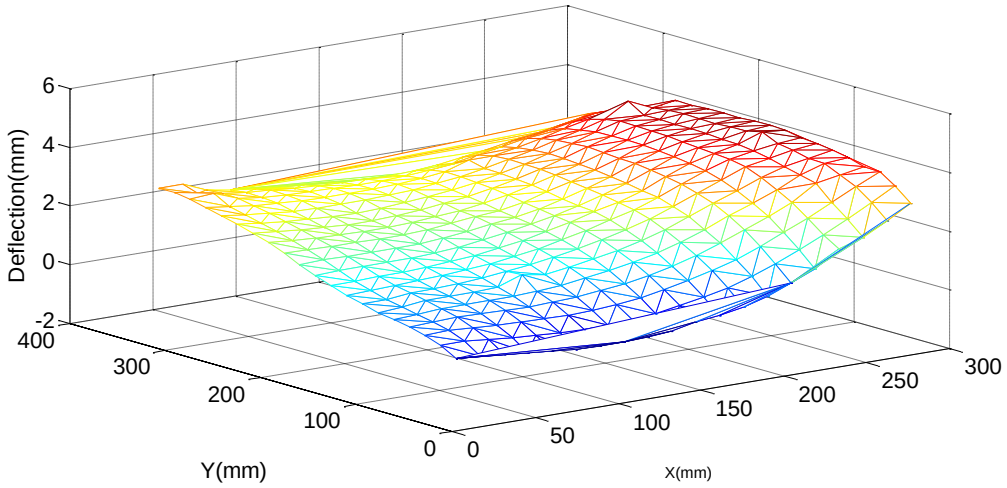

Figure 46: The CMM profile of the deflected Al7050 part (Depth of cut of 2mm, Spindle speed of 8000 rpm, feed per tooth 0.2 mm/rev)

The gradient of the deflection can be visualised. In fact, the part is deflected more in one extremity. The deflection is increasing from the non deflected part to the most deflected. The deflection intensity for the real machined part is about 4 mm.

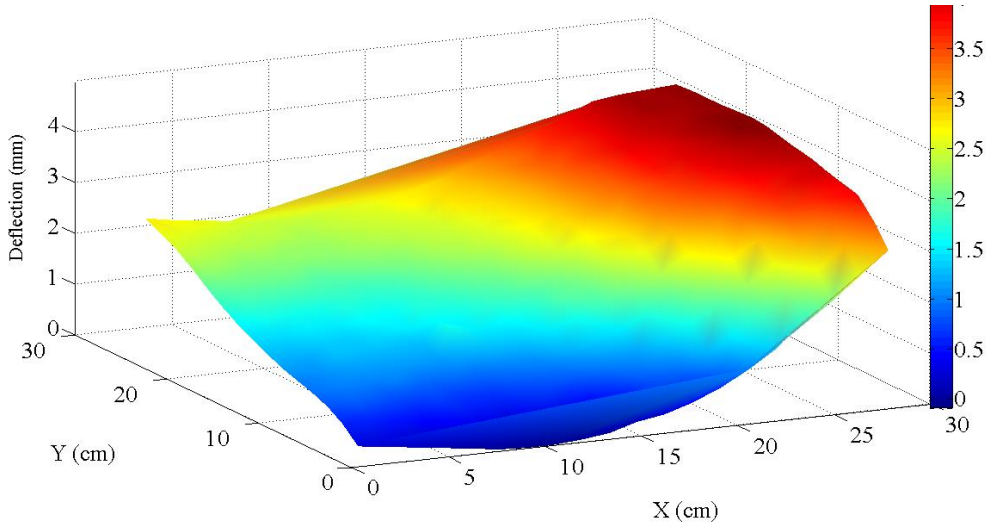

Figure 47: CMM profile side view (Depth of cut of 2mm, Spindle speed of 8000 rpm, feed per tooth 0.2 mm/rev)

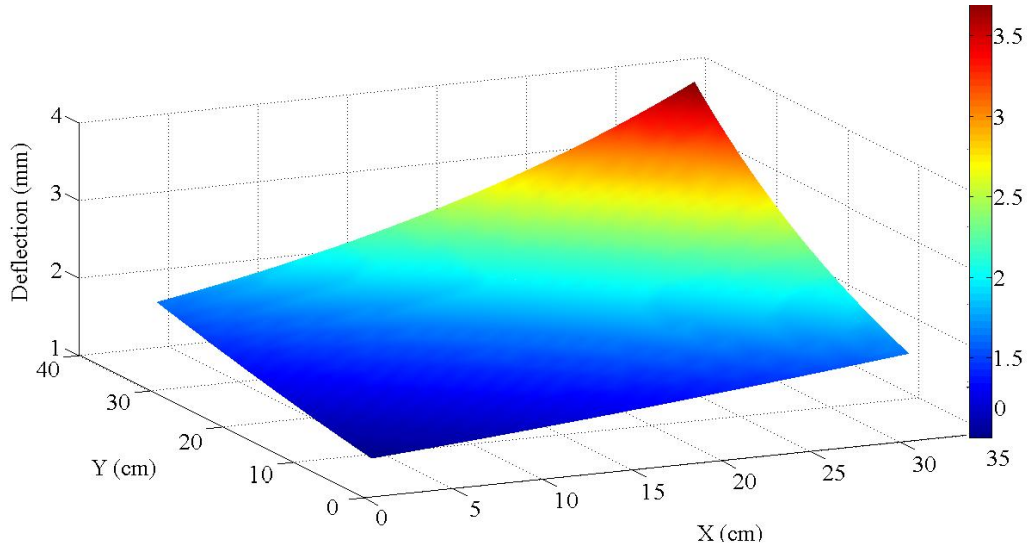

Figure 48: Simulated deflection

The simulation's objective was to simulate the deflection of a simple geometry. For this case, a thin part from Al7050 was simulated. The relaxed strain distribution was used as input of the deflection calculation. This strain was obtained from the residual stress model that takes the same amount of generated forces during the cutting using the following conditions, Depth of cut of 2mm, Spindle speed of 8000 rpm, feed per tooth 0.2 mm/rev. Figure 44 and 45 shows the results of the simulations for the same cutting parameters. The estimated maximal deflection is about 3.5 mm. The gradient of the deformation taking place and deflection amount were predicted. The small magnitude difference may be due to two reasons. Firstly, it can be due to the transformation of the cutting forces to pressure distribution; in fact the distribution of pressure is an approached model for the reality. Secondly, it can be due to the fact that we are not taking into account the hydrostatic pressure applied by the thermal stress on the surface, which is when it is superposed to the mechanical pressure distribution can increase the intensity.

Other distortions were investigated in this research for understanding purposes, in two other extremes: micro parts and very large parts. Figures 50 and 51 show the simulation

results. Concerning the micro machining, a validation was made using white light interferometer. For this work a different experimental setup was used as shown in the figure bellow. The experiments are done for the well known engineering material widely used in aero-space industry Al 7050.

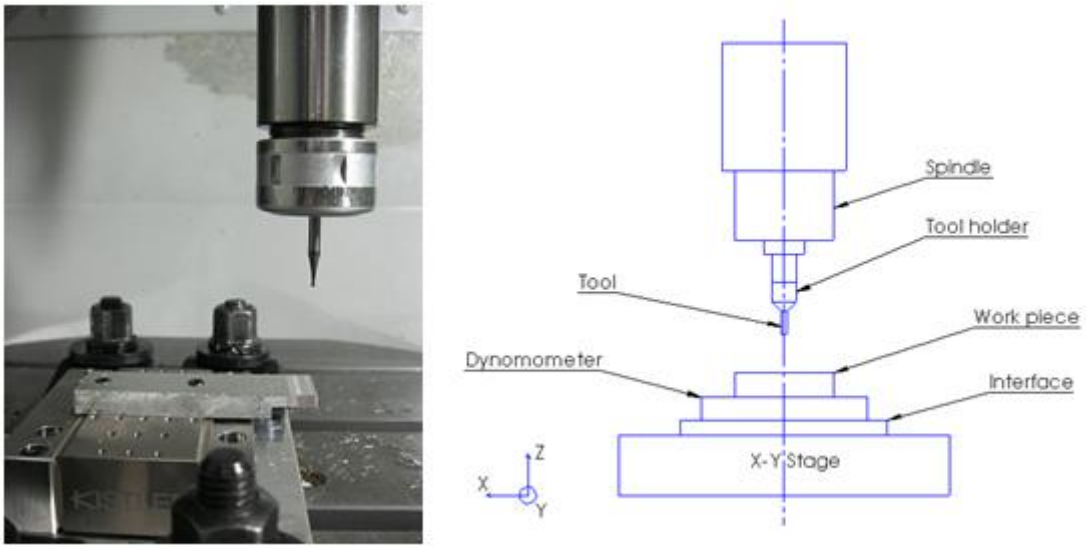

Figure 49: Micro milling experimental setup

The cutting process was performed by 1.5 mm diameter Tungsten Carbide (WC) end-mill presented in figure. Experiments are performed at 20.000 rpm spindle speed, 200μm depth of cut slot milling at different feed per tooth. Experiments were held on Mori Seiki NMV5000DCG CNC machine using Nikken high speed air turbine. Force measurements were done by Kistler 9256C micro dynamometer as shown in Figure 49.

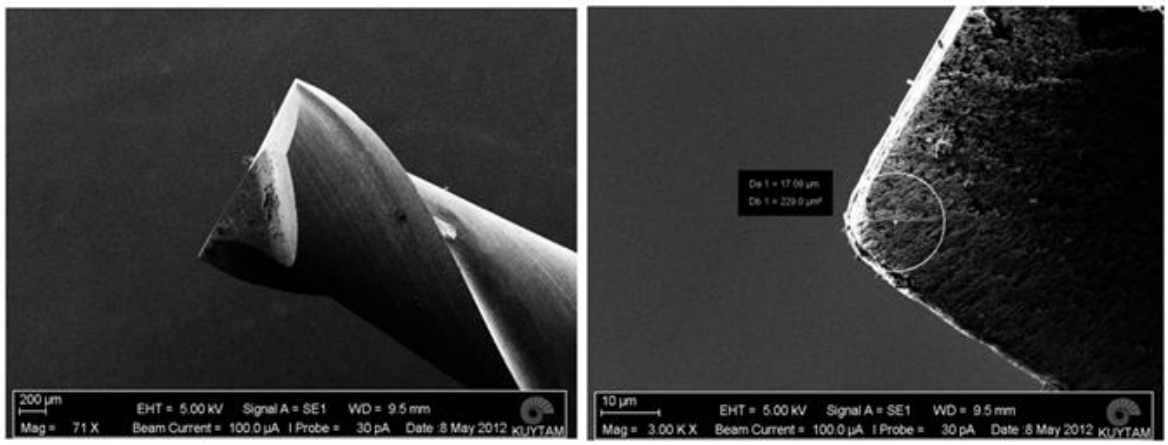

Figure 50: Tool used

The simulations results were made for the same cutting conditions and the obtained results are shown in Figure 51.

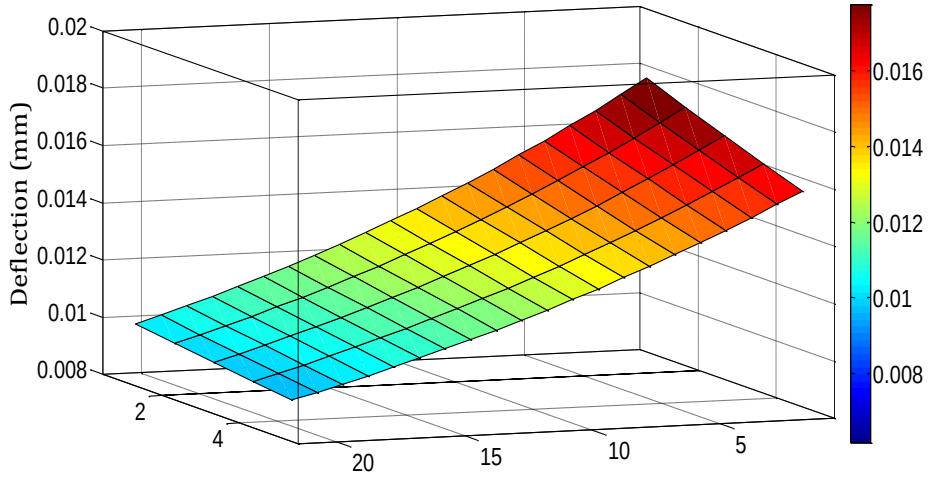

Figure 51: Micro deflection (20x5 mm)

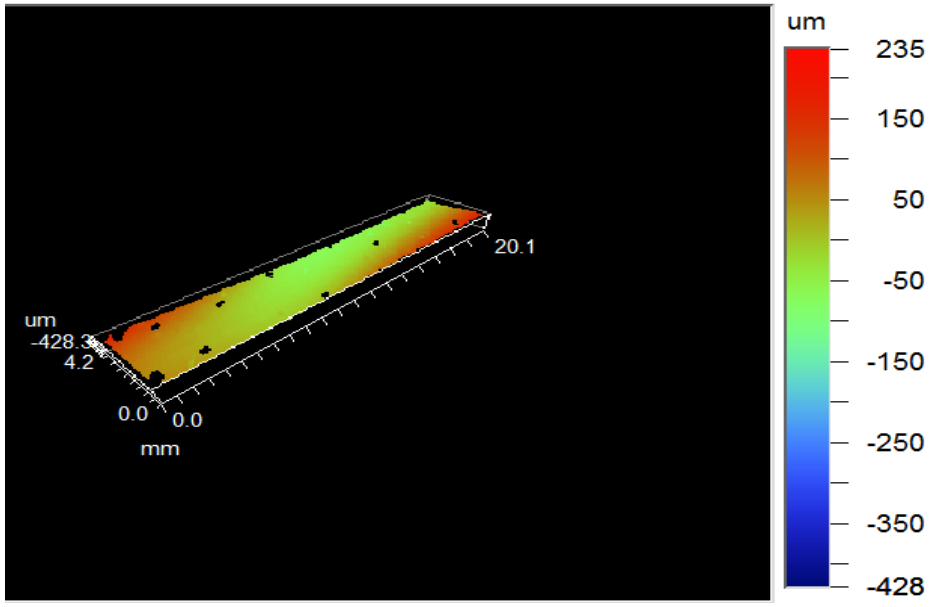

Figure 52: White light interferometer obtained result

Figure 52 shows the experimental results obtained using a white light interferometer. The deflection form is predicted and the deflection amount is not yet accurate. In fact, a study about the indentation is to be held. The contact length is complicated to be determined. Though, the better is the understanding about the contact area, the more accurate the results are.

5.3 Residual stress

The residual stress analysis involved different materials and different machining aspects. Table 5 shows the different parts and the different parameters tested. The simulation code links the cutting parameters to the residual stress and distortion. The first objective of this study was to establish a new methodology to approach the residual stress problem in the milling process. The second objective is to make this new modeling approach related to the cutting parameters. In fact, this should be enhanced more. However,

some first simulations especially for Steel 2842 have shown a correlation with the experimental results. Figure shows the simulation results for different cutting parameters; the next figures show the experimental results for the same cutting parameters.

	S01	**S02**	**S03**	**Af1**	**Af2**	**Aw1**	**Aw2**
Material	Steel2842	Steel2842	Steel2842	Al7050	Al7050	Al7050	Al7050
Feed Rate(mm/rev)	0.075	0.10	0.2	0.075	0.2	0.075	0.2
Spindle Speed(rpm)	4000	4000	4000	8000	8000	8000	8000
Axial Depth of Cut(mm)	2	2	2	1	1	1	1
Number of cutters	2	2	2	2	2	2	2
Wear	fresh	fresh	fresh	fresh	fresh	worn	worn

Table 7: Cutting parameters for residual stress

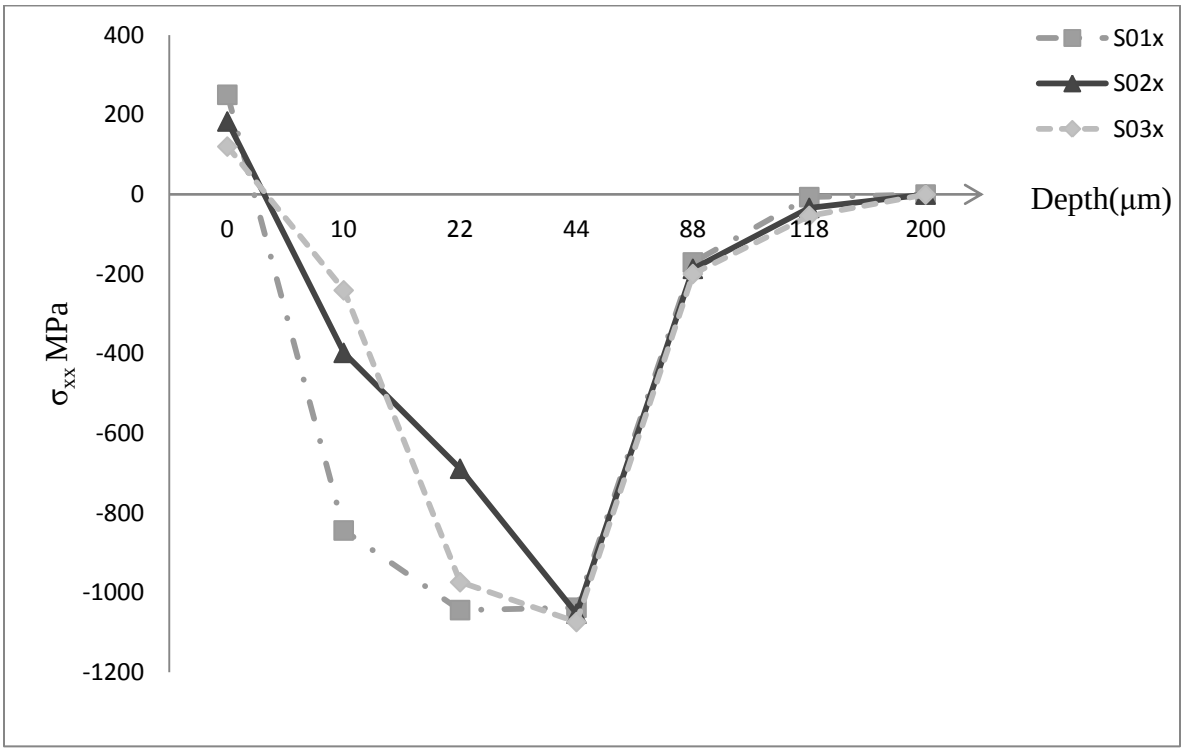

Figure 53: Experimental residual stresses in the x direction of Steel 2842 for (S01, S02, S03)

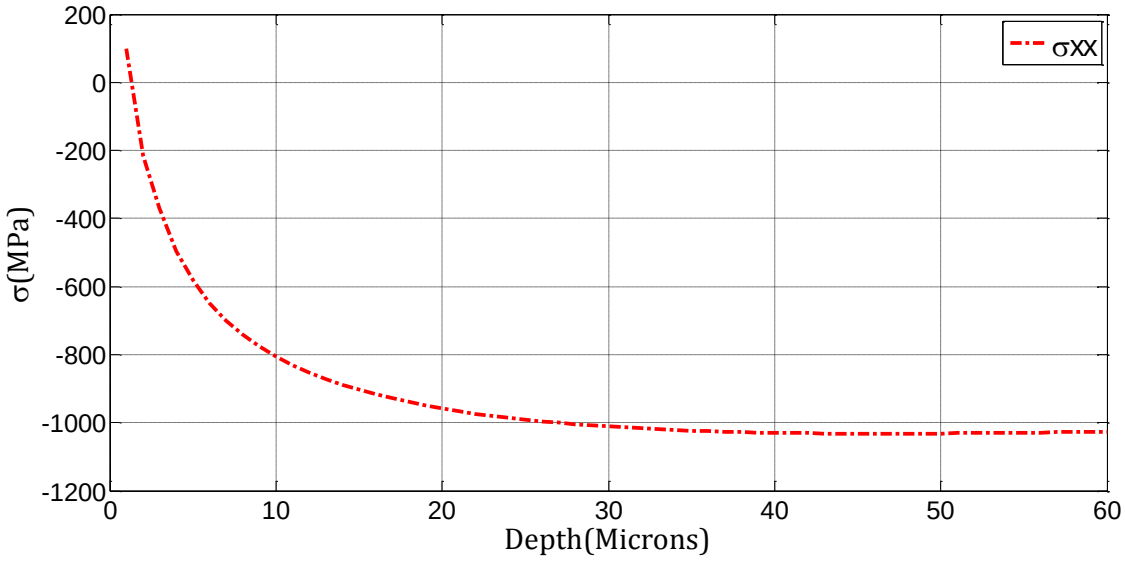

Figure 54: Simulated residual stress in x direction for the case S01, Steel 2842

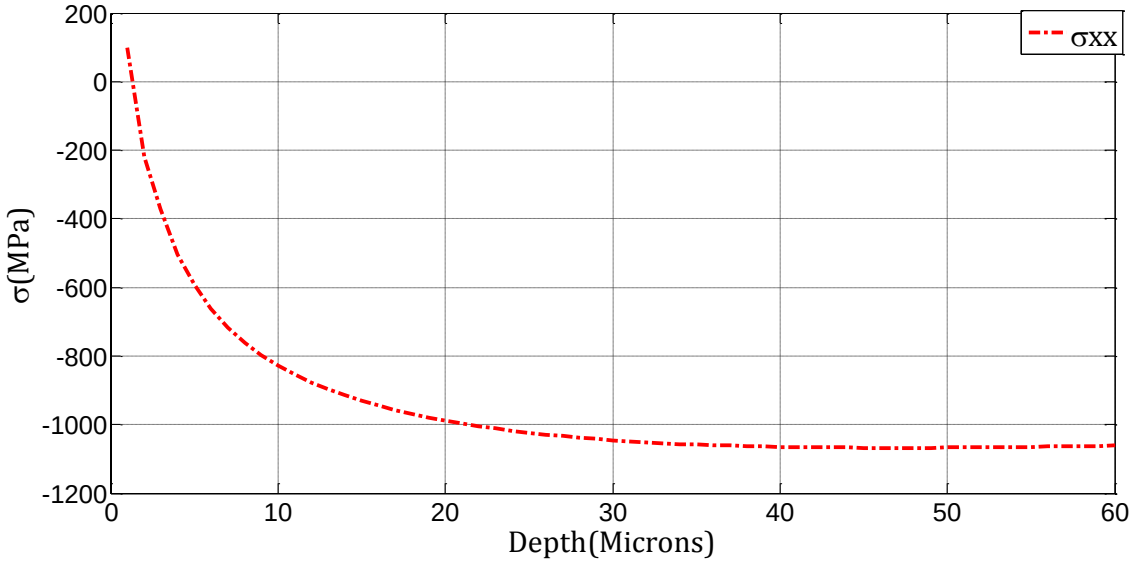

Figure 55: Simulated residual stress in x direction for the case S02, Steel 2842

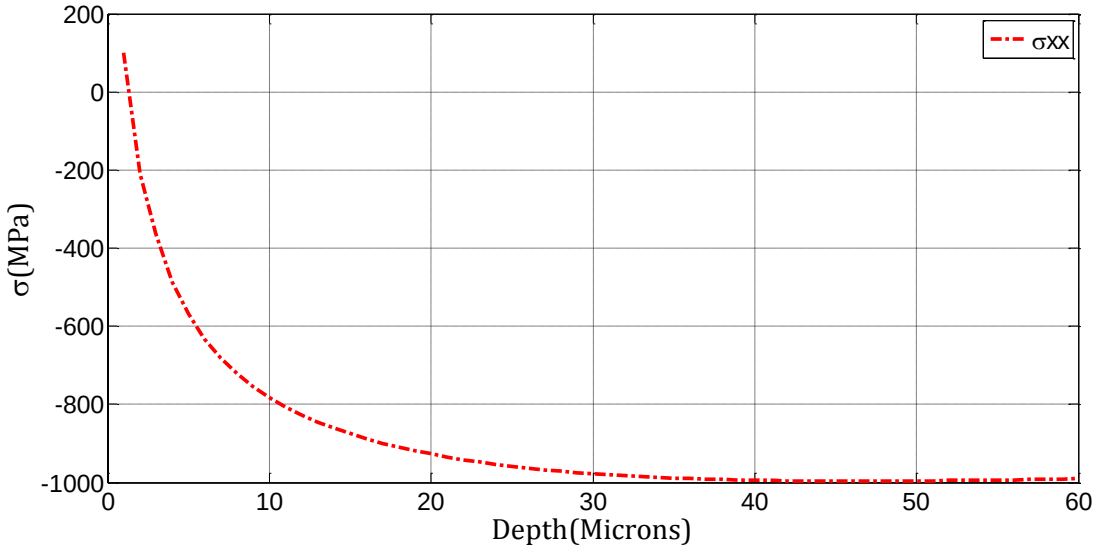

Figure 56: Simulated residual stress in x direction for the case S03, Steel 2842

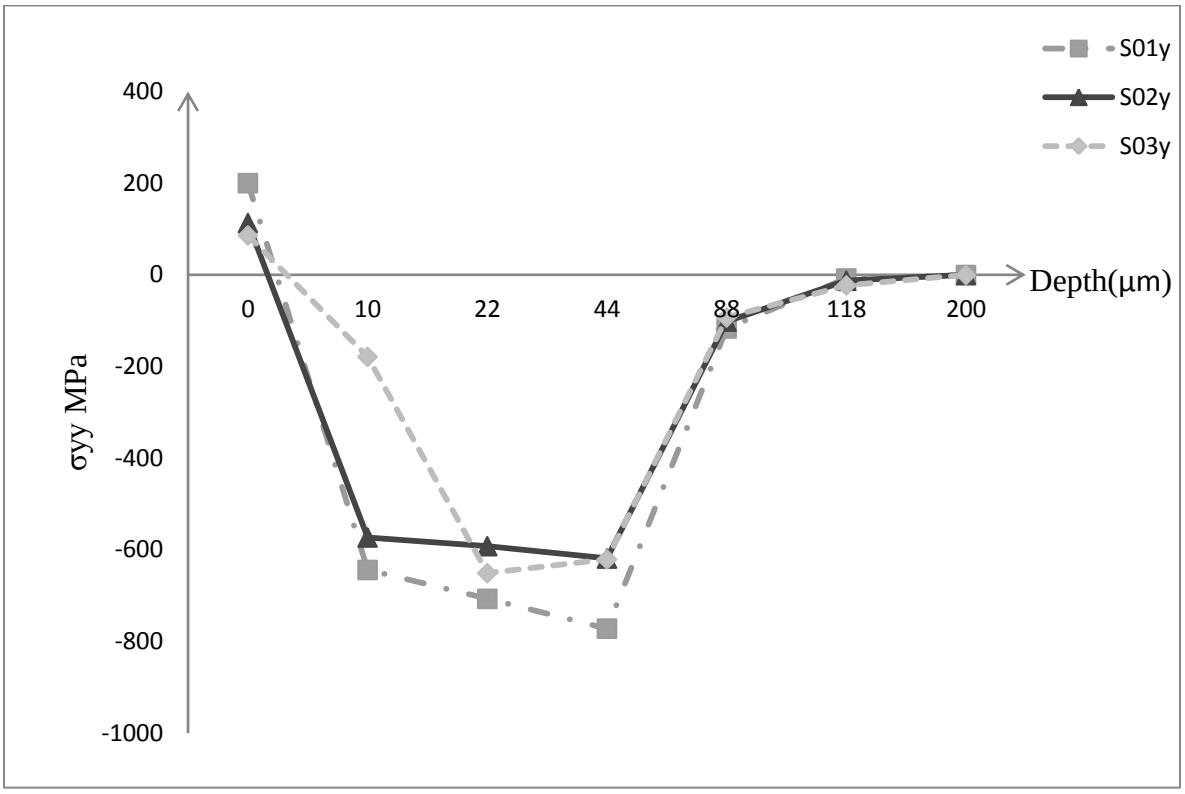

Figure 57: Experimental residual stresses in the y direction of Steel 2842

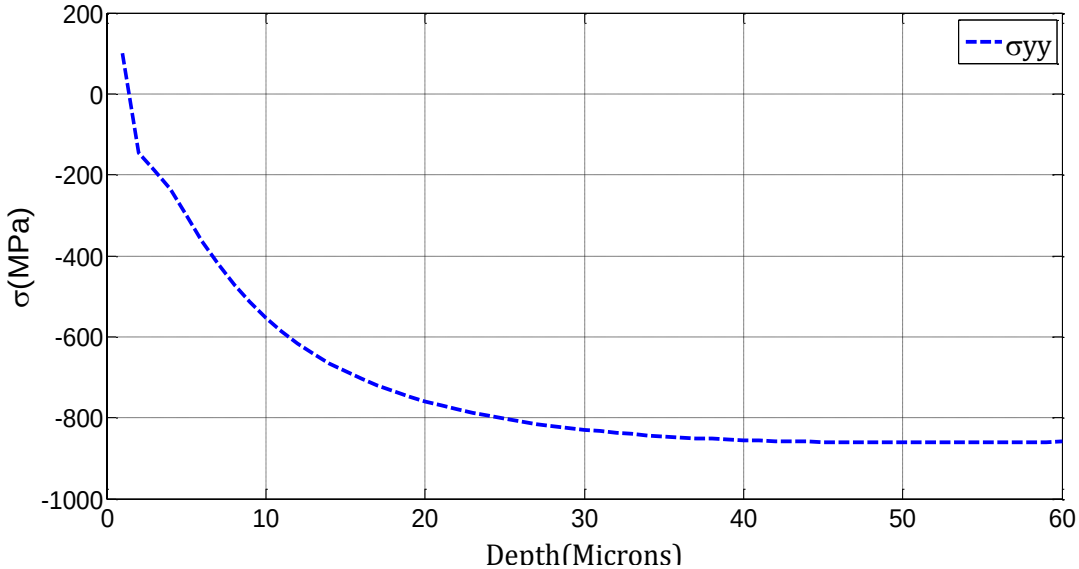

Figure 58: Simulated residual stresses in the y direction for the case S01 of Steel 2842

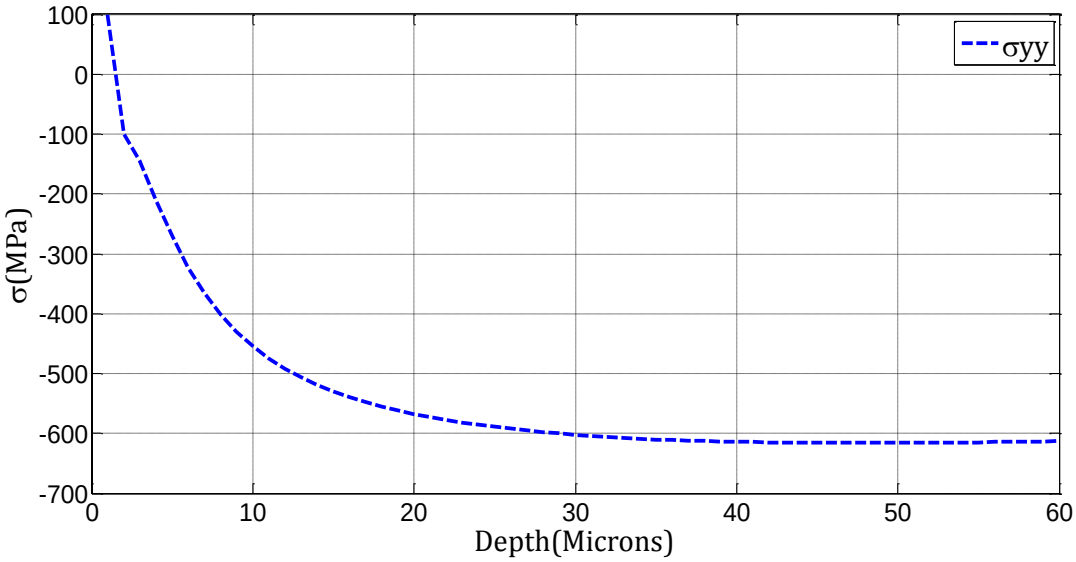

Figure 59: Simulated residual stresses in the y direction for the case S02 of Steel 2842

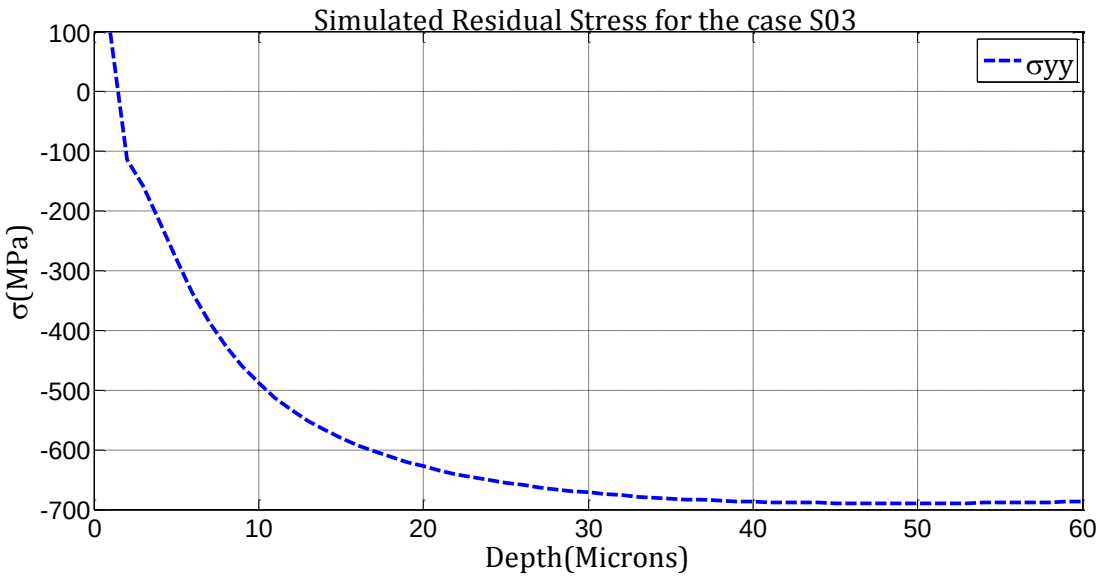

Figure 60: Simulated residual stresses in the y direction for the case S03 of Steel 2842

For aluminium, the simulation results were not successful to define the full profile. For the aluminium test, two levels of cutting conditions were defined. Also, the wear of the tool was taken into account. In fact, this domain is to be investigated. The experimental results show that the fresh tool is generating a compressive residual stress on the surface, which is very beneficial for the part quality and resistance to crack and fatigue. However the worn tool is generating an intense tensile residual stress. The following figures show the cutting conditions that can be found in table.7 and the wear of the tool.

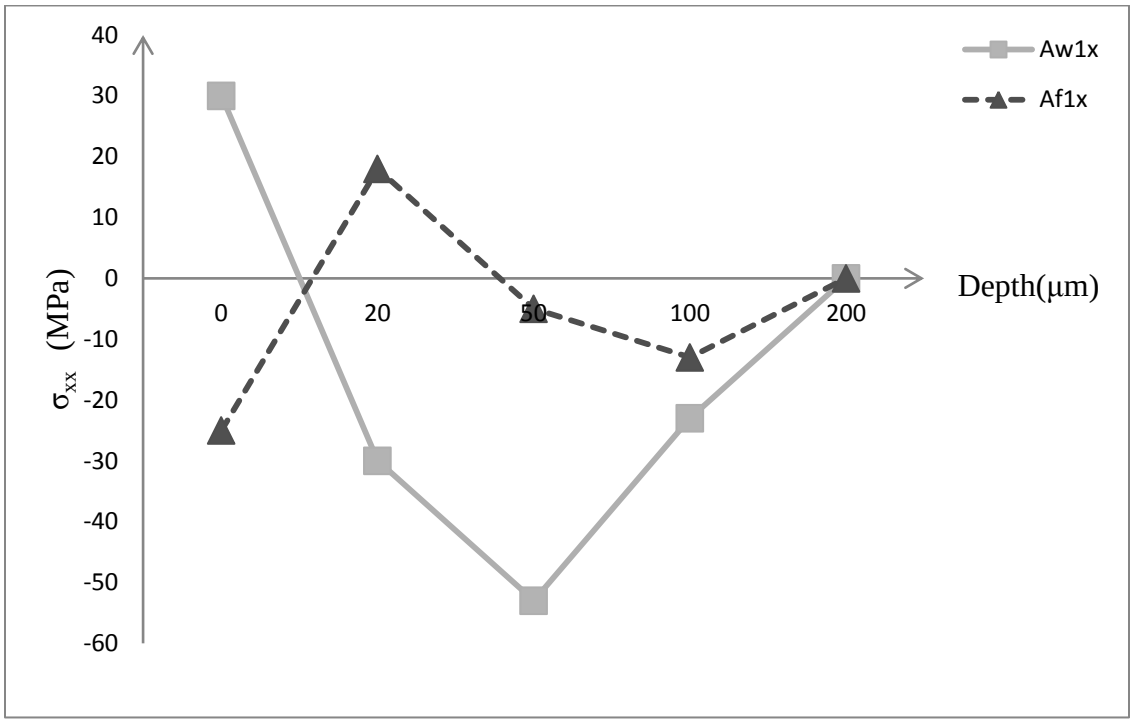

Figure 61: Experimental residual stress for Al7050 (Feed 0.075, Spindle speed of 8000 rpm, depth of cut 1mm), x direction

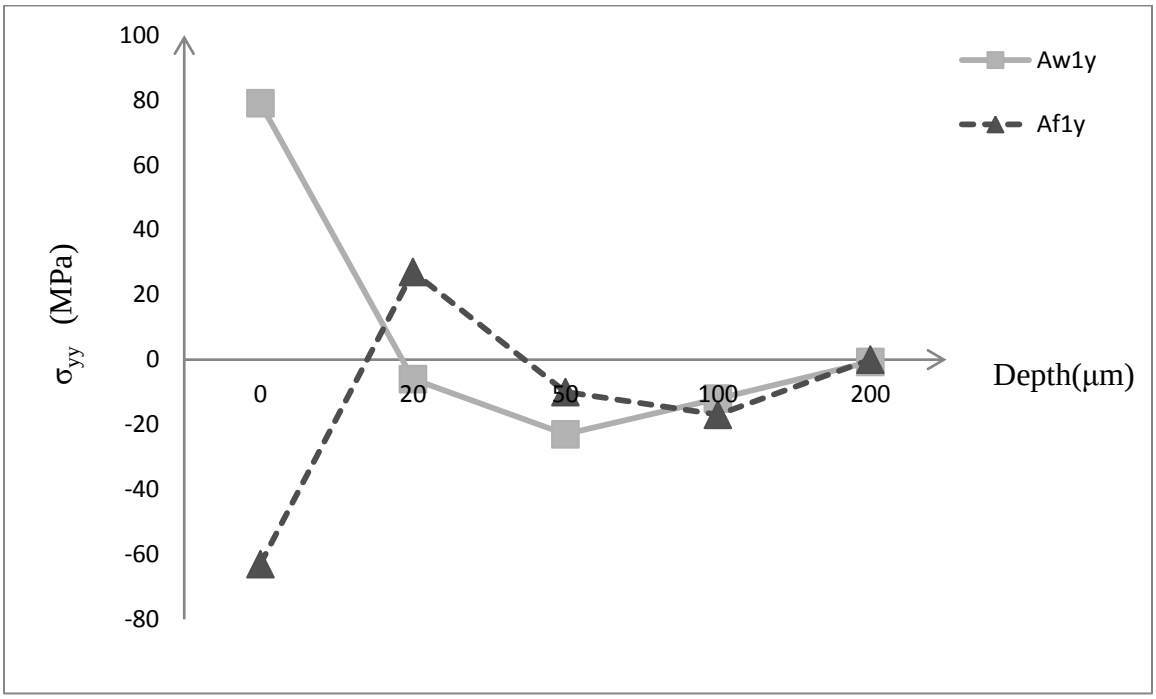

Figure 62: Experimental residual stress for Al7050 (Feed 0.075, Spindle speed of 8000 rpm, depth of cut 1mm), y direction

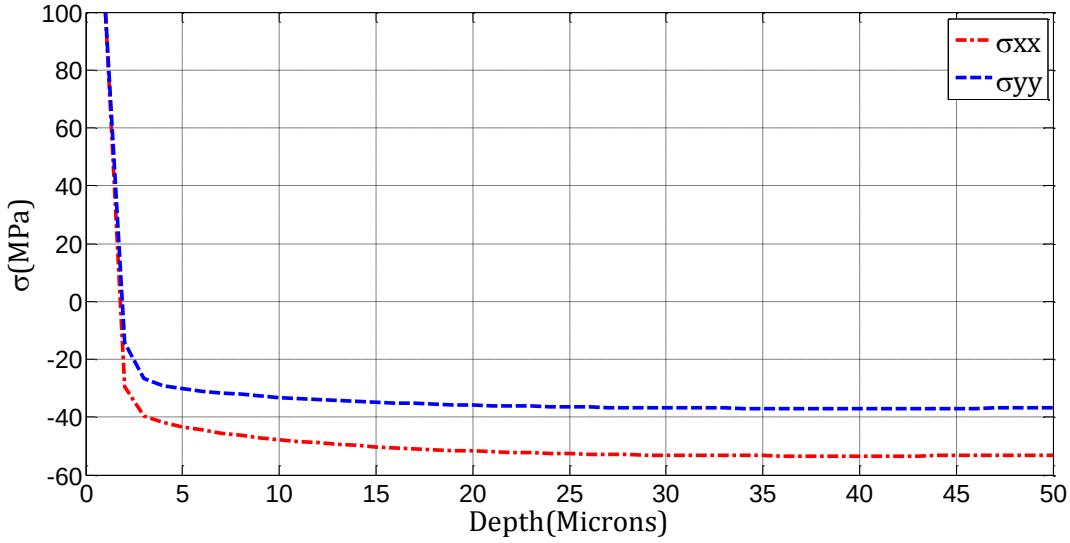

Figure 63: Simulated residual stress for Al7050 (Feed 0.075mm/rev, Spindle speed of 8000 rpm, depth of cut 1mm)

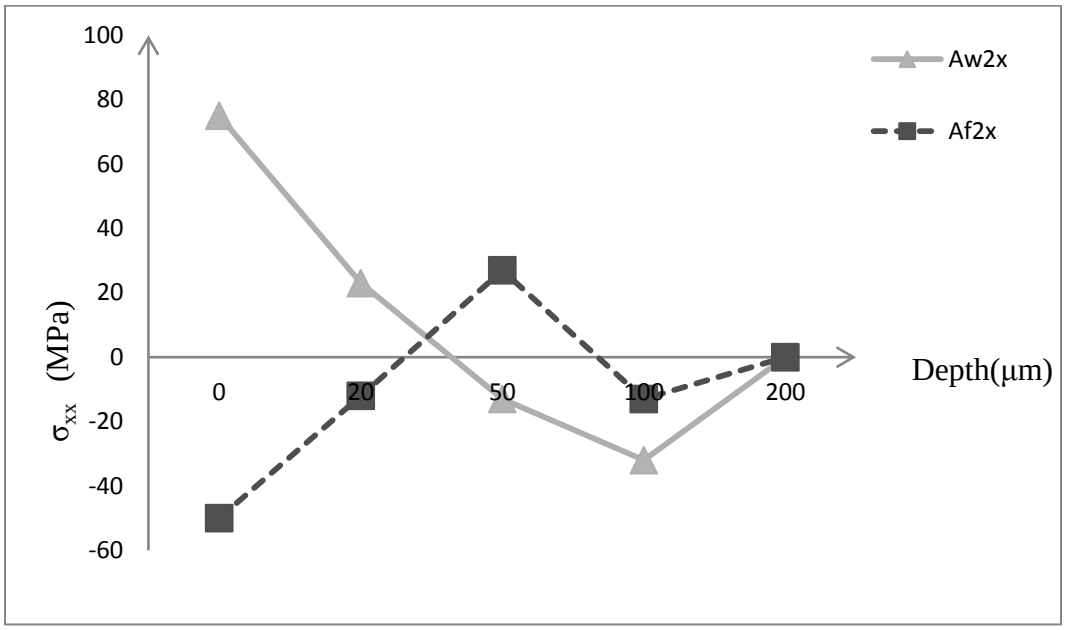

Figure 64: Experimental residual stress for Al7050 (Feed 0.2 mm/rev, Spindle speed of 8000 rpm, depth of cut 1mm), x direction

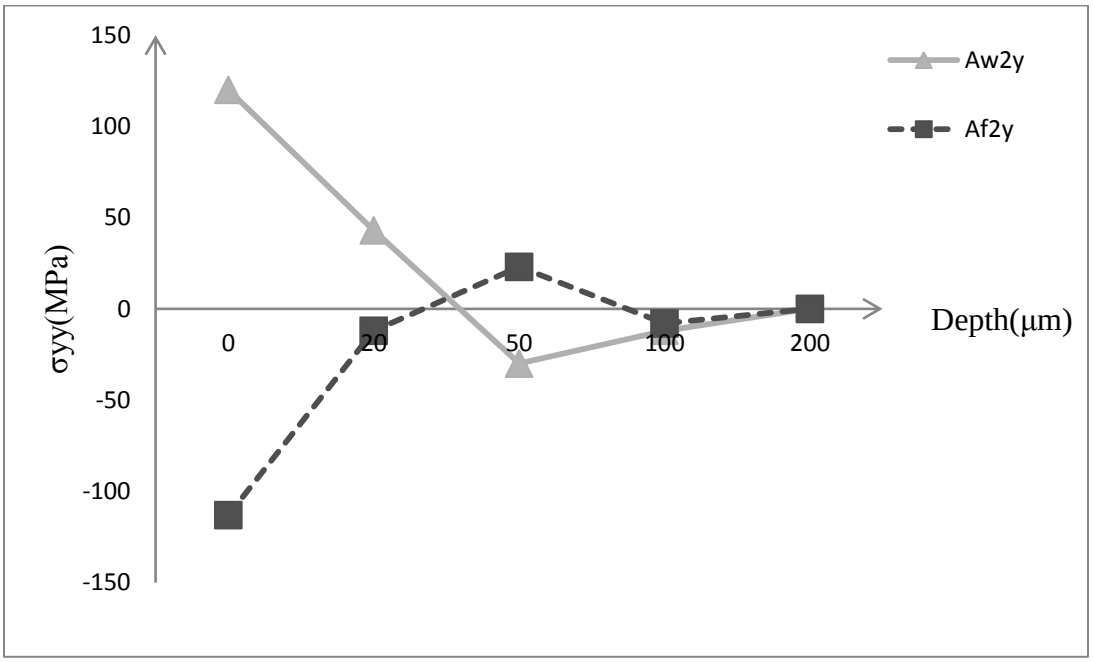

Figure 65: Experimental residual stress for Al7050 (Feed 0.2 mm/rev, Spindle speed of 8000 rpm, depth of cut 1mm), y direction

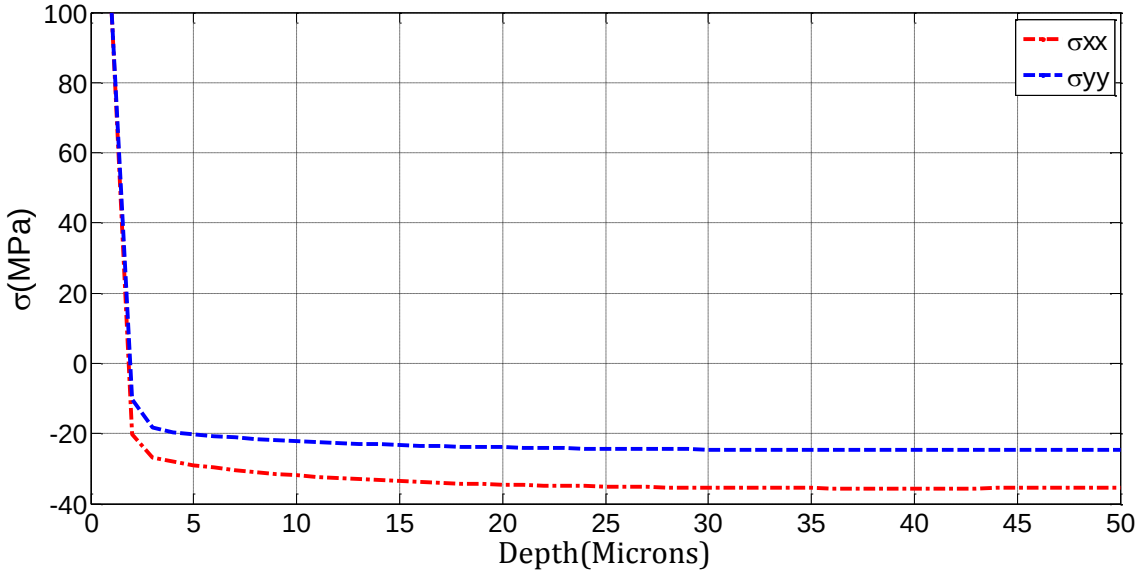

Figure 66: Simulated residual stress for Al7050 (Feed 0.2 mm/rev, Spindle speed of 8000 rpm, depth of cut 1mm)

From this first investigation, a deeper work can be oriented to the effect of the tool wear on residual stress. The effect of the tool wear and the physics behind can be explored. Some first analysis shows that shear operation done by a worn tool is generating a very irregular cutting; therefore the relaxation of the atomic structure after the cutting is not occurring. On the other hand a fresh and sharp tool is cutting the atomic structure in a very regular way. The generated forces are very regular and therefore the atomic structure is relaxing after the shear operation. This phenomenon generates a compressive behaviour of the structure. These predictions have to be validated using texture analysis on AFM (Atomic Force Microscope).

5.4 Hardness and residual stress

The hardness of a material is a very important characteristic to be surveyed. In this part, the effect of milling on the surface hardness is studied. The pre and post machining hardness was investigated. The analysis was made on Steel 2842. Figure.67 shows the hardness before and after the milling operation.

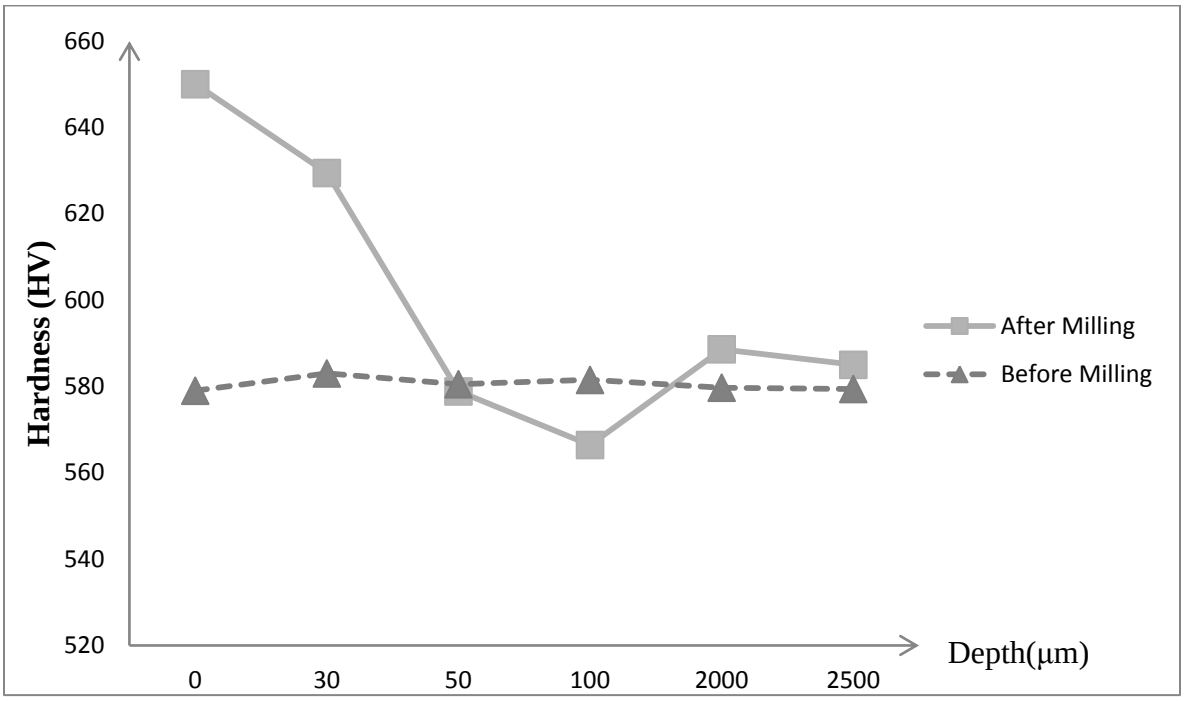

Figure 67: Harness before and after milling on Steel 2842

Beyond the evident changes of hardness due to the milling of steel, a typical curve appeared and was correlating with the residual stress variation in the same concerned depth. The whole profile of residual stress variation is correlating with a sudden change of the hardness. The hardness decreased from its high new value to the original hardness value. All these microstructure changes in the first 100 μm are related to the effect of the stress and large strain induced by the cutting operation. In fact, there exists a pseudo linear relationship between both of them.

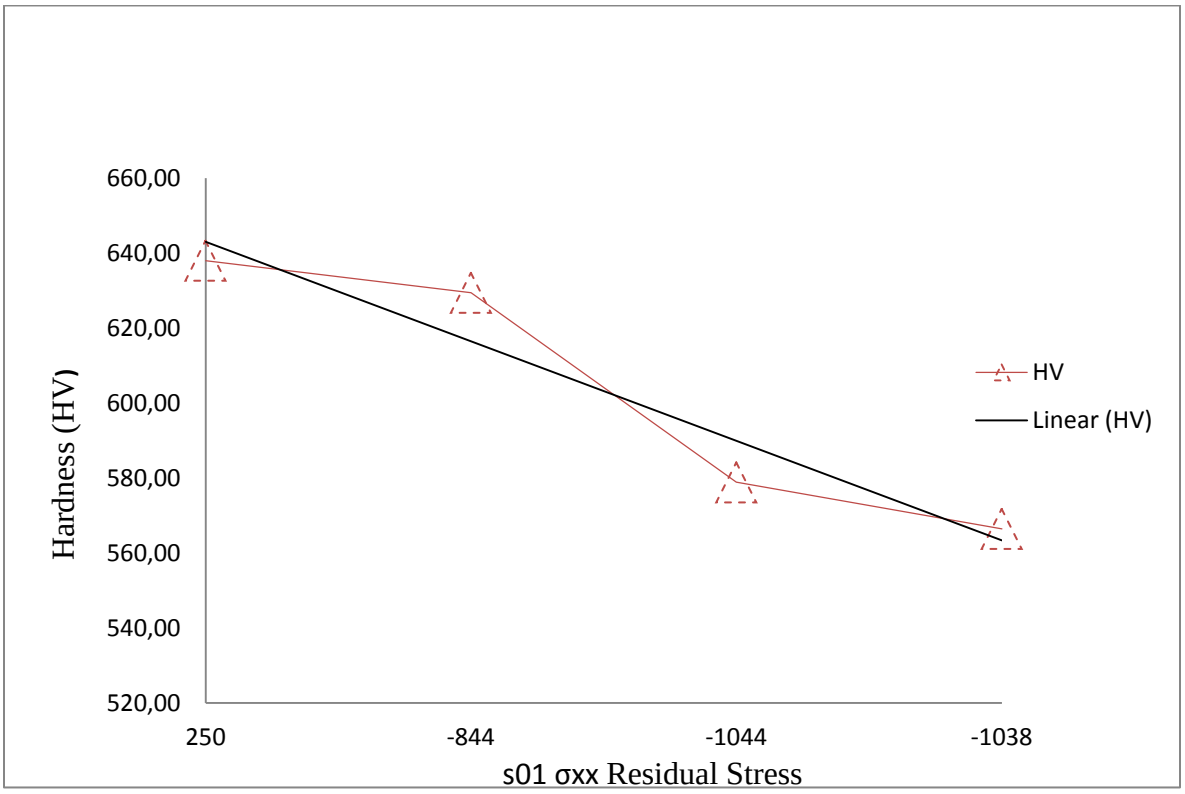

Figure 68: Hardness vs. residual stress

5.5 Similarities between SPD and milling

SPD methods are used to convert coarse grain metals and alloys into ultrafine grained (UFG) materials. Obtained UFG materials then possess improved mechanical and physical properties which destine them for a wide commercial use. Severe plastic deformation (SPD) is one of the methods of obtaining very fine crystalline structure in different bulk metals and alloys, which possess different crystallographic structure. SPD causes the formation of micrometer and sub-micrometer sized subgrains in the initially coarse grain materials. As a result of that enhanced mechanical performance is observed. The mechanism responsible for this effect is still under investigation, however, it is

believed that short and long-range intersecting shear bands produced by plastic deformation play a major role at grain subdivision and local dynamic recovery and recrystallization processes contribute to grain refinement. Sufficiently large deformation leads to a distinct structure of dislocation-free and highly disoriented fine grains. The structural changes caused by SPD are reflected in improved mechanical properties of metals. The reported effects include increased hardness and yield stress, both featuring tendency to saturation. The drawback of ultrafine grained structure materials is their limited ductility. Some other research revealed increased ductility and toughness as well as improved dumping and physical properties. The fine grained structure of UFG materials obtained by SPD leads to super plastic behaviour of these materials at lower temperatures and yet with higher deformation rates.

This section aims to build the first observations about the similarities between the SPD and the machining operations. During the machining process, the cheap removal is inducing a very large strain. Many researchers have studied the machining process and compared it to the SDP, [45] investigated the strains that generates SPD. They made a FEM simulation to estimate strain during the orthogonal machining process. They also did a microstructure analysis to validate their results.

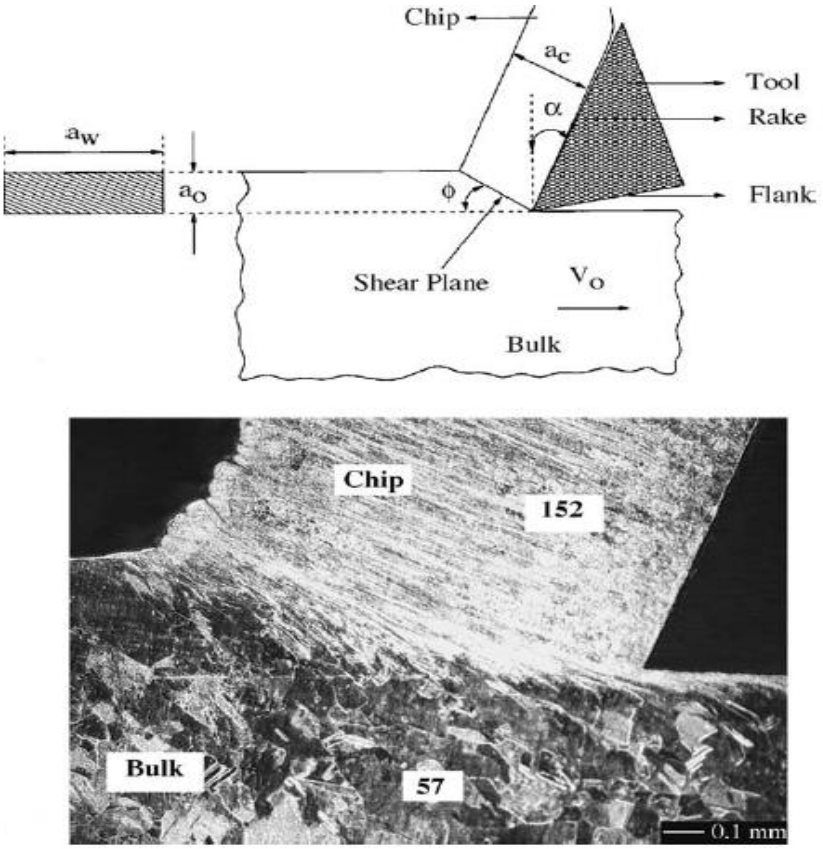

Figure 69: Chip formation process [45]

The large strain in the shear plane is therefore generating on the machined surface some characteristics that are similar to what we obtain during the SPD process. An increase of the surface hardness was predictable due to the decrease of the grain size. This was validated experimentally. In this study, the SPD aspect of the machining operation is partially validated. Further investigations about the texture should be studied.

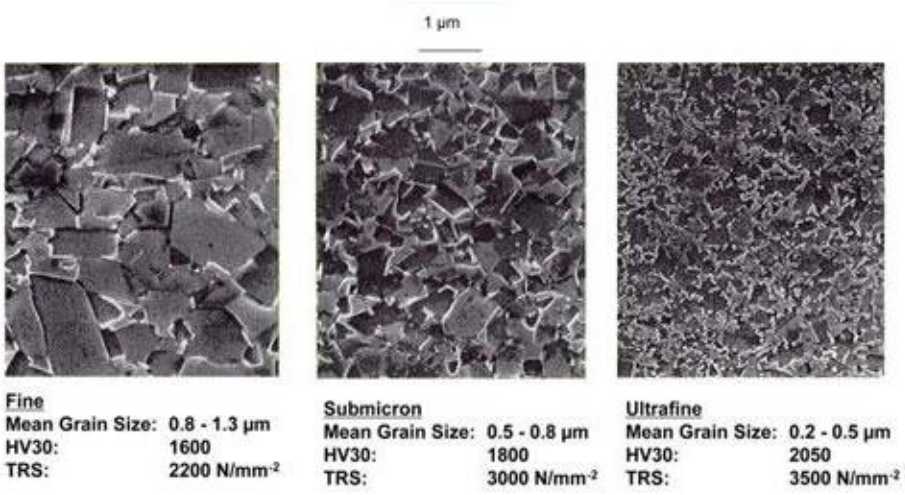

Figure 70: The change of the grain size during the machining [45]

Conclusion

The research on residual stress induced by machining is complex due to the mathematical challenges and it interdisciplinary aspect. In fact, a deep understanding of the physics of cutting is necessary but not sufficient. The material behaviour during and after the cutting operations is also critical. Although the modeling of such phenomenon is complicated, the experimental validations are not easier and ask a lot of experiences and very advanced experimental setup such as (x-ray, SEM, XPS, AFM, dynamometers ...). In this study, the first objective was to investigate the residual stress in the oblique cutting. While working on that, we enhanced our knowledge and we ended up proposing a new technique for residual stress modeling in milling. This technique is based on a hybrid model that associates experimental calibration and analytical simulation. During the research, many experts were involved from theoretical material sciences to experimental approach on X-ray diffraction.

For the first time, a hybrid model is proposed to simulate residual stress in milling. This model was tested on two different materials, Steel 2842 and Al7050. During the experimental work, the effect of new parameters rather than the cutting inputs were investigated. During the machining of Al7050, the effect of the wear on the residual stress was investigated. The results show that the fresh tool is always generating compressive stress on the surface of the Al 7050 part. After a certain amount of cutting, the tool starts generating undesirable tensile residual stress on the surface. This point where the compressive stresses become tensile can be used in the industry as a wear indicator. In fact

most of the manufacturing industries try to avoid tensile stress on the surface. The simulations giving residual stress were validated experimentally for steel 2842. Hardness profile for Steel 2842 was investigated before and after milling. An increase in the hardness always appeared after the machining process. The hardness change in the first 50 microns is correlating with the area where residual stresses change. The experimental results show a pseudo-linear relation between the hardness and the residual stress. This is partly due to the change of the grain size of the material. Therefore, a similarity study was proposed to understand the how milling can enhance the surface characteristics of a part by making a comparative study with SPD.

The deflection of a thin part was simulated for Al7050. Validation tests have been conducted successfully. The model is still under validation for other materials such as Titanium alloys. The deflection profile was close to the simulated one, the amplitude of the deflection was 10% to 30% close to the simulated one depending on different parameters such as contact area and cutting parameters. This is partly due to the fact that thermal effect on the residual stress was not considered in this work. The deflection model is valid for simple geometry and cannot be used for difficult geometries. This is due to the analytical aspect of the solution. However the model gives very accurate results in a very short time. Other solutions such as FEM take many hours for the same results. Other research is conducted to validate the deflection in the micro machining domain.

This thesis is a first step for a larger research on residual stress effect on surface milled part. It gives first ideas and results on some of the most used materials in the manufacturing industry. It also gives a first model that predicts the deflections induced by the machining residual stress. Further, the global computing time is much shorter than FEM simulation. This work can constitute the bases for different research topics

- *The modeling of residual stress in milling: In this study, the kinematics and the kinetics of the milling process was linked to the residual stress distribution in the part. The relation between the force profile, the cutter position and the equivalent stress on the surface was proposed in this study. The 3D field can produced in the future for a better understanding.*
- *Introducing a residual stress parameter into the wear theory: Many researchers have been investigation the wear of tool based on the same parameters (Temperature, Forces, material properties ...etc). In this research, we propose a more pragmatic approach to define the wear. In fact, wear should be studied based on the non desirable effect of it. Here, we found that the fresh tool is generating desirable compressive stress, however the warn tool is generating tensile stress on the surface. The changing point from compressive to tensile stress should be investigated and linked to the removed volume.*
- *The investigation of the surface microstructure and residual stress: for many years, the material properties were associated to different kind of parameters such as the grain size, the texture, or the chemical composition. From this study, a relation between the microstructure and the residual stress was proposed. It is experimentally validated. Further theoretical work should be done to define stronger links between all these parameters.*

BIBLIOGRAPHY

[1] Noyan, I.C. and J.B. Cohen, Residual Stress :Measurement by Diffraction and Interpretation. 1987, New York: Springer-Verlag. x, 276 p.

[2] Henriksen, E.K., Residual Stresses in Machined Surfaces. American Society of Mechanical Engineers -- Transactions, 1951. **73**(1): p. 69-76.

[3]Liu, C.R. and M.M. Barash, Variables Governing Patterns of Mechanical Residual Stress in a Machined Surface. Journal of Engineering for Industry, Transactions ASME, 1982. **104**(3): p. 257-264.

[4] Xie, Q., et al. A Study on Residual Stresses and Tool Wear Induced by the Machining Process. in NAMRC XVII. 1989: SME.

[5] I.Lazoglu An enhanced analytical model for residual stress prediction in machining, CIRP Annals - Manufacturing Technology 57 (2008) 81–84

[6] Merwin, J.E., Johnson, K.L., *An Analysis of Plastic Deformation in Rolling Contact.* Proeedings, Institution of Mechanical Engineers, London, 1963. **177**(25): p. 676-685.

[7] Jacobus, J.K., R.E. DeVor, and S.G. Kapoor, Machining-Induced Residual Stress: Experimentation and Modeling. Journal of Manufacturing Science and Engineering, 2000. 122: p. 20-31.

[8] Merwin, J.E., Johnson, K.L., An Analysis of Plastic Deformation in Rolling Contact. Proeedings, Institution of Mechanical Engineers, London, 1963. 177(25): p. 676-685.

[9] Mittal, S. and C.R. Liu, Method of Modeling Residual Stresses in Superfinish Hard Turning. Wear, 1998. 218(1): p. 21-33.

[10] E.J.A. Armarego and N.P. Deshpande, Force Prediction Models and CAD/CAM Software for Helical Tooth Milling Processes, I, Basic approach and Cutting Analyses, International Journal of Production Research 31 (1993), 1991-2009.

[11] E.M. Lim, H.Y. Feng, C.H. Menq, The Prediction of Dimensional Errors for Machining Sculptured Surfaces Using Ball-End Milling, in K.F. Ehmann, editor, Manufacturing Science and Engineering, 149-156. ASME Winter Annual Meeting, New Orleans, USA, 1993, PED-Vol.64.

[12] Okushima, K. and Y. Kakino, Residual Stress Produced by Metal Cutting. CIRP Annals, 1971. 20(1): p. 13-14.

[13] Lin, Z.-C., Y.-Y. Lin, and C.R. Liu, Effect of Thermal Load and Mechanical Load on the Residual Stress of a Machined Workpiece. International Journal of Mechanical Sciences, 1991. 33(4): p. 263-278.

[14] Shih, A.J., *Finite Element Analysis of the Rake Angle Effects in Orthogonal Metal Cutting.* International Journal of Mechanical Sciences, 1996. **38**(1): p. 1-17.

[15] Hua, J., et al., Effect of Feed Rate, Workpiece Hardness and Cutting Edge on Subsurface Residual Stress in the Hard Turning of Bearing Steel Using Chamfer + Hone Cutting Edge Geometry. Materials Science and Engineering A, 2005.394(1-2): p. 238-248.

[16] Hua, J., D. Umbrello, and R. Shivpuri, Investigation of Cutting Conditions and Cutting Edge Preparations for Enhanced Compressive Subsurface Residual Stress in the Hard Turning of Bearing Steel. Journal of Materials Processing Technology, 2006. 171(2): p. 180-187.

[17] K.C. Ee, O.W. Dillon Jr., I.S. Jawahir, Finite element modeling of residual stresses in machining induced by cutting using a tool with finite edge radius International Journal of Mechanical Sciences 47 (2005) 1611–1628

[18] Liu, C.R. and M.M. Barash, Mechanical State of the Sublayer of a Surface Generated by Chip-Removal Process Part 2: Cutting with a Tool with Flank Wear. Journal of Engineering for Industry, Transactions ASME, 1976. **98 Ser B**(4): p. 1202-1208.

[19] Matsumoto, Y., M.M. Barash, and C.R. Liu, Effect of Hardness on the Surface Integrity of AISI 4340 Steel. Journal of Engineering for Industry, Transactions ASME, 1986. **108**(3): p. 169-175.

[20] Wu, D.W. and Y. Matsumoto, Effect of Hardness on Residual Stresses in Orthogonal Machining of AISI 4340 Steel. Journal of Engineering for Industry, Transactions of the ASME, 1990. **112**(3): p. 245-252.

[21] Fuh, K.-H. and C.-F. Wu, Residual-Stress Model for the Milling of Aluminum Alloy (2014-T6). Journal of Materials Processing Technology, 1995. **51**(1-4): p. 87-105.

[22] Chen X., Xue J., Tang D., Chen H., Qu S., 2009, Deformation prediction and error compensation in multilayer milling processes for thinwalled parts. International Journal of Machine Tools and Manufacture, vol. 49, pp. 859-864.

[24] Sakkiettibutr, J .Vollertse, F. 2011, Possibilities and limitations of geometric simplifications for calculations of residual stresses and distortions. Production Engineering Research and Development (WGP),

[25] Zäh, M., Brinksmeier, E., Heinzel, C., Huntemann, J.-F., Föckerer, T. (2009), Experimental and numerical identification of process parameters of grindhardening and resulting part distortions. Production Engineering – Research and Development Vol. 3 , p. 271-279

[24] Xie., J.-I. Beyoumi, and A. Tsukuda, Effect of Tool Nose Radius and Tool Wear on Residual Stress Distribution in Hard Turning of Bearing Steel. Journal of Materials Processing Technology, 2004. **150**(3): p. 234-241.

[26] Gang L., 2009, Study on deformation of titanium thin-walled part in milling process. j. of materials processing technology,vol. 209, pp. 2788-2793.

[27] I.S. Jawahir, E. Brinksmeier, R. M'Saoubi, D.K. Aspinwall, J.C. Outeiro, D. Meyer, D. Umbrello, A.D. Jayal , 2011, Surface integrity in material removal processes: Recent

advances Original Research Article CIRP Annals - Manufacturing Technology, Volume 60, Issue 2, Pages 603-626

[28] Sakkiettibutr, J.; Vollertse, F. 2011, Possibilities and limitations of geometric simplifications for calculations of residual stresses and distortions. Production Engineering – Research and Development (WGP),

[29] Zäh, M., Brinksmeier, E., Heinzel, C., Huntemann, J.-F., Föckerer, T. (2009), Experimental and numerical identification of process parameters of grindhardening and resulting part distortions. Production Engineering – Research and Development Vol. 3 , p. 271-279

[30] Gang L., 2009, Study on deformation of titanium thin-walled part in milling process. Journal of materials processing technology,vol. 209, pp. 2788-2793.

[31] Love, a. e. h., 1952, a treatise on the mathematical theory of elasticity, 4th ed. cambridge university press, Cambridge

[32] Y.h. an, Lh. He, 2009, Surface deformation of an elastic half-space with attenuating eigenstrain in a striped region, international journal of engineering science 47 866–874

[33] Fuh, K.-H. and C.-F. Wu, Residual-Stress Model for the Milling of Aluminum Alloy (2014-T6). Journal of Materials Processing Technology, 1995. 51(1-4): p. 87-105.

[34] Mittal, S. and C.R. Liu, Method of Modeling Residual Stresses in Superfinish Hard Turning. Wear, 1998. 218(1): p. 21-33.

[35] Heinrich Hertz 1882 "On the contact of elastic solids" ("Ueber die Berührung fester elastischer Körper") by Heinrich Hertz

[36] Yusuf altintaş, Automation and Manufacturing, Cambridge edition

[37] T H Lin & T. K Tung, ‘The stress field produced by plastic slip at a free surface’, Journal of Applied Mechanics, September 1962.

[38] R. D Mindlin, ‘ Forces at a point in the interior of a semi infinites Solid’, Proceedings of the First Midwestern Conference of Solid Mechanics, 1953, pp. 56-59.

[39] A. E. Love, ‘ On stress Produced in a semi-infinite solid by pressure on a part of the boundery’, Philosophical Transactions of the Royal Society, series A, Vol.228, 1929, p. 337

[40] T.Mura, ‘Micromechanics of defects in solids’ Martinus Nijhoff, The hague/Boston/London, 1982.

[41] Martelotti (Tlusty & MacNeil, 1975)

[42] Jiang Y, Sehitoglu H (1994) An Analytical Approach to Elastic-Plastic Stress Analysis of Rolling Contact. Journal of Tribology 116:577–587.

[43] Chiu Y.P., 1977, “On the Stress Field Due to Initial Strains in a Cuboid Surrounded by an Infinite Elastic Space,” ASME J. Appl. Mech., 44, 587−590.

[44] Chiu Y.P., 1978, “On the Stress Field and Surface Deformation in a Half-Space With a Cuboidal Zone in which Initial Strains Are Uniform,” ASME J. Appl. Mech., 45, 302−306.

[45] M. SEVIER, H.T.Y. YANG, S. LEE, and S. CHANDRASEKAR, “Severe Plastic Deformation by Machining Characterized by Finite Element Simulation” metallurgical and materials transactions b volume 38b, december 2007—927

[46] A. Ramesh, S.N. Melkote, L.F. Allard, L. Riester, T.R. Watkins, “Analysis of white layers formed in hard turning of AISI 52100 steel” Materials Science and Engineering: A, Volume 390, Issues 1–2, 15 January 2005, Pages 88-97

[47] Eshelby, J. D. (1951). "The Force on an Elastic Singularity". Philosophical Transactions of the Royal Society A: Mathematical, Physical and Engineering Sciences 244 (877): 87. doi:10.1098/rsta.1951.0016

[48] Johnson, K. L. (1985) Contact Mechanics (Cambridge University Press, Cambridge)

[49] Y. Altintas, S. Engin, 2001, Generalized Modeling of Mechanics and Dynamics of Milling Cutters, CIRP Annals - Manufacturing Technology, Volume 50, Issue 1, Pages 25.

[50] Johnson, G.R, Cook H.W, “A constitutive model and data for metals subjected to large strains, high strain rates and high temperatures”. Proceedings for the 7th International Symposium on Ballistics, The Hague, The Netherlands, April 1983

[51] Drucker, D. C. and Prager, W. (1952). Soil mechanics and plastic analysis for limit design. Quarterly of Applied Mathematics, vol. 10, no. 2, pp. 157–165.

Vitae

Omar Fergani is a graduate research assistant in the Department of Mechanical Engineering at Koc University. He is working under the supervision of Dr. Ismail Lazoglu at the Manufacturing and Automation Research Center. He obtained his B.Eng in Mechanical Engineering from Reims University and ENSAM ParisTech in France. He is also holder of a national diploma in political science from Sciences Po Paris.

After finishing his MS study at Koc University, he will be joining The George W. Woodruff School of Mechanical Engineering Department at Georgia Institute of Technology for his Ph.D. study.